Anodizing of Ti c.p and Ti6Al4V alloy in high pH solutions for applications of high wear performance

David Alberto Quintero Giraldo

Doctoral Thesis

CIDEMAT

Centro de Investigación, Innovación y Desarrollo de Materiales

UNIVERSIDAD DE ANTIOQUIA
1 8 0 3

Anodizing of Ti c.p and Ti6Al4V alloy in high pH solutions for applications of high wear performance

David Alberto Quintero Giraldo

Doctoral Thesis in Materials Engineering

Supervisors:

Prof. Félix Echeverría
Prof. Juan G. Castaño

Centro de Investigación, Innovación y Desarrollo de Materiales – CIDEMAT
Facultad de Ingeniería
Universidad de Antioquia
Medellín, Colombia
2013 - 2016

Centro de Investigación, Innovación y Desarrollo de Materiales

CIDEMAT

Sede de Investigación Universitaria – SIU

Universidad de Antioquia

Cr 53 # 61 – 30

Medellín, Colombia

The Doctoral thesis is based on the experimental work carried out at the Research Center, Innovation and Development of Materials - CIDEMAT, in the University of Antioquia, Medellin – Colombia, within the framework of the project "Desarrollo de implantes quirúrgicos empleando tecnologías avanzadas" funded by Sistema General de Regalias, the Universidad de Antioquia and the University of Manchester; “ Estrategia de Sostenibilidad” of the Universidad de Antioquia; LATEST 2 funded by the engineering and Physical Sciences Research Council (UK).

Some results are from research internships in the laboratory of interfacial electrochemistry in the Hokkaido University, Japan under the supervision of Prof. Hiroki Habazaki and the Corrosion and Protection Center in the University of Manchester, UK under the supervision of Profs. Peter Skeldon and Michele Curioni.

Acknowledgements / Agradecimientos

Quisiera agradecer de forma muy especial a mi familia, a mi padres, Alba y José David, a mis abuelos, Nelly y José Dolores, y hermanos, Laura, Darío y Edison, quienes han sido un apoyo incondicional y siempre me han motivado a seguir mis metas y ser mejor persona. Un agradecimiento muy especial para mi familia, ya que siempre me apoyaron en todas las etapas de este proceso de formación, especialmente a la tía Carmen. Finalmente quiero agradecer a Natalia, dado que me dio su apoyo y cariño en esta etapa final de mi proceso de formación.

Le agradezco profundamente a mis tutores, Félix Echeverría y Juan Castaño, quienes siempre me guiaron en este proceso, contribuyendo de manera integral a mi formación como persona, investigador, compañero y en muchos otros aspectos. Sus enseñanzas serán de mucha importancia para los retos que se vendrán después de mi proceso de formación doctoral. Igualmente, quiero agradecer a los profesores Jorge Calderón y Maryory Gómez, quienes han sido un apoyo incondicional durante este proceso.

First, I would like to thanks to Prof Hiroki Habazaki for accepting me in your lab and allowing me to conduct some research at the laboratory of interfacial electrochemistry in the Division of Materials Chemistry of the Hokkaido University, Japan under his supervision. His suggestions and comments were very helpful to achieve the aims of my research. Moreover, I would like to thanks to the students of the Lab KAIMEN for your help both in the lab and during my stay in Japan.

I would like to thanks, Prof Peter Skeldon and Michele Curioni for accepting me as their student in the Corrosion and Protection Centre in the School of Materials of the University of Manchester. His teachings were of vital importance to my PhD formation process. I would like to thanks all the students of the D10 office for giving me your help and friendship during my stay in Manchester. It was a very great time for me.

Muchas gracias a todos los colegas y amigos del Centro de Investigación, Innovación y Desarrollo de Materiales - CIDEMAT, por toda su ayuda y los momentos vividos durante estos 8 años, los cuales fueron de gran importancia para poder terminar esta etapa de formación doctoral.

Igualmente quiero expresar mis agradecimientos a todos los compañeros y amigos de los procesos sociales en los que he participado, ya que siempre han contribuido a mi proceso de formación como persona y han sido un apoyo incondicional durante esta etapa de mi vida. Entre ellos a todos los compañeros de la corporación CORUM.

También quiero agradecer el apoyo económico brindado por el Departamento Administrativo de Ciencia, Tecnología e Innovación – COLCIENCIAS a través de su programa de formación Doctoral “Francisco José de Caldas – Generación del Bicentenario”.

Abstract

Titanium and its alloys have excellent physical and mechanical properties for a large number of applications. Unfortunately, these applications are restricted due to their poor wear and corrosion resistance. An approach to overcome this issue is to form a coating on the surface metal to avoid direct contact with the environment and improve the surface properties of these materials. A number of coating technologies are available in order to improve the corrosion resistance and the tribological performance of the titanium alloys. Anodizing process, especially the plasma electrolytic oxidation (PEO), is gaining popularity given that by anodizing, a wide range of coatings is formed on the metal surface. It is an economically and eco-friendly process and the coatings obtained have good adhesion to the substrate. This doctoral thesis is aimed to obtain coatings on titanium alloys by PEO in alkaline solutions in order to improve the wear performance and the corrosion resistance looking to increase the number of applications of these materials.

Anodic coatings were obtained in alkaline solutions in two different substrates; Ti c.p and Ti6Al4V alloy and characterized by scanning electron microscopy (SEM), X-ray diffraction (XRD), Microwave energy dispersive X-ray (EDS) and profilometry in order to study the composition, morphology, roughness and porosity distribution of the coatings. The coatings were obtained both under galvanostatic and potentiostatic conditions. In order to form the coatings on the titanium alloys, two alkaline base solutions were used. The first set of solutions was based on sodium hypophosphite with different additives looking for the incorporation of species useful for biomedical applications. The second set of solutions was

based on sodium aluminate with different additives with the aim to form hard ceramic coatings that improve the mechanical and tribological properties of the titanium alloys. These alkaline solutions were used due to the few information in the literature and seeking the formation of other crystalline phases into the coatings in order to evaluate their corrosion and wear performance.

The wear behavior of the coatings was assessed using a ball-on-disc tribometer, and the corrosion behavior was evaluated by electrochemical impedance spectroscopy (EIS). The results were correlated with the structure, morphology and composition of the coatings. The coatings obtained under potentiostatic conditions showed a better corrosion resistance and wear performance due to their low porosity. The coatings obtained with the addition of sodium metasilicate showed a better corrosion resistance. Finally, the progress of the formation of the coatings was investigated in two solutions with different electrical parameters. A significant different was observed in the coating formation for the films obtained in the sodium aluminate-based solution with the addition of sodium metasilicate due to the abundant gas evolution during anodizing of the coating obtained on Ti c.p, which reduced the efficiency the process. For the coatings obtained in the sodium-hypophosphite-based solution with the addition of sodium metasilicate, the anodizing process shows a similar behavior for both substrates.

Research Output

The thesis is a summary of the following papers:

Control of the Physical Properties of Anodic Coatings Obtained by Plasma Electrolytic Oxidation on Ti6Al4V Alloy

D. Quintero, O. Galvis, J.A Calderón, M.A Gómez, J.G Castaño, F. Echeverría, H. Habazaki

Surface and coating technology. 283 (2015) 210–222

Properties of alumina - titanate and alumina - mullite coatings obtained by PEO on Ti6Al4V: influence of the electrochemical parameters and solution composition

D. Quintero, J.A Calderón, M.A Gómez, J.G Castaño, M. Curioni, F. Echeverría, H. Habazaki, P. Skeldon, G.E Thompson

In preparation

Effect of pre-anodizing on the tribological and corrosion properties of titanium following plasma electrolytic oxidation under potentiostatic conditions

D. Quintero, J.A Calderón, M.A Gómez, J.G Castaño, F. Echeverría, M. Curioni, H. Habazaki, Peter Skeldon, G.E Thompson

In preparation

Kinetic aspects, morphological and chemical changes during the formation anodic coatings on titanium alloys obtained in alkaline solutions by PEO

D. Quintero, J.A Calderón, M.A Gómez, J.G Castaño, F. Echeverría, M. Curioni, H. Habazaki, Peter Skeldon, G.E Thompson

In preparation

In addition, other papers have been completed but they are not included in the thesis:

Effect of electrochemical parameters on the formation of anodic films on commercially pure titanium by plasma electrolytic oxidation

D. Quintero; O. Galvis; J.A Calderón; J.G Castaño; F. Echeverría

Surface and coating technology. 258 (2014) 1223–1231

Titanium anodic films obtained in aluminate solutions by spark anodizing: Effect of OH^- and $WO4^{-2}$ additions on the tribological properties

D. Quintero; M.A Gómez; J.G Castaño; E. Tsuji; Y. Aoki; F. Echeverría; H. Habazaki
Surface and coating technology. 310 (2017) 180-189.

Accepted publications as a co-author in related subjects:

Morphological transitions of coatings formed on titanium by plasma electrolytic oxidation in H_2SO_4 / H_3PO_4 electrolytes.
O.A. Galvis, D. Quintero, J.G. Castaño, H. Liu, G.E. Thompson, P. Skeldon, F. Echeverría.
Surface and Coatings Technology. 269 (2015) 238–249

Osseointegration Improved by Plasma Electrolytic Oxidation of Modified Titanium Alloys Surfaces.
M. Echeverry, O. Galvis, D. Quintero, J. Pavón, J. L Lacomba, E. Jiménez, M. Anglada, S.M. Robledo, J.G Castaño, F. Echeverría.
Journal of Materials Science. 26 (2015) 1–18

Manuscripts in preparation in related subjects

Effect of the anodizing parameters on the corrosion and wear properties of anodic coatings obtained on Nb by PEO in alkaline solutions.
D. Quintero, J.A Calderón, M.A Gómez, J.G Castaño, F. Echeverría.

Formation of nanotubular TiO_2 structures with varied surface characteristics for biomaterial applications.
R. Aguirre, D. Quintero, M. Echeverry, J.G Castaño, S.M Robledo, F. Echeverría.

Improved two-step electropolishing of aluminum alloys in Brytal process
L .M. Sepúlveda, D. Quintero, J.G Castaño, F. Echeverría
Submitted to Corrosion Science

Congress and meetings in the thesis subject

D. Quintero, O. Galvis, J.G Castaño, F. Echeverría. VII Congreso Internacional de Materiales. "Effects of the parameters on the formation of the anodic films on pure titanium by PEO". Medellín, Colombia, 2013.

D. Quintero, O. Galvis, J.G Castaño, F. Echeverría. V Simposio SIU – Superficies e Interfaces. "Caracterización superficial de recubrimientos anódicos sobre Ti c.p obtenidos a diferentes tiempos de anodizado". Medellín, Colombia, 2013.

D. Quintero, O. Galvis, J.A Calderón, M.A Gómez, J.G Castaño, F. Echeverría. Second International Symposium on Anodizing Science and Technology. "Plasma electrolytic oxidation of Ti6Al4V alloy in alkaline solutions: Effect of OH^- ion. Sapporo – Japan, 2014.

D. Quintero, M Curioni, P. Skeldon. PGR Student Conference. "Effect of pre-anodizing on the tribological and corrosion properties of Ti6Al4V alloy following plasma electrolytic oxidation under potentiostatic conditions". Manchester, UK. 2016.

D. Quintero, M. Gómez, J.A Calderón, J.G Castaño, F. Echeverría, P. Skeldon, M Curioni, G. E. Thompson, E. Tsuji; Y. Aoki; H. Habazaki. International Conference on Processing and Manufacturing of Advanced Materials – THERMEC 2016. "Control of Physical Properties of Anodic Coatings Obtained by Anodizing in Aluminate Solutions". Graz, Austria. 2016

Congress and meetings in related subjects

R. Aguirre, D. Quintero, J.G Castaño, F. Echeverría. VIII Congreso Internacional de Materiales - CIM 2015. "Formation of nanotubes on titanium c.p by anodizing technique using different fluoride sources". Boyacá, Colombia, 2015.

Table of Contents

Introduction

Light alloys, such as aluminum, magnesium and titanium, are the choice for a wide range of applications due to their unique properties [1], [2]. For example, in the transport and aerospace industries, the low density and the high strength-to-weight ratio made these materials suitable for these applications. Weight reduction in transport translates directly to fuel saving and a decrease in CO_2 emissions, important facts for an ecologically and economically sustainable development. The above remarks have made these materials the main choice for the aerospace industry for more than four decades, especially titanium alloys. In view of their unique combination of properties, there is an increasing demand for these materials into non-aerospace sectors such as biomedical, performance sports, automotive, power generation, general engineering and architecture [1], [3]–[8]. In addition, light alloys are attractive for some specific applications; for example, outstanding biocompatibility makes titanium alloys the material choice for body implants [9]–[12]. Nevertheless, in some cases, the surface properties of these materials do not provide enough protection, generating a serious barrier in many sectors and industries; i.e. magnesium alloys have a bad reputation

for their poor corrosion protection in most environments which is essential in many applications [1], [13]–[17]. Currently, in the automotive and the biomedical sector, titanium alloys have been used as a substitute of steel components due to their biocompatibility properties and the possibility of the mass reduction of the components. Nonetheless, light alloys are known by their poor tribological properties in sliding conditions since these materials exhibit low load-bearing capacity and low abrasion resistance, which are related to low hardness, high adhesion tendency, high ductility, and high reactivity features. Therefore, light alloys are restricted to sectors in which tribological performance is not critical. On the other hand, light alloys are susceptible to surface degradation in some environments, especially in acidic media. In different fields such as biomedical applications, chemical industry, gas and oil industries and some aerospace applications, improving the corrosion protection of these materials is important in order to increase their life cycle under demanding operating conditions [18]–[26].

One approach to overcome these issues is to form a coating on the metal base in order to modify the surface characteristics of these materials improving their behavior against corrosion and wear. Among the different surface modification techniques (CVD, PVD, ion implantation, electroplating, plasma nitriding, thermal oxidation, electroless Ni-P), the anodic oxidation has become increasingly important since it has some advantages over other surface modification techniques [27]–[29]. The main advantages of the anodizing process are as follows: no degradation of the mechanical properties of the substrate, high bonding strength of the coatings to substrate, successful coatings on complex geometric shapes of the substrate, inexpensive and ecologically friendly process [20], [23], [27]–[35]. Anodizing is

an electrochemical process in aqueous solutions that generates an oxide layer, generally thicker than those formed in a naturally way, that improves the surface characteristics of the substrate. The anodizing process is classified into two groups depending on the potential range. The conventional anodizing generates thin coatings (20 - 500 nm) and generally is a process carried out at low potentials. The coatings obtained are generally dense layers that improve the corrosion protection of the substrate. By adding some additives to the solution, the formation of nanotubular layers has been observed; these coatings have different functional properties and potential use in applications such as gas sensors, photocatalysis, solar cells, biosensors and electronic applications. Nevertheless, thin coatings do not provide an effective protection against wear as well as a good corrosion protection in some aggressive environments [36]–[53]. Plasma electrolytic oxidation, PEO, is an anodic oxidation of the substrate in an aqueous solution under conditions of plasma discharge, which needs high-applied potentials. Sparking happens during anodizing due to dielectric breakdown of the oxide at high potential. The presence of plasma produces local high temperature regions leading to the formation of a crystalline and adherent coating on the surface of the substrate. The coating thickness growth generates systemic changes in the surface topography, which gives the possibility to obtain different morphologies and surface features and consequently to determine the appropriated properties [19], [30], [54]–[58].

One important fact of the PEO process is that the chemical composition of the coatings depends on the species in the solution, allowing the formation of different crystalline phases during the process [1], [49], [59]–[61]. Different solutions, acid, neutral or alkaline, have been used to obtain coatings on titanium alloys. The acid and neutral solutions allow the

formation of coatings that improve mainly the corrosion protection of these materials. Coatings obtained under PEO conditions reveal the formation of a porous structure, which is important in many applications, especially in the biomedical sector. The chemical composition is mainly TiO_2 with the incorporation of species from the solution [7], [28], [46], [48], [49], [62]–[68]. Alkaline solutions allow the formation of a wide range of crystalline phases, among which stand out the formation of Al_2O_3 and Al_2TiO_5, which exhibit good wear behavior and superior mechanical properties than TiO_2. This fact allows the formation of coatings with a better performance against corrosion and wear due to the range of crystalline phases that are obtained during anodizing. The formation of other crystalline phases into the coating by anodizing in alkaline solutions has allowed new applications of PEO coatings [18], [24], [25], [61], [69]–[71]. For example, the formation of barium titanate ($BaTiO_3$) on titanium allows using these materials in electronic applications [72], [73], the formation of Al_2O_3, SiO_2 and ZrO_2 into the coating allows the formation of electrically insulating coatings, the formation of mullite into the coating allows the application of PEO coatings as a thermal barrier and the formation of phosphates species into the coating allows the formation of bioactive coatings for biomedical applications [74]–[77]. The chemical composition of the coating has a significant effect on its final properties; but the morphological distribution in the coating can improve or deteriorate these properties. For example, a porosity increase reduces the hardness and the wear and corrosion resistance of the coatings and also reduces the thermal conductivity that benefits the applications of thermal protection. The coating adhesion depends on many factors, such as the chemical composition, the porosity distribution, and the coating thickness, among others. The control of the coating topography affects the wear behavior, given that rough surfaces have higher friction coefficients,

nonetheless, rough surfaces can improve the adhesion of paints or the bonding of two surfaces [1], [78]–[80]. Different studies have demonstrated the critical influence of the electrochemical parameters on the oxide properties as well as on the growth mechanism of the anodic coatings. For example, a high growth rate of the coating generates mechanical damage, fatigue cracking and stress, decreasing the mechanical and tribological properties. The coating growth rate depends mainly on the electrical parameters of the process (potential and current). Another important parameter of the process is the solution temperature given that increases the dissolution of the coating, rises the coating porosity and affects the size of the micro-discharges; the latter generates large pores and increase the voids and pores near the coating base, affecting the coating adhesion. Therefore, by controlling the anodizing parameters such as concentration and nature of the anodizing solution, pH, temperature, process time and electrical parameters of the process (potential and current density), the surface properties can be modified depending on their final applications [14], [81]–[86].

Plasma electrolytic oxidation (PEO) is a very attractive surface engineering technique given that it is an economic (compared with CVD and PVD) and ecological process that allows improving the surface characteristics of titanium alloys as well as other metals. A wide range of crystalline phases with different properties can be produced by PEO, which can effectively improve the tribological and corrosion properties. In particular, PEO is a unique and irreplaceable technique to fabricate functional coatings for specific applications [85], [87]–[94]. Nevertheless, it is necessary to further study the fundamentals of the PEO technique and understand clearly the relationship between the anodizing parameters and the morphological characteristics of the coatings. Besides, it is important to relate these

morphological characteristics with the corrosion behavior and wear of the anodic coatings. On the other hand, the formation of other crystalline phases or combination of new crystalline phases with oxides that have been widely studied could generate new functional coatings. In addition, new solutions or the effect of various additives on the traditional alkaline solutions could be explored, allowing improvement of the morphological characteristics of the coatings. The thickness of wear-resistant coatings is usually ≥ 10 μm. Thin coatings to be used in tribological applications are not widely explored, as these coatings, regularly, do not provide an effective protection against wear and corrosion. However, in some cases, the formation of thin coatings with good mechanical and tribological performance could be useful for applications where no significant dimensional changes are required, like screws and pistons. In this research, some of these technological challenges were explored and the results obtained are summarized in the following chapters.

Document Overview

Chapter 1 presents the results of the coatings obtained in sodium hypophosphite-based solutions with different electrical parameters. Dense coatings exhibit a better performance against corrosion and wear. The porosity of the coatings is influenced by the anodizing solution and the electrical parameters. Coatings obtained under potentiostatic conditions and in the solution composed of sodium hypophosphite and sodium metasilicate have low porosity and therefore, good corrosion resistance and wear performance.

Chapter 2 presents the results of the coatings obtained in sodium aluminate-based solutions with different electrical parameters. Coatings obtained under potentiostatic conditions reveal a better corrosion and wear resistance due to the formation of dense coatings. In the coatings

obtained under galvanostatic conditions, the formation of mullite in the alumina matrix improves the wear resistance significantly. The chemical composition of the coatings obtained under potentiostatic conditions is similar due to the formation of small micro-discharges that have a low intensity that does not allow the formation of other crystalline phases.

Chapter 3 presents the effect of the anodizing parameters on the tribological and corrosion properties. In the galvanostatic coatings, the increase of the current density decreases the wear resistance of the coatings due to the decrease in the inner layer thickness. In the potentiostatic coatings, the initial current density has a significant effect on wear and corrosion properties and finally, the anodizing solution affects the size and intensity of the micro-discharges, which generates different coating characteristics (morphology, thickness, porosity, topography).

Chapter 4 presents the grow mechanism of the coatings obtained in both substrates in the alkaline solutions with the addition of sodium metasilicate. It was found that the anodizing process is influenced by both, the anodizing solution and the substrate. In the coatings obtained in the sodium hypophosphite-based solution, the anodizing process has a similar behavior; however, a difference in composition of the coatings is evidenced. In the coatings obtained in the sodium aluminate-based solution, the coating obtained on Ti exhibits an abundant gas evolution during anodizing which affects the anodizing process and reduces the efficiency of the process.

Objectives

General Aim

To obtain anodic films on Ti c.p and Ti6Al4V alloy by anodizing technique in alkaline pH solutions in order to improve the tribological properties for demanding wear applications.

Specific Aims

To set the parameters of the anodizing process on Ti c.p and Ti6Al4V alloy that allow the formation of anodic films homogeneously distributed throughout the anodized area.

To determine the mechanical and tribological properties of anodic coatings obtained under different parameters of the process.

To determine the effect of process parameters on the morphological distribution and chemical composition of anodic films obtained using different surface and compositional characterization techniques (SEM/EDS, XRD, Raman and AFM).

To determine the anticorrosive properties by electrochemical impedance spectroscopy of the anodic films that showed good tribological behavior.

To study the possible mechanisms of formation of the anodic films that showed good tribological behavior.

1. Chapter 1

Anodic coatings obtained in sodium hypophosphite-based solutions

Abstract: Spark anodizing has been performed in two alkaline solutions using different electrical parameters in order to study the coating formation. The surface features show a dependence on the shape and distribution of the electric micro-discharges. In addition, the surface features and the chemical composition of the coatings are dependent on the anodizing solution employed. The tribological properties of the coatings formed are correlated with the morphology and the internal structure of the coatings. The variation of the internal structure of the coatings was evidenced by EIS analysis. Results indicate that it is possible to control the physical properties of the anodic film by an adequate selection of

the process parameters. A porous structure is obtained using a solution mainly composed of hypophosphite, which exhibits a good tribological performance. Low porosity and compact structure can be obtained in the anodic film by using an anodizing solution composed of hypophosphite and metasilicate; furthermore, these coatings exhibit a good corrosion protection, especially on Ti6Al4V alloy. The best wear resistances were observed in coatings formed at potentiostatic mode, as demonstrated by the results of ball-on-disc wear tests.

Keywords: PEO, titanium alloys, tribological behavior, phosphorous solutions, corrosion resistance, anodic coatings, property.

1.1. Introduction

The formation of coatings on light alloys using solutions composed by phosphates species has been widely studied [26,27,94–98]. The phosphate-based solutions have some benefits on the formation of anodic coatings due to the incorporation of phosphorous or the formation of phosphates species into the coating that assists the osseointegration processes in biomedical applications. In addition, the coatings formed have low friction coefficient, an important aspect of the tribological performance. Moreover, the use of phosphate as an additive in alkaline solutions allows reducing the porosity of the coating. A porosity reduction, especially in the coating base, improves the adhesion of the coating, which in turn improves its wear resistance [18], [19], [23], [25], [31], [78]. In this research, different phosphorous sources were used to obtain anodic coatings on titanium alloys. However, better results were obtained when using sodium hypophosphite-base solutions. On the other hand, literature reports using sodium hypophosphite as a phosphorus source to obtain anodic films

on titanium alloys are scarce. In this chapter, anodic coatings obtained in two hypophosphite-base solutions are studied. The coatings were obtained with different electrical perturbations, in both galvanostatic and potentiostatic modes. EIS analysis was performed with the purpose of correlating the electrical properties of the coatings with internal structure changes. Results indicate that, by an appropriate selection of process parameters, it is possible to control the physical properties of the anodic coatings, with potentiostatic coatings exhibiting the best tribological performance. Moreover, the plasma characteristics are influenced by changes in the electrical properties of the coating generated by elements incorporated from the anodizing solution. This fact is of a special interest in titanium alloy processing, looking for an accurate control of the anodic film formation.

1.2. Experimental

Samples, with dimensions of 10 x 10 x 1 mm, were cut from a titanium sheet of Ti6Al4V alloy (AMS 4911) and Ti c.p grade 2. The samples were mechanically polished progressively with SiC paper up to 1200 grit size, degreased with acetone using an ultrasound bath for 10 min, and then washed with distilled water and dried in a cool air stream. Titanium wire was used to hold the samples in the anodizing solution. The wire with a U-shape in one side holds the sample by pressure as observed in Fig. 2. The titanium wire area was taken into account to calculate the total current applied. The anodizing process was carried out using a Kepco Power Supply BHK 500-0.4 MG in an electrochemical cell of 1 L of volume immersed in a cooled water bath, using a stainless steel beaker as a cathode. During the process, the solution was stirred vigorously in order to homogenize the solution and maintain a uniform temperature (20 ^{o}C). Table 1 shows the anodizing solution composition and the electrical

parameters employed to obtain the anodic coatings. The chemical composition of the solutions was established in order to obtain homogeneous coatings on titanium alloys. For P solution, the concentration of NaOH for both materials was slightly modified for the purpose of generating a stable anodizing process without high variations of potential, allowing the formation of coatings with a homogeneous morphology. Both substrates allowed the formation of coatings with a homogeneous morphology in the P-Si solution. Ca is added in the P solution seeking its incorporation into the coating for biomedical applications where wear resistance is also required [97], [100]–[103]. In the P-Si solution, silicate addition looks to improve the corrosion and wear resistance, as well as induce bone formation, as demonstrated in previous studies by other authors [104]–[108]. The coatings were obtained both in galvanostatic and potentiostatic mode. Galvanostatic coatings were obtained applying a constant current and recording the potential variation with time. For potentiostatic coatings, after a short galvanostatic stage, current changes were recorded. During the process, the micro-discharge behavior was monitored using a Canon 7D camera with a 100 mm F2.8 Macro lens, filming at 60 frames per second. Once anodic oxidation was completed, the samples were taken out from the solution, washed with deionized water in an ultrasonic bath for 15 minutes to clean the surfaces and then dried in a cool air stream. All the experiments were performed in triplicate to ensure reproducibility of the anodizing process.

Table 1 Solution concentrations and electrical parameters used to obtain the anodic coatings in sodium hypophosphite-based solutions

Solution ID	Solution concentration (g L^{-1})	pH	Conductivity (mS cm^{-1})	Anodizing parameters	Time (s)
P (Ti6Al4V)	$NaH_2PO_2.H_2O$: 10.0 $EDTANa_2$: 7.4 $(CH_3COO)_2Ca$: 1.8 NaOH: 4.0	14	20.1	50 mA cm^{-2} 250 V	600 600
P (Ti c.p)	$NaH_2PO_2.H_2O$: 10 $EDTANa_2$: 7.4 $(CH_3COO)_2Ca$: 1.8 NaOH : 3.0	13.2	17.2	50 mA cm^{-2} 300 V	600 600
P - Si	NaH_2PO_2: 10.0 $Na_2SiO_3.9H_2O$: 5.0	13.7	10.7	50 mA cm^{-2} 400 V	1000 1000

Top views and cross-section views of the coatings were observed using scanning electron microscopy in a JEOL JSM 6490 LV instrument, equipped with energy dispersive X-ray spectroscopy (EDS – 20 kV). For examination of the cross-sections, the samples were mounted in resin and polished to a 0.3 µm alumina finish. The arithmetic average roughness (R_a) of the coating surfaces was assessed using a DektaK XT profilometer (Bruker). The phase compositions of the coatings were evaluated by X-ray diffraction (Empyream PANalytical), using Cu K_α radiation with a scanning range in the 2θ = 10 – 90º. The tribological performance of PEO coatings was evaluated using a ball-on-disc tribometer. The test was carried out under unlubricated condition at ambient atmosphere, with a sliding speed of 60 rpm, a wear track with a radius of 2 mm, a sliding distance of 22 m, a load of 4 N and using a stainless ball AISI 420 of 6 mm diameter as counter-body. The wear rate was calculated by weight loss using a micro balance Mettler Toledo UMX5 with an accuracy of ±

0.1 µg. To calculate the wear rate, the following equation (1) was used:

$$Wear\ Rate = \frac{m}{d\ x\ F} \qquad (1)$$

Where **m** is the weight loss during the test, **d** is the sliding distance and **F** is the normal force applied. All tribological tests were stopped before reaching the substrate.

The electrical properties of the anodic coatings were determined by electrochemical impedance spectroscopy (EIS). EIS measurements were performed using a Potentiostat/Galvanostat IM6e BAS Zahner at open circuit potential (OCP), in potentiostatic mode with a 10 mV of amplitude perturbation and a frequency scan from 10^5 to 0.005 Hz. Measurements were performed at room temperature and potentials were measured with respect to an electrode of Ag/AgCl. The solution used was NaCl 3.5 g L^{-1}. The EIS results were analyzed and fitted using the software Gamry Echem Analyst version 6.11, which fits the experimental results using a least-squares approximation.

1.3. Results

Potential-time and current density-time curves of the anodizing processes are shown in **Figs.** 1 (a,b) and (c,d) respectively. The figures show the behavior characteristic of PEO condition for all anodizing parameters [1]. For the coatings obtained in P solution, a steep increase of the potential is observed up to ~ 150 V; the slope of the curve decreases and the potential continues ascending to a critical potential value and the formation of micro-discharges and evolution of gas is evidenced on the surface of the material. For the coating obtained on Ti c.p, a higher potential is reached at the end of the process (**Fig.** 1a).

The coatings obtained in P-Si solution reveal the same regions in the anodizing curves as well as similar behavior for both materials. However, the potential reached at the end of the process is higher than the coatings obtained in P solution (**Fig.** 1b). For the coatings obtained under potentiostatic conditions (**Fig.** 1c), the initial galvanostatic stage is followed by a rapid decrease in current density until the end of the process. Throughout this process, evolution of gas and micro-discharges with small size were observed with smaller micro-discharges than the galvanostatic process. A similar behavior is evidenced for the coating obtained in P-Si solution (**Fig.** 1d).

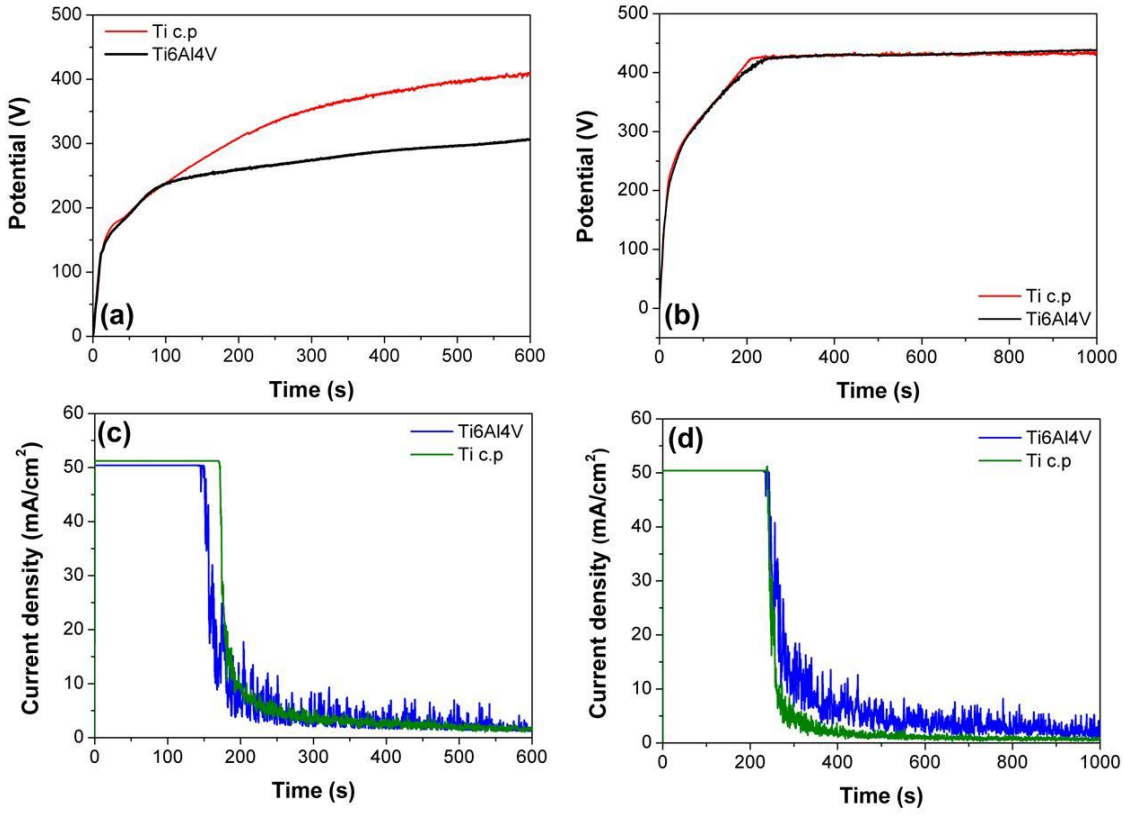

Figure 1. Potential-time curves for the coatings obtained under galvanostatic conditions (50 mA cm^{-2}) in (a) P solution and (b) P-Si solution and current-time responses for the coatings obtained under potentiostatic conditions in (c) P solution and (d) P-Si solution.

The anodic coatings were obtained using the alkaline solutions mentioned in **Table** 1. The solution conductivity changed depending on the chemical species in the anodizing solution. During the plasma electrolytic oxidation process, gas evolution and electric micro-discharges were observed on the substrate surface [25]. The maximum voltage reached during the process was different for the various anodizing solutions, several researchers [109], [110] have reported on the relationship between solution conductivity and breakdown potential. The lower the solution conductivity, the higher the breakdown potential value reached during anodizing, as observed for the anodizing solutions evaluated.

In PEO process, the nature of the anodizing solution has a significant effect on the size and shape of the micro-discharges; **Fig.** 2 shows the appearance of the spark discharges during the anodizing process. For the anodic coatings obtained in the same anodizing solution, the spark discharges show a similar appearance; nevertheless, the spark density changes according to the anodizing conditions. A surface color change is observed, due to the formation of an insulating thin film at initial stages of the PEO process. Then, surface gas evolution is observed on titanium anode at 30 s and after this, the formation of sparks on the surface is observed for all anodizing solutions. Nevertheless, some changes in the sparks appearance are observed according to the solution; at early stages of the process, small sparks distributed over the surface of the material are observed. In the final stages of the process, sparks increase in size with time and their color changes into yellow. In the anodic coatings obtained in P-Si solution, the spark size and density are greater. Concerning the coatings obtained under potentiostatic conditions, the sparks density is reduced notably, especially during the transition from the initial galvanostatic process into the potentiostatic mode, whereas spark sizes do not show significant changes during the process. Micro-discharge

appearance for both materials is similar in the same anodizing solution.

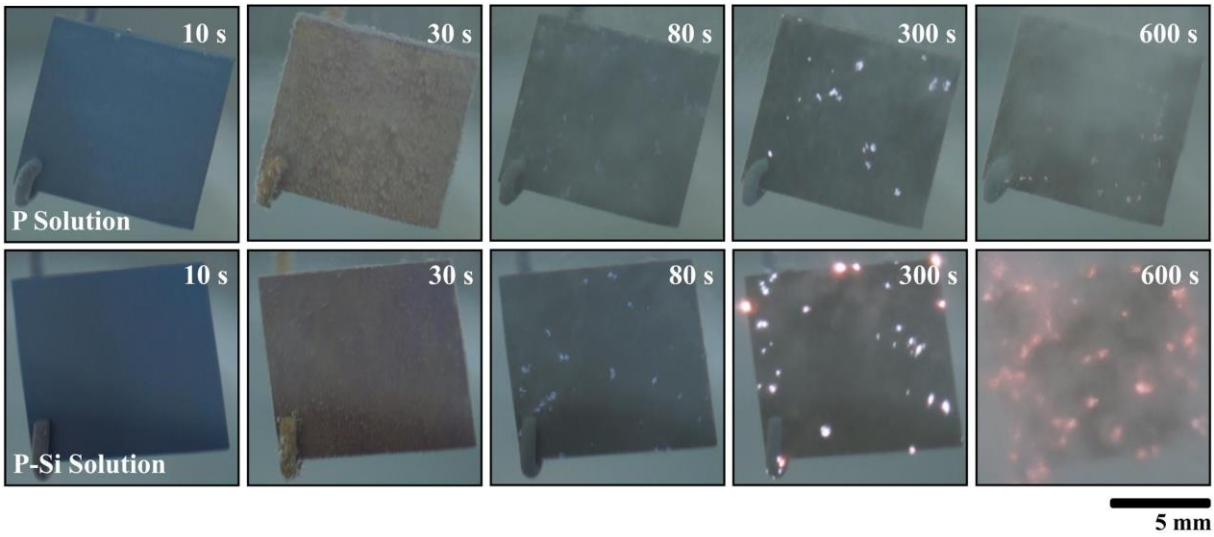

Figure 2. Micro-discharges appearance at various stages of PEO process of the anodic coatings obtained at galvanostatic mode on Ti6Al4V using 50 $mAcm^{-2}$ in P solution and P - Si solution respectively.

The surface morphology of the anodic coatings depends on both the nature of the anodizing solution and the electrical parameters employed to obtain the coatings [77,79]. **Fig.** 3 shows SEM micrographs of the surface morphology of the anodic coatings obtained, evidencing the formation of a porous structure, typical of the PEO process [111]–[113]. The surface morphology of coatings obtained in P solution revealing circular pores for galvanostatic coatings with the formation of volcano-shaped pores only in Ti c.p. As observed in the galvanostatic coatings, circular pores are also formed in potentiostatic coatings; nevertheless, on Ti6Al4V alloy the formation of some coalescent pores is also shown and the pore density, in this case, appears higher than in the other conditions. Concerning the surface morphology of the anodic coatings obtained in P–Si solution. In

general, the addition of silicate to the hypophosphite solution decreases the coatings surface porosity, in particular in the coatings obtained on Ti6Al4V alloy under galvanostatic conditions. Circular pores are evident in the coatings obtained under potentiostatic conditions. As in the P solution, the coating obtained on Ti6Al4V alloy shows the formation of pores with a higher size. These morphological variations generate changes in the roughnesses of the coatings obtained.

Surface roughnesses of the coatings are shown in **Fig.** 4. For the coatings obtained in P solution, the highest roughness occurred in the coating produced on Ti c.p due to the formation of volcano-shaped pores (in agreement with SEM analysis), while the surface roughness for the other anodizing conditions has similar values (**Fig.** 4a). In the coatings obtained in the P - Si solution, a similar topography roughness is evidenced, regardless of the electrical parameters (**Fig.** 4b).

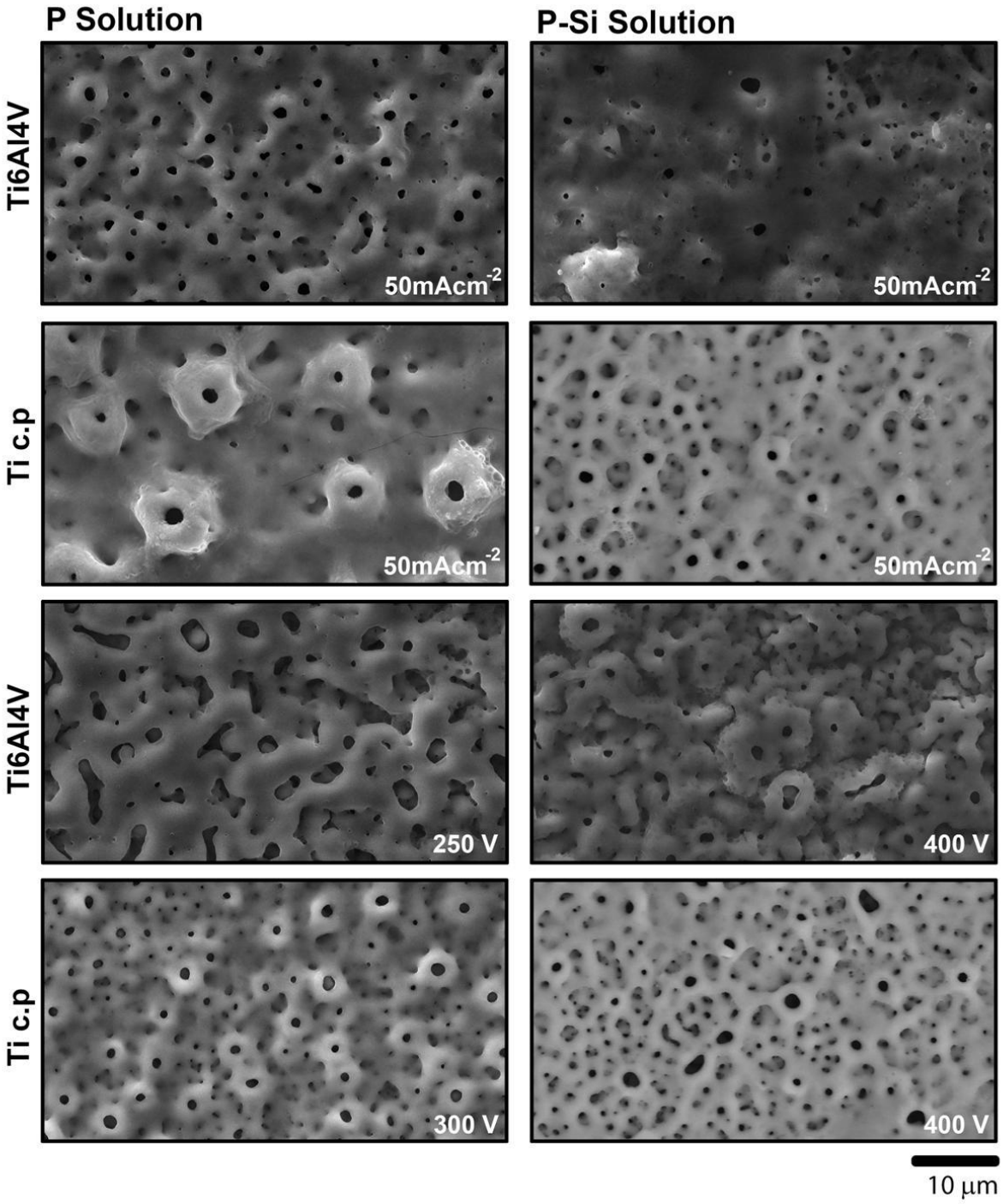

Figure 3. SEM micrographs (SE) of the coatings formed under the conditions listed in Table 1.

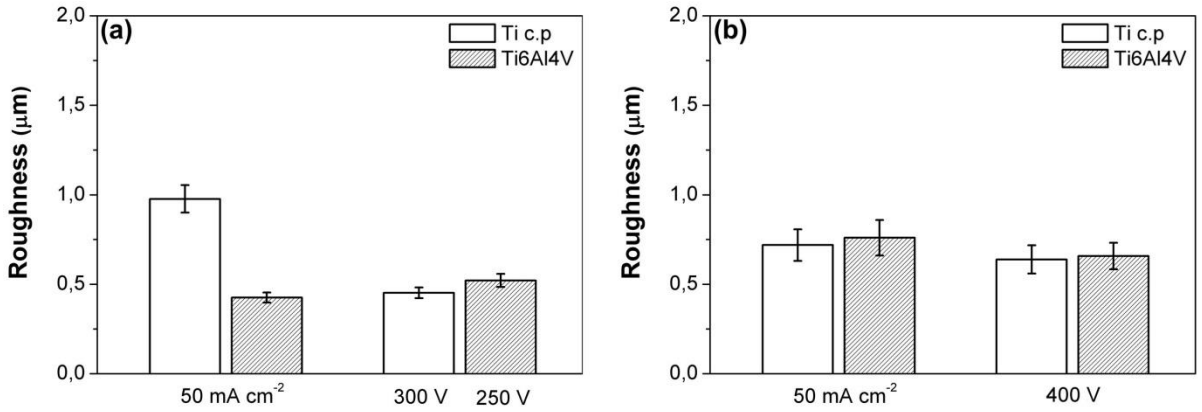

Figure 4. Roughness determined by AFM of the coatings obtained in the following solutions (a) P and (b) P - Si

Fig. 5 shows the cross-sections of the anodic coatings formed and **Fig.** 6 shows the average thickness of all anodic coatings. It is observed that the nature of the anodizing solution and the anodizing parameters have a significant effect on the coating thickness and internal porosity. Coatings obtained under galvanostatic conditions has higher thickness than coatings obtained under potentiostatic conditions in both solutions. In P solution, the coatings obtained on Ti6Al4V alloy have lower thickness than the coatings formed on Ti c.p (**Fig.** 6a). The highest thickness was obtained in the coating obtained in P solution on Ti c.p at 50 mA cm^{-2}. In the P-Si solution, coatings obtained on Ti6Al4V alloy has a higher thickness in comparison with the coatings formed under the same electrical parameters on Ti c.p (**Fig.** 6b). From the cross-section SEM images, the formation of a dual-layer structure is evidenced, due to the existence of temperature gradients between the inner and outer layer, (a dense inner layer and a porous outer layer) and the development of pores and holes associated with dielectric breakdown, accompanying the micro-discharges during the PEO [114]. Crossing pores and big pores concentrated towards the metal-oxide interface are formed in coatings

obtained in P solution. Potentiostatic coatings show a decrease in porosity, especially near the metal-oxide interface. Dense coatings are formed in P–Si solution on Ti6Al4V alloy and some pores and cracks (possibly formed during cross-section polishing) near the metal-oxide interface are observed. On the coatings obtained on Ti c.p, the formation of pores and voids are observed, especially near the coating base.

The composition of the coatings was assessed by EDS and summarized in **Table** 2. Phosphorous, silicon, oxygen, sodium and calcium are incorporated into the coatings from the solution. Moreover, the coatings contain titanium derived from the substrate, vanadium is not evident into the coatings obtained on the Ti6Al4V alloy. The Al signal detected in the EDS analysis could be associated with the aluminum incorporated in the coating or the aluminum in the substrate. In the coatings obtained in P solution, the incorporation of Ca and P is revealed, nevertheless, the concentration of the elements does not exhibit a tendency with the electrical parameters. In the coating formed in P-Si solution, silicon and phosphorous are the main elements incorporated from the solution into the coatings. **Fig.** 7 shows EDS line scan analysis across the coatings formed. Incorporation of elements from the anodizing solutions is observed through the coating and an inhomogeneous distribution of some elements is evident. All the anodic coatings have incorporation of phosphorous, located mainly in the middle of the coating whereas oxygen signal indicates a homogeneous distribution across the film. Calcium is also observed in the outer part of anodic coatings formed in P solution (**Fig.** 7a). Likewise, the anodic coatings obtained in P–Si solution exhibit an enrichment of silicon in the outer part of the coating (**Fig.** 7b).

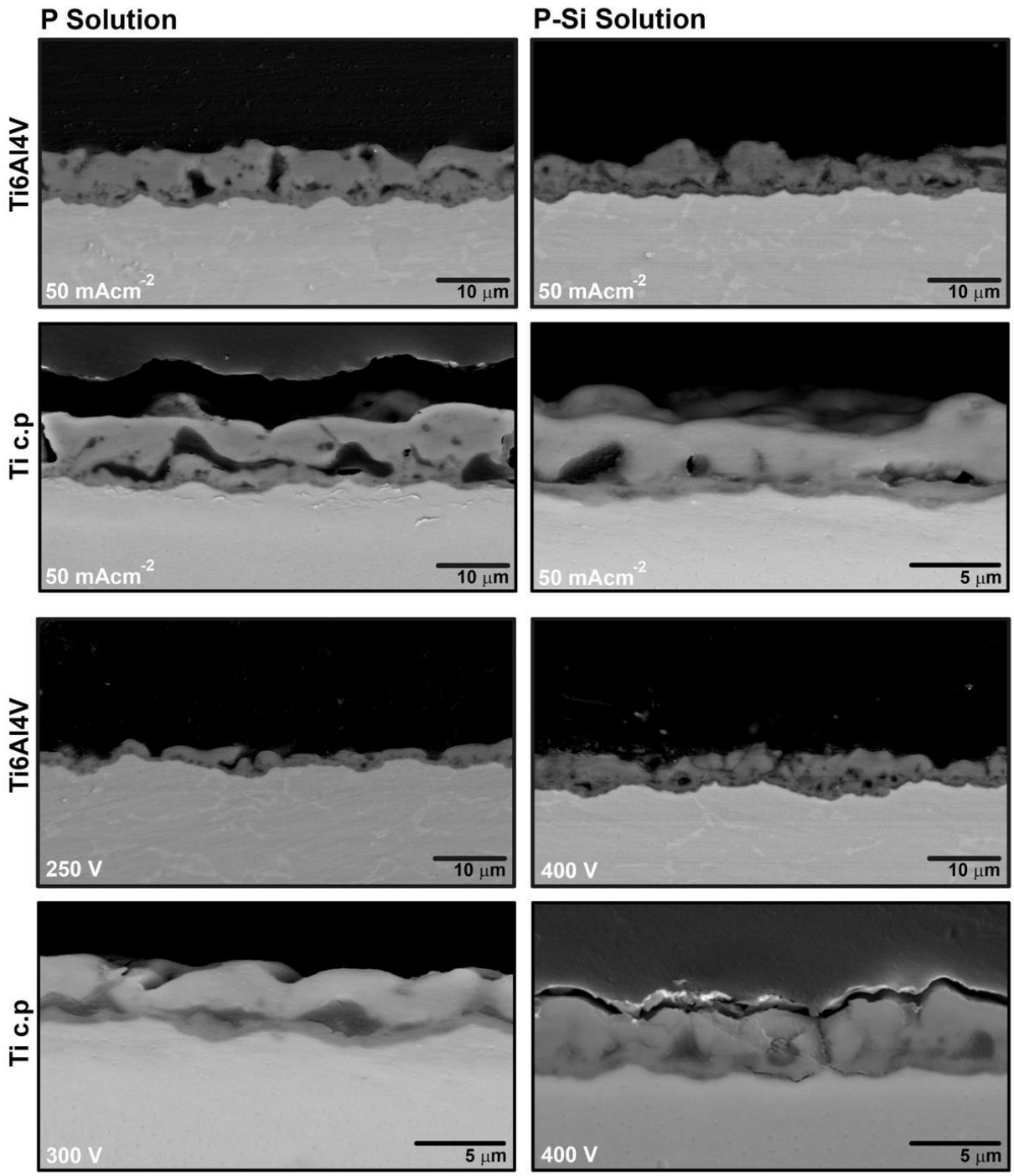

Figure 5. SEM cross-section micrographs (BSE) of the coatings formed under the conditions listed in Table 1

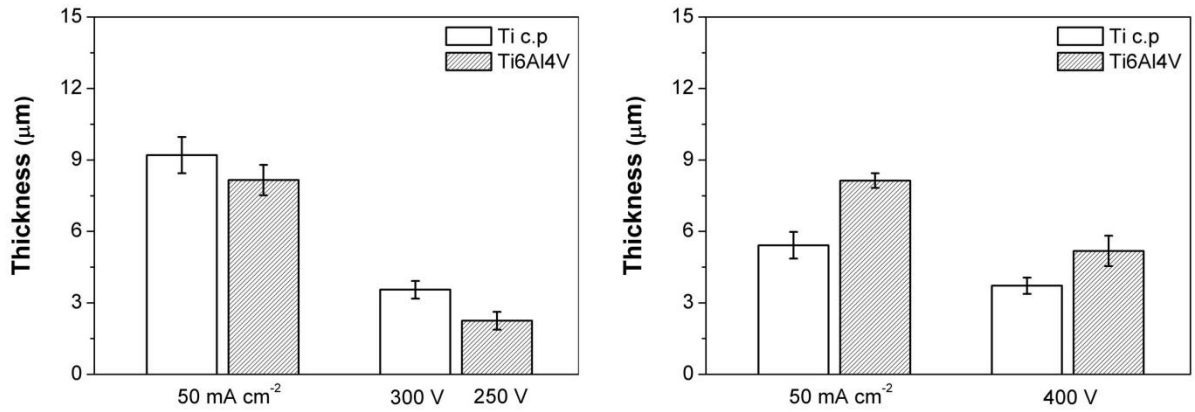

Figure 6. Thickness of the coatings obtained in (a) P solution and (b) P-Si solution

Table 2. Chemical composition of the main components of the anodic coatings obtained

Solution ID	Electrical Parameter	Material	% Al	% O	% Ti	% P	% Si	% Na	% Ca
P	50 mA cm^{-2}	Ti c.p	---	68.58	20.46	7.96	---	0.48	2.52
		Ti6Al4V	1.34	70.67	19.98	5.88	---	0.46	1.66
	300 V	Ti c.p	---	69.70	20.91	6.42	---	0.52	0.90
	250 V	Ti6Al4V	1.43	70.47	19.19	7.07	---	0.66	1.17
P - Si	50 mA cm^{-2}	Ti c.p	---	70.03	21.92	4.85	3.20	0.34	---
		Ti6Al4v	1.43	70.75	13.77	5.15	8.45	0.38	---
	400 V	Ti c.p	---	70.16	20.49	5.18	4.18	0.52	---
		Ti6Al4V	1.42	71.70	14.89	4.60	6.72	0.68	---

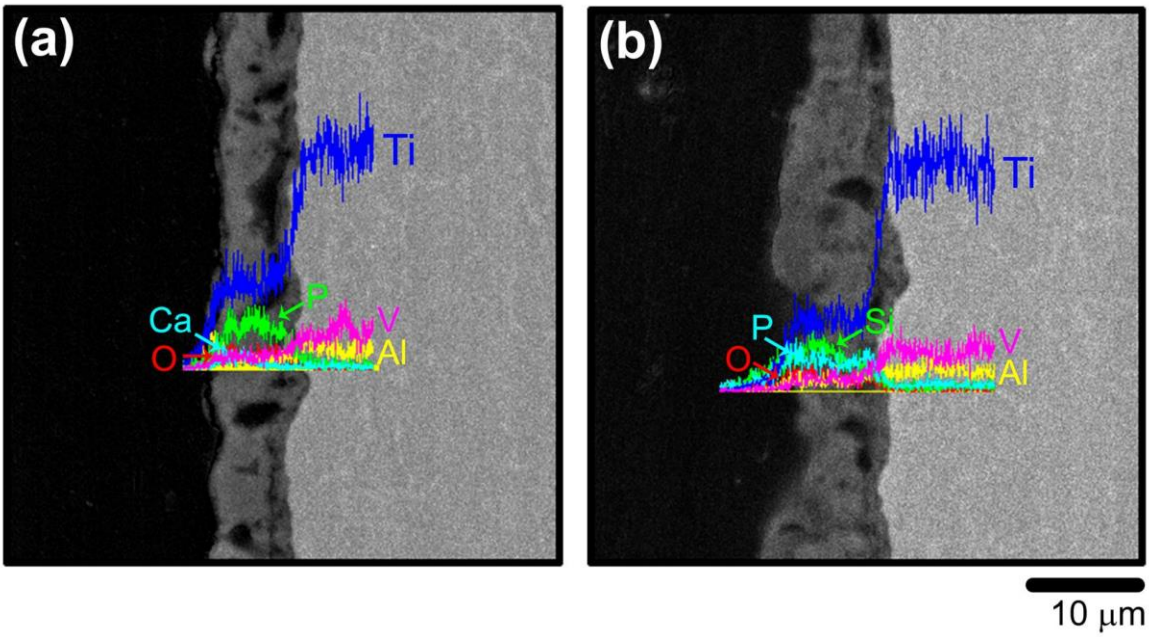

Figure 7. EDS analysis of the cross-section of the coatings obtained on Ti6Al4V alloy in (a) P solution (50 mA cm^{-2}) and (b) P–Si solution (50 mA cm^{-2})

The crystal structure of the anodic coatings assessed by XRD is shown in **Fig.** 8. The XRD patterns show the characteristic peaks of titanium dioxide both in anatase and rutile phases; additionally, peaks of the substrate are also observed. In the coatings obtained on Ti c.p, anatase phase is the main crystalline phase in all the coatings, showing a higher intensity in the coatings obtained under galvanostatic conditions (**Figs.** 8 a,b). In the coatings obtained on Ti6Al4V alloy, anatase is the main crystalline phase and rutile is observed in minor proportion for all conditions (**Fig.** 8 c,d). As in the coatings formed in P solution, galvanostatic coatings peaks has a higher intensity than potentiostatic coatings.

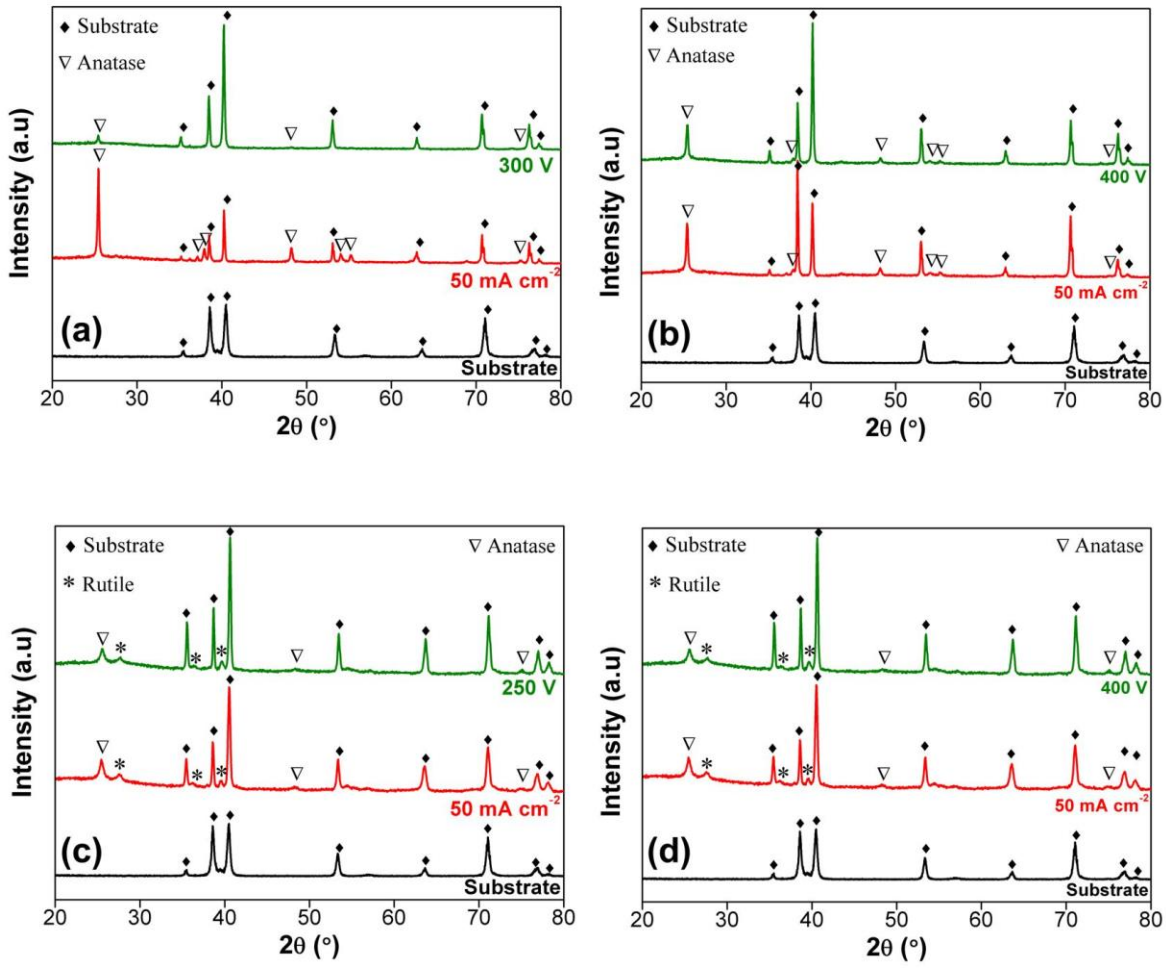

Figure 8. XRD patterns of the anodic coatings obtained on (a,c) Ti c.p and (b,d) Ti6Al4V alloy using the following solutions (a,c) P solution and (b,d) P–Si solution

Fig. 9 shows the friction coefficient obtained for the anodic coatings and the surface appearance of the sample surface and the counter-body after the tribological test. A stable friction coefficient was observed for all coatings after a while that the test had started and only the substrate exhibits some fluctuations. P coatings have a similar friction coefficient behavior both in galvanostatic and potentiostatic conditions (**Fig.** 9a), while P–Si coatings formed at 400 V show the lower friction coefficients values (**Fig.** 9b). The same behavior was

observed for the coatings obtained on Ti c.p; therefore, only the friction coefficient responses on Ti6Al4V alloy are shown. SEM analysis of the wear path after the test, clearly shows, for all coatings, that the wear test does not reach the substrate (**Fig.** 9c) and the counter-body showed wear after the test, as observed in **Fig.** 9d.

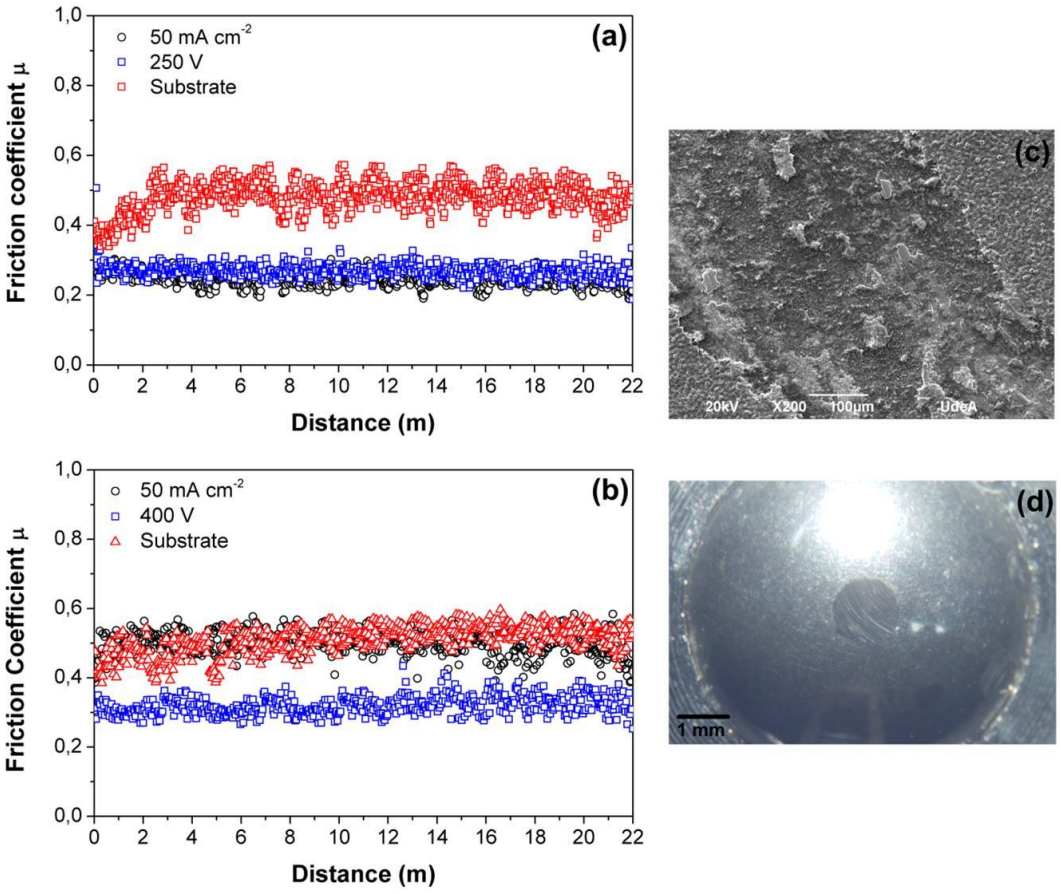

Figure 9. Friction coefficient register of the anodic coatings obtained on Ti6Al4V alloy in (a) P solution, (b) P–Si solution, c) SEM image of the surface of the anodic coating formed on Ti6Al4V alloy in P–Si solution at 50 mA cm^{-2} and d) OM image of the counterbody after the wear test

The wear rate of the anodic coatings is shown in **Fig.** 10. All the anodic coatings improve the wear resistance of the substrate (4.28 x 10^{-9} Kg/N.m for Ti6Al4V alloy and 18.7 x 10^{-9} Kg/N.m for Ti c.p), with the potentiostatic coatings showing a better tribological performance than the galvanostatic coatings. The lowest wear rates were measured in the anodic coatings formed at 250 V in P solution and 400 V in P–Si solution on Ti6Al4V alloy. The negative value of wear rate for the P coating formed at 250 V on Ti6Al4V alloy (see **Fig.** 11f) is due to adhesion of counter-body debris to the coating surface, which increases the weight of the sample. As the anodic coatings obtained in P solution, the P–Si potentiostatic coatings exhibit a better tribological performance than galvanostatic coatings (see **Fig.** 10b), especially the coatings obtained on Ti6Al4V alloy. In general, the coatings obtained on Ti6Al4V alloy have lower wear rates than the coatings obtained on Ti c.p.

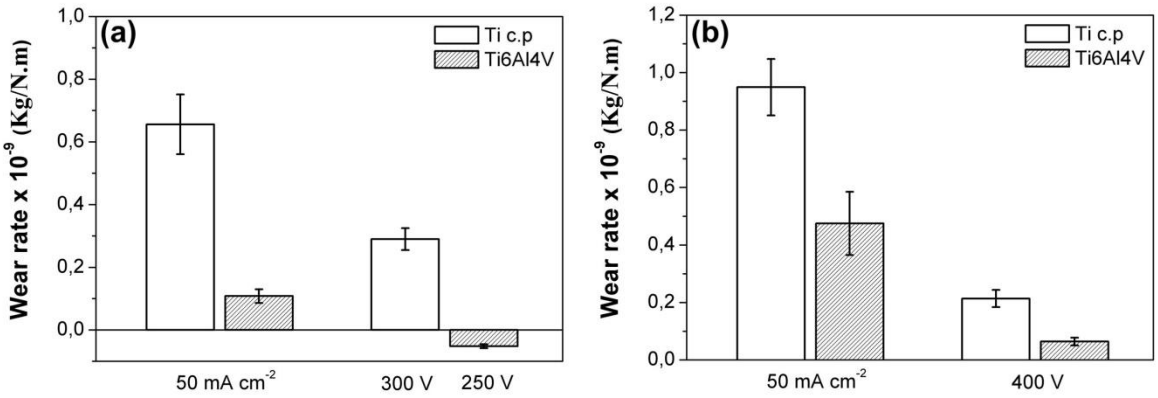

Figure 10. Wear rate of the coatings obtained in (a) P solution and (b) P-Si solution.

Results of SEM analysis for some coatings after wear tests are shown in **Fig.** 11. The EDS analysis (**Fig.** 11e) on the wear path of the coating formed at 400 V in P - Si solution on Ti c.p, confirmed the presence of debris from the counter-body on the surface of the anodic coating. In the anodic coating formed at 50 mA cm^{-2} in P solution on Ti c.p (see **Fig.** 11 a,b), adhesion and mainly spalling are the wear mechanisms observed. Nonetheless, in the anodic coating obtained at 400 V in P-Si solution on Ti c.p, adhesion is the main wear mechanism; due to the anodic coating which does not show a significant surface damage after the wear test, as shown in **Fig.** 11 c,d; this result evidences different tribological behavior between galvanostatic and potentiostatic coatings. For the coatings formed on Ti6Al4V alloy, a similar behavior is observed; the galvanostatic coatings show spalling and adhesion as the wear mechanisms (**Fig.** 11 h,i) and the potentiostatic coatings show adhesion as the main wear mechanism (**Fig.** 11 f,g).

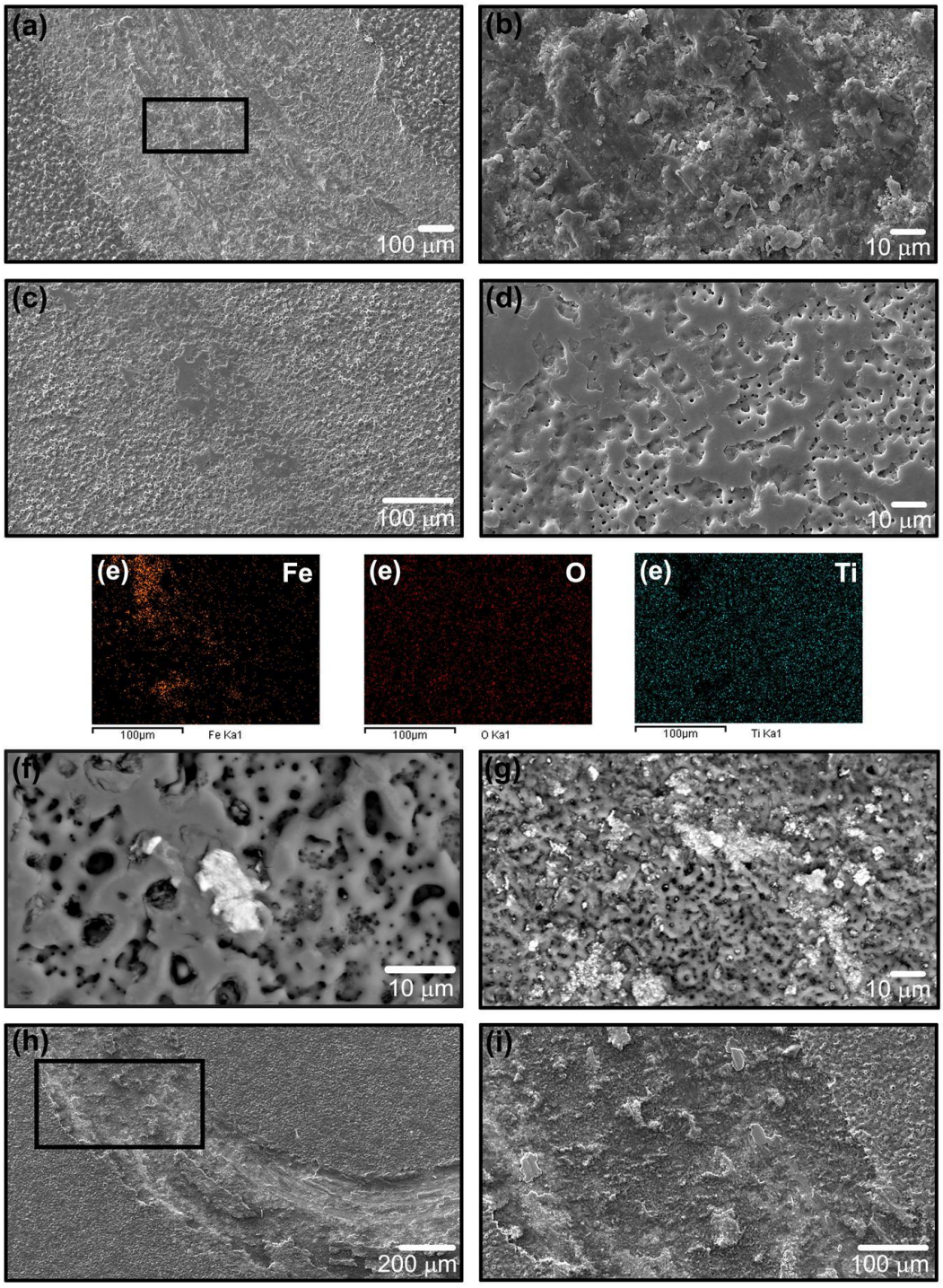

Figure 11. SEM micrographs of wear paths of the coatings obtained in (a,b) P solution on Ti c.p (50 mA cm^{-2}), (c,d) P - Si solution on Ti c.p (400 V), (d) elemental mapping of the wear path of the coating obtained in P-Si solution (Fig. 11c), (f) P solution on Ti6Al4V alloy (250 V), (g) P–Si solution on Ti6Al4V alloy (400 V) and (h,i) P solution on Ti6Al4V alloy (50 mA cm^{-2})

Fig. 12 shows Bode diagrams of the anodic coatings formed in the solutions mentioned in **Table** 1. The diagrams show two capacitive loops, indicating the formation of a duplex structure in the anodic coatings (a dense inner layer and a porous outer layer), as has been mentioned by other authors [46], [104], [114], [115]. According to literature reports, the first capacitive loop corresponds to the porous outer layer and the second one corresponds to both the dense inner layer and the relaxation of the electrical double layer [116]. The relaxation processes of both the inner layer and the electrical double layer have similar values of time constant so that only one capacitive loop at low frequencies appears in the impedance diagram. **Figs.** 12(a,c) shows the impedance spectra for the coatings formed in P solution. The potentiostatic coatings exhibit a higher impedance module than the galvanostatic coatings as shown in the Bode diagram. Moreover, the time constant of the porous layer (high frequencies) shows variations in its characteristic frequency, indicating changes in the electric properties of the coating obtained on Ti6Al4V alloy in P solution. **Fig.** 12(c,d) shows the impedance spectra of the coatings formed in P–Si solution. Like the coatings formed in P solution, the impedance module is higher for the potentiostatic coatings. Time constants in both the porous layer and the inner dense layer do not show changes in the characteristic frequency as a result of variations in anodizing parameters. Finally, the highest impedance modules are observed in the coatings formed in the P–Si solution on Ti6Al4V alloy and the characteristic frequency of the porous layer is greater than in other solutions.

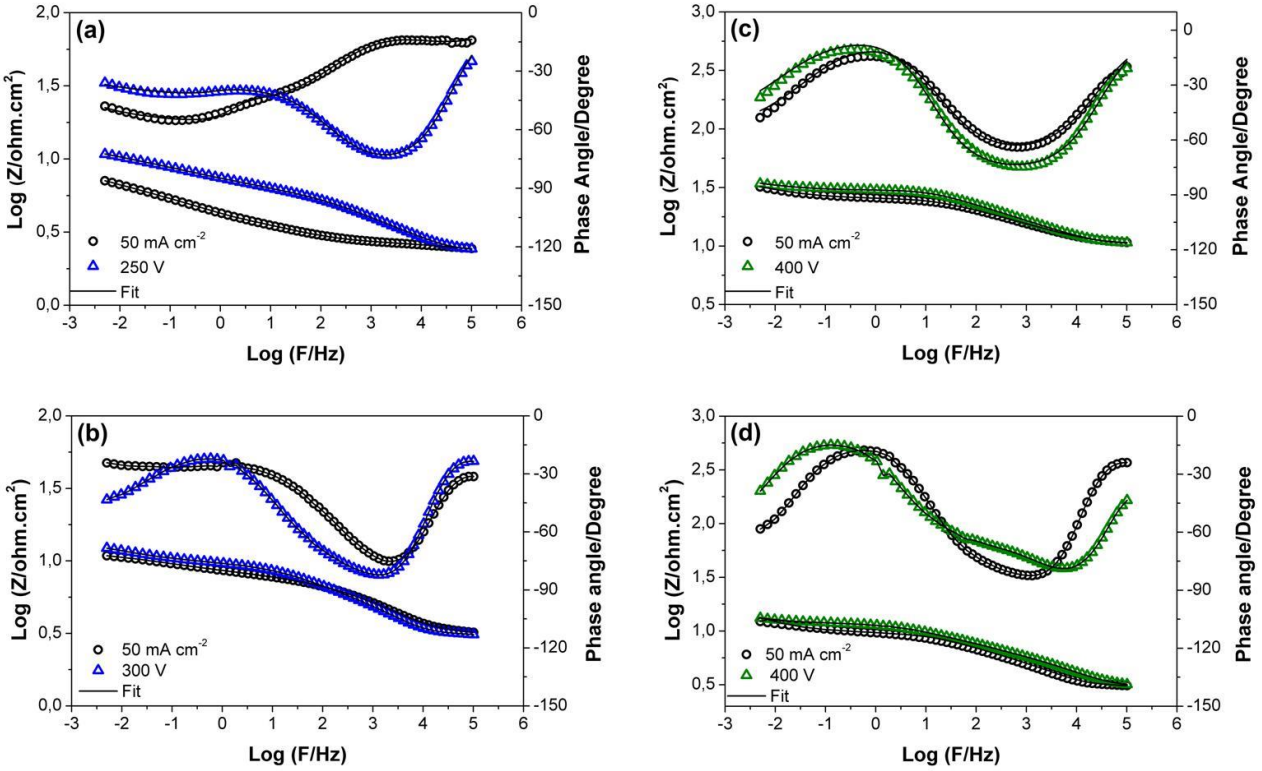

Figure 12. Bode spectra for the coatings obtained on Ti6Al4V in (a) P solution and (b) P-Si solution and Bode spectra for the coatings obtained on Ti c.p in (c) P solution and (d) P-Si solution

Impedance data were analyzed using different equivalent circuits. The circuit shown in **Fig.** 13 corresponds to the better fit of the experimental data and gives an adequate physical meaning of the electrical parameters of the coatings. The cascade circuit shown in **Fig.** 13 allows to take into account the parallel combination of the electric double layer capacitance and the charge transfer resistance, because the inner layer is not completely homogeneous and has nanometric pores that allow contact between the Ti substrate and the solution. The capacitances of both the inner layer and the porous layer present in the coating were related to constant phase elements (CPE), which are associated with heterogeneities in the coating. In the equivalent circuit shown in **Fig.** 13, R_p and Q_p represent the resistance and the

pseudo-capacitance of the porous layer, R_b and Q_b represent the resistance and the pseudo-capacitance of the inner layer and R_{tc} and C_{dc} refer to the charge transfer resistance and the capacitance of the electrical double layer. **Fig.** 12 shows the simulations for the anodic films obtained at mode galvanostatic and potentiostatic (solid line). It is observed that there is a high correlation between experimental and theoretical values according to the model proposed.

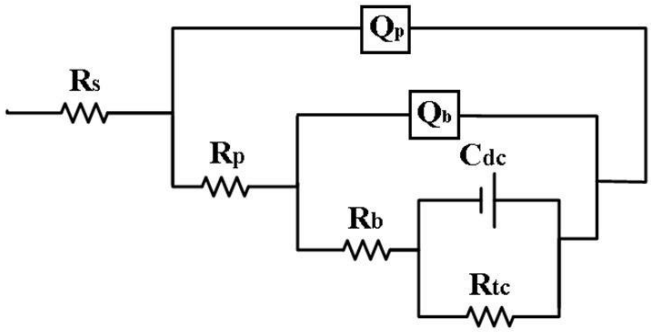

Figure 13. Equivalent circuit model used for the adjustment of impedance data of the anodic films obtained. Solution resistance (R_s), porous resistance layer (R_p), Inner resistance layer (R_b), porous layer pseudo capacitance (Q_p), inner layer pseudo capacitance (Q_b), electrical double layer capacitance (C_{dc}) and charge transfer resistance (R_{tc}).

The values of effective capacitance were calculated from the parameters of the constant phase elements in accordance to the following equations [68]:

$$C_{eff} = Q^{1/n} Re^{(1-n)/n} \quad \text{Surface distribution} \quad (1)$$

$$C_{eff} = Q^{1/n} Rf^{(1-n)/n} \quad \text{Normal distribution} \quad (2)$$

The surface distribution (**Equation** 1) was used to calculate the effective capacitance of the inner layer. The surface distribution is used to calculate the effective capacitance in the case of which admittance is influenced by the electrode surface; this is the case of the inner layer due to the roughness generated in the interface metal – oxide. Q and n are the parameters of CPE and R_e is the resistance in series with the constant phase element. In this case, R_e corresponds in the equivalent circuit to R_p. Furthermore, the normal distribution equation (**Equation** 2) was used to calculate the effective capacitance of the porous layer due to the heterogeneous distribution of the coating and the porosity. In this case, Q and n are the parameters of CPE and R_f is the resistance in parallel with CPE, which corresponds in the equivalent circuit to R_p. The values of the electrical parameters provided by the equivalent circuit for the anodic films obtained are shown in **Table** 3.

Table 3. Electrical parameters of the coatings obtained by the fitting of the EIS experimental results

Solution ID	Electrical parameter	Material	Electrical parameter provided by the EIS fitting									
			R_p (KΩ cm^2)	R_b (MΩ cm^2)	R_{tc} (MΩ cm^2)	C_p (μF cm^{-2})	n_b	C_b (μF cm^{-2})	n_p	C_{dc} (μF cm^{-2})	$Z_{f=0.005}$ (KΩ cm^2)	Goodness of fit x 10^{-3}
P	50 mA cm^{-2}	Ti c.p	18.61	3.984	29.01	0.065	0.52	0.041	0.91	1.50	430.29	3.19
		Ti6Al4V	0.36	0.01	1.21	0.43	0.55	1.30	0.60	8.12	22.33	0.10
	300 V	Ti c.p	31.94	7.787	239.20	0.056	0.63	0.010	0.97	4.60	739.54	4.46
	250 V	Ti6Al4V	42.32	3.370	19.42	0.051	0.89	0.075	0.46	1.21	367.43	0.20
P - Si	50 mA cm^{-2}	Ti c.p	100.36	0.19	2.12	0.050	0.63	0.215	0.92	18.45	612.79	3.76
		Ti6Al4V	5.88 x 10^5	9.34 x 10^5	4.71	4.73 x 10^{-8}	0.77	1.49 x 10^{-5}	0.61	12.34	2.74 x 10^5	1.22
	400 V	Ti c.p	197.35	0.95	88.25	0.020	0.64	0.029	0.95	4.45	948.66	0.81
		Ti6Al4V	1.72 x 10^6	9.17 x 10^7	105.05	5.26 x 10^{-7}	0.87	1.05 x 10^{-5}	0.60	1.52	7.89 x 10^5	1.25

1.4. Discussion

Real-time images of the PEO process evidenced that the chemical composition of the anodizing solution affects the appearance of micro-discharges (**Fig.** 2), as well as the surface morphology and the internal porous structure during the coating formation (**Figs.** 3 and 5). Larger micro-discharges are formed in P-Si solution in the final steps of the process; several researches have reported the formation of large and intense sparks by using metasilicate in the anodizing solution [18], [90], [96]. Based on Optical Emission Spectroscopy data [117], temperature analyses during spark discharges show the formation of two micro-regions during sparking: A hot core with temperatures up to 8000 to 10000 K and a relatively cold bubble (2000 K) separating the core from the solution. The high temperature generated during the process leads the formation of crystalline phases into the coatings. In the present study, addition of metasilicate in the P-Si anodizing solution does not generate the formation of SiO_2 phases as has been reported by other researchers [18], [89], [96]. In the XRD spectra (**Fig.** 8), the increase in the intensity of the characteristic bands of anatase or rutile in some coatings is related to the increase in coating thickness as evidenced in cross-section SEM images. The EDS analysis shows the incorporation of some elements from the anodizing solution in the anodic coatings (**Fig.** 7); the phosphorus found mainly in the inner parts of the coatings is the result of phosphate anions being incorporated through the discharge channels under a high electric field [32]. In addition, silicon species are also observed on the surface of the coatings formed in P-Si solution and calcium species are evidenced in the coatings obtained in P solution as reported in the literature [118], [119]. EDS analysis does not clearly show incorporation of aluminum or vanadium in the coating; according to literature reports, high solubility of vanadium oxides or vanadium compounds is the cause of low incorporation

of vanadium into the film and the low concentration of aluminum is not conducive to formation of aluminum oxides [61], [120].

Porosity in the anodic coatings formed in P solution varied with anodizing conditions, both at the surface (**Fig.** 3) and inside of the anodic film (**Fig.** 5), showing lower porosity coatings obtained under potentiostatic conditions. The later can be explained since the potentiostatic mode allows controlling the size and density of micro-discharges, especially at low potentials. Analysis by EIS evidenced structural changes in the coatings due to changes in the electrical parameters of the coating layers (**Table** 3). In all P coatings, the overall resistance depends mainly on the dense inner layer given that the resistance of this layer (R_b) is greater than the porous layer resistance (R_p), in agreement with other researchers [1], [114], [121]. For the galvanostatic P coatings, the coating obtained on Ti c.p exhibit a better corrosion resistance than the coating obtained on Ti6Al4V alloy. **Table** 3 shows that R_p is higher for the coating obtained in Ti c.p due to the formation of a thicker coating (**Fig.** 5), consequently causing the decrease of C_p in comparison with the coating obtained on Ti6Al4V alloy. Regarding the inner layer, R_b is higher for the coating obtained on Ti c.p, indicating the formation of a thicker and denser inner layer (**Fig.** 5). Consequently, C_b rises for the coating obtained on Ti6Al4V alloy. Therefore, coatings obtained on Ti c.p exhibit a better corrosion resistance since the resistance depends on mainly of the inner layer. The charge transfer resistance represents the inner layer blocking electron transfer. For that reason, R_{tc} and C_{dc} show a similar behavior than R_b and C_b. The electrical parameters of the potentiostatic P coatings show a similar behavior; nevertheless, R_p, R_b and R_{tc} are greater due to the formation of a dense coating. The coatings obtained on Ti c.p appear to be similar according

to n_p parameter of CPE, which refers to the uniformity of porosity through the coating (see **Table** 3). On the other hand, n_b refers to the roughness of the metal-oxide interface; n_b values in **Table** 3, indicate that this interface is smoother for potentiostatic coatings on Ti6Al4V alloy, due to the smaller micro-discharges occurring in this anodizing condition [116]. These internal changes might influence the mechanical and tribological properties of the coating. Potentiostatic coatings show a better tribological performance due to the formation of denser coatings (**Fig.** 5) and the wear mechanism of these coatings is mainly adhesion, which is less severe than the wear mechanisms showed by the galvanostatic coatings. Besides, R_b is greater for the coatings obtained under potentiostatic conditions, indicating a dense inner layer and consequently improving coating adhesion to the substrate. Similar results have been reported, where a reduction in porosity in the metal-oxide interface improved the wear performance [122]. Additionally, the literature suggests that the greater the coating thickness, the weaker the strength of adhesion of the coating to the substrate [1]. The better wear performance of the coatings obtained on Ti6Al4V alloy is due to the formation of rutile into the coating. It has been reported that the good adherence of the rutile phase on titanium improved wear resistance and reduces the friction coefficient. Rutile-like oxide phases exhibited low shear strength due to the particular crystallographic shear plane and behaved like a solid lubricant [23]. The similar friction coefficients observed for all coatings are related to little variation on surface roughness. Besides, coatings obtained on phosphates solutions exhibit low friction coefficient values as has been reported [18], [19].

In the coatings formed in P-Si solution, high electrical resistances of these coatings indicate that these coatings exhibit higher corrosion resistances (**Table** 3), especially on Ti6Al4V alloy, as already reported by other authors [46], [90]. These coatings show differences in electrical parameters for the inner and the outer layer, more significant than the coatings obtained in P solutions. In this solution, the better corrosion resistance is evidenced in the coatings obtained on Ti6Al4V alloy due to the formation of coatings with low porosity (**Fig**. 5), therefore R_b and R_p are higher and consequently, C_b and C_p decreases. As in P coatings, the overall resistance of the coating depends mainly on the inner layer. Correspondingly, the highest impedance module is obtained in the coating formed at 400 V (**Table** 3) on Ti6Al4V alloy. As in the coatings formed in P solution, the heterogeneity of the porous layer is similar for the two materials evaluated and the interface metal-oxide is smoother for the potentiostatic coating obtained on Ti6Al4V alloy according to parameters of CPE (n_b, n_p). Likewise, the potentiostatic coatings show a better tribological performance, especially the coating formed on Ti6Al4V alloy due to the formation of rutile as a second crystalline phase in the coating (**Fig.** 10), which also exhibits the lower friction coefficient. As the coatings obtained in P solution, the wear mechanism of the potentiostatic coatings is less severe than the wear mechanisms of the galvanostatic coatings.

In the chapter, it has been found that anodic coatings obtained in P and P-Si solutions exhibit good tribological performance, especially anodic coatings formed in potentiostatic mode. Besides, potentiostatic coatings showed a better corrosion resistance due to the increase of the resistance of the inner layer (Rb), indicating the formation of a denser and thicker inner layer. This is due to the size and the lifetime of the micro-discharges in

potentiostatic mode, which are smaller than in galvanostatic mode. Xuelin Zhang et al [116] analyzed by EIS the grow of anodic coatings with time, finding that a potential increase is not beneficial for the growth of the inner layer due to the increase in both the size of the micro-discharges and the porosity. Large discharges contribute to the formation of some deep pores inside the coating and also decreases the smoothness of the coating-substrate interface. These results indicate that density, intensity and lifetime of sparks can be related to surface morphology of the coating, particularly to the porosity. Moreover, the variation of electrical parameters in the coating by the fitting of the EIS experimental results, evidence internal structural changes generated in the coating by changing the anodizing conditions.

1.5. Conclusions

Anodic coatings have been obtained in alkaline solutions by plasma electrolytic oxidation. The effect of different additives was studied seeking to improve the wear resistance of the titanium alloy. The conclusions of the work are as follows:

1. Plasma electrolytic oxidation carried out in different alkaline solutions indicate that both shape and size of the spark discharges together with the chemical composition of the anodizing solution have a significant influence on the surface morphology of the coatings.

2. Anodic coatings obtained in P-Si solution had lower porosity respect to the other anodic coatings obtained and, consequently, higher corrosion resistance.

3. Anatase crystalline phase was the main structure formed whilst rutile phase was detected in minor proportion only in the coatings obtained on Ti6Al4V alloy. Conversely, in the coatings obtained on Ti c.p, anatase phase is the only crystalline phase.

4. Potentiostatic coatings showed a better tribological performance than coatings grown under galvanostatic control; it is especially true for the anodic coatings obtained on Ti6Al4V alloy in P (250 V) and P-Si (400 V) solutions, which showed the lowest wear rate values.

5. EIS analysis allowed characterization of the electrical properties of the anodic coatings. These electrical parameters were found to be closely related to changes in the coating internal structure, which can be achieved by variation of the anodizing conditions.

2. Chapter 2

Anodic coatings obtained in sodium aluminate-based solutions

Abstract: PEO coatings have been obtained using an aluminate-based solution with additions of NaH_2PO_2 and Na_2SiO_3. The effect of the solution composition and the electrical parameters on the corrosion and wear performance were studied. The chemical composition of the coatings is mainly Al_2O_3 and Al_2TiO_5. Nevertheless, in the coatings obtained under galvanostatic conditions, the formation of other crystalline phases due to the additives in the solution was evidenced; $Na_4Ti_5O_{12}$ phase was observed into the coatings obtained in the solutions with the addition of NaH_2PO_2 whereas mullite was evidenced in the coating obtained on Ti6Al4V alloy with the addition of Na_2SiO_3. The formation of mullite into the alumina matrix improves significantly the tribological behavior of the coatings obtained

under galvanostatic conditions as evidenced in the wear tests. The coatings obtained under potentiostatic condition exhibit better tribological properties due to the formation of a dense coating. Coatings obtained with Na_2SiO_3 in the solution exhibited a better corrosion resistance due to the decrease of the coating porosity. The morphology changes of the coatings are related to the electrical parameters calculated by the fitting of the EIS experimental results.

Keywords: PEO coatings, titanium alloy, wear resistance, mullite – alumina coatings**,** corrosion resistance, property.

2.1. Introduction

Alkaline solutions containing aluminates have been often used to form hard oxides containing Al_2O_3 and Al_2TiO_5 phases. These crystalline phases promote the formation of coatings with good wear performance as well as good adhesion [18], [20], [23], [25], [30], [33].. The Al_2TiO_5 phase is formed by a eutectic reaction between Al_2O_3 and TiO_2 and the ratio of phases into the coating depends on the anodizing parameters, especially of the anodizing solution. Moreover, the distribution of the crystalline phases in the coating affects properties such as adhesion, hardness and the mechanical and tribological behavior [22], [61], [70], [94], [122]–[126]. In coatings formed in aluminate-based solutions, the formation of a secondary crystalline phase in the alumina matrix increases the fracture toughness of the coating and thereby provides an improvement of the wear resistance; for example, the formation of aluminum titanate improves the adhesion of the coating as well as the wear resistance [17], [25], [77], [127]–[129]. Another crystalline phase that improves the properties of the alumina matrix is the mullite due to its relatively lower specific weight. The

combination of alumina and mullite in the coating at an optimal ratio might increase the wear resistance, in addition this crystalline phase has high thermal stability and acts as a thermal barrier. Many studies of PEO on aluminum that form alumina - mullite coatings have demonstrated their good wear resistance and thermal properties as well as their good corrosion resistance [75], [76], [130], [131]. Besides the chemical composition of the coatings, that has an important effect on the coating properties, the control of the morphological characteristics such as porosity, roughness, morphology distribution, pore diameter and homogeneity of the coating thickness, has an important effect on the coating properties, especially the porosity. The decrease in the porosity increases the hardness and therefore the tribological behavior of the coating. A smooth surface allows reducing the friction coefficient in wear applications, which is very important to obtain a good wear performance. On the other hand, the formation of a dense coating, especially near the coating base, improves the adhesion of the coating and the corrosion resistance. These morphological characteristics depend on the electrical parameters (current density, potential, time) of the anodizing process, indicating that a good selection of the process parameters allows controlling the characteristics of the coating, improving the mechanical and tribological properties [1], [13], [36], [78].

The formation of wear resistant coatings on titanium alloys using aluminate-based solutions has been studied widely. However, the formation of secondary phases in the alumina matrix like other aluminate phases, mullite and aluminum oxides, combined with other elements for wear demanding applications, has not been explored extensively [32], [61], [94], [96]. In aluminum, the formation of these phases by PEO anodizing has been widely explored with good results; nonetheless, titanium exhibits a strength-density ratio higher than

aluminum, which could be important for many applications [1], [28]. In this chapter, anodic coatings were obtained in aluminate-based solutions containing alumina - titanate and alumina - mullite as the main chemical composition. The influence of the solution composition and the electrochemical conditions on the coatings properties was assessed. The coatings obtained under potentiostatic condition showed a better wear resistance despite being coatings relatively thin. Potentiostatic control allows the formation of coatings with low porosity, decreasing the wear rate and improving the corrosion resistance of the coatings.

2.2. Experimental

The anodizing procedure and the characterization of the coatings were described in Chapter 1. Aluminate-based solutions with various additions, which are listed in **Table** 4, were employed to form the coatings. The NaH_2PO_2 additions to the aluminate-based solutions were made to promote the incorporation of phosphorus species into the coatings, which has been reported to reduce the porosity and the friction coefficient of the coatings [18], [22], [31]; and to enhance their wear resistance [78]. The Na_2SiO_3 addition was selected to incorporate silicon species which has been reported to improve the corrosion protection and lead to the formation of mullite within the coatings [31], [78], [132]. The galvanostatic anodizing was carried out at 50 mA cm^{-2} for 1000 s; the potential was recorded during the process. The potentiostatic mode employed a first period of anodizing at galvanostatic mode until the potential reached 400 V and a second period in which the potential was held at 400 V during 1000 s; the current density was recorded during the process.

Table 4. Solution concentrations and electrical parameters used to obtain the anodic coatings in sodium aluminate-based solutions

Solution ID	Solution composition (g L^{-1})	pH	Conductivity (mS cm^{-1})	Anodizing condition	Time (s)
Al – P	$NaAlO_2$: 12.24 $NaH_2PO_2.H_2O$: 3	13.34	13.60	50 mA cm^{-2} 400 V	1000
Al - Si	$NaAlO_2$: 12.24 $Na_2SiO_3.9H_2O$: 1	13.74	12.32	50 mA cm^{-2} 400 V	1000

The friction coefficients and wear-resistances of the coatings were determined by dry sliding tests using a ball-on-disc tribometer. The tests were carried out under unlubricated conditions in the ambient atmosphere (25 ºC and 50 % Humidity) with a rotation rate of 60 rpm, a wear track of 6 mm of diameter and a sliding distance of 200 m; a SUJ2 steel ball of 6 mm diameter was used as a counterbody, with an applied load of 5 N. The wear rate was determined from the weight loss of the sample as was described in chapter 1.

2.3. Results

The potential-time and current density-time curves for the galvanostatic and potentiostatic anodizing processes are shown in **Figs.** 14 (a,b) and (c,d) respectively. Each figure compares the results for the two materials in the solutions given in **Table** 4. The curves are of the typical forms for anodizing under the respective two modes [133], [134]. In **Fig.** 14 a, a steep increase of the potential is observed up to ~ 200 V. The slope of the curve then decreases until reaching a stable potential. Both materials have the same behavior in this

solution. In **Fig.** 14 b, a steep increase of the potential is observed up to ~ 200 V. The slope of the curve then decrease, especially for the coating obtained on Ti c.p, which coincides with abundant gas evolution and the formation of small micro-discharges on the sample surface. Further a stable potential is reached in the Ti6Al4V alloy sample whilst it is not observed on the Ti c.p sample. For the coatings obtained under potentiostatic conditions (**Figs.** 14 c,d), the current density in the potentiostatic period initially decreased rapidly, followed by a final region of slow change. Throughout the potentiostatic period, both evolution of gas and micro-discharges were observed on the sample surface, these micro-discharges which were smaller than those formed in the galvanostatic process. The time necessary to reach the potentiostatic control is influenced by both the solution and the substrate. In Al-P solution, both materials show a similar behavior (**Fig.** 14 c), whereas in Al-Si solution. The process on Ti c.p takes more time to reach the definite potential, which is accompanied by an abundant evolution of gas (**Fig.** 14 d).

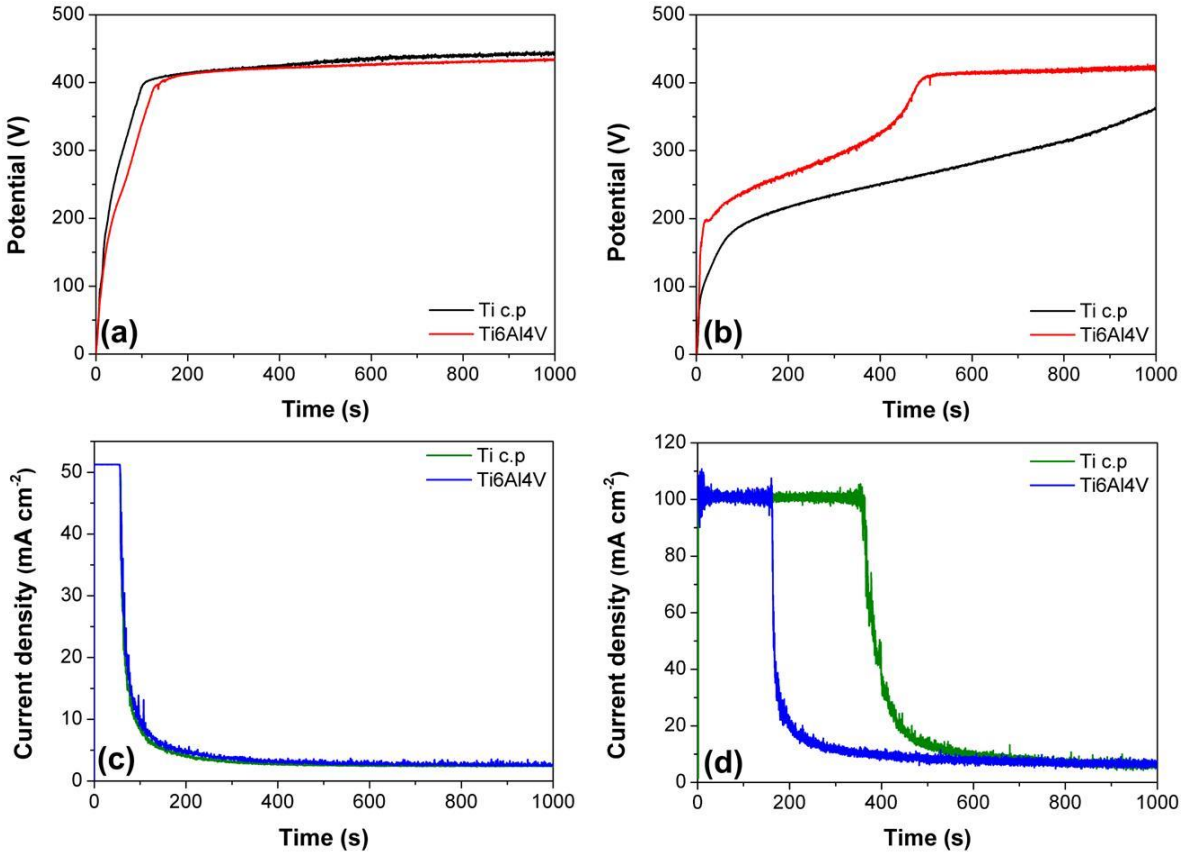

Figure 14. Potential-time curves for the coatings obtained applying 50 mA cm^{-2} in (a) Al-P solution and (b) Al-Si solution and current-time responses for the coatings obtained applying 400 V in (c) Al-P solution and (d) Al-Si solution. The anodizing solution temperature is 20 ºC.

Fig. 15 shows the micro-discharge appearance for both galvanostatic and potentiostatic processes at different times for the Ti6Al4V alloy. In the galvanostatic mode, the micro-discharge appearance is similar for all conditions. Nevertheless, in the first stages of the process, differences in size of the micro-discharges are evidenced and they are related with the potential-time response (**Fig**. 14 a,b). For the coatings formed in the Al - P solution, the micro-discharge size is higher during the initial first stages as the highest potential value is reached in a shorter time (**Fig.** 14 a). Comparing the micro-discharge appearance for both

modes evidence that the size of the micro-discharges is largely different in both processes after 200 s. In the galvanostatic mode, the micro-discharges increase in size until the end of the process (**Fig.** 15 a). In contrast, the size of the small micro-discharges formed on the specimen surface in the potentiostatic mode (**Fig.** 15 b), remains about the same but their density increases until the process changes to potentiostatic mode. Then after, the density and size of sparks remained unchanged despite the sharp decay of the current during potentiostatic control stage (**Fig.** 14 c,d).

Top views of the coatings formed under galvanostatic and potentiostatic conditions are shown in **Fig.** 16. The surface morphology of the anodic coatings obtained shows a porous structure, which is typical of the anodic films formed under sparking. Coatings formed under galvanostatic condition in Al - P solution show the formation of coatings with a low surface porosity and a similar surface morphology. Nevertheless, the morphology for coatings obtained in Al - Si solution is different for both materials. In Ti6Al4V alloy, the formation of volcano shaped pores is evident, that modifies the coating roughness, while in Ti c.p, a lower surface porosity is obtained and the formation of small circular pores is revealed in all surface. The potentiostatic control during the anodizing process modifies the surface morphology of the coatings. The porosity of the coatings is reduced in comparison with the galvanostatic coatings and small pores are formed on the surface of the coating homogeneously distributed on the coating surface. The morphology of the coatings obtained under potentiostatic conditions is similar in all conditions and in both materials.

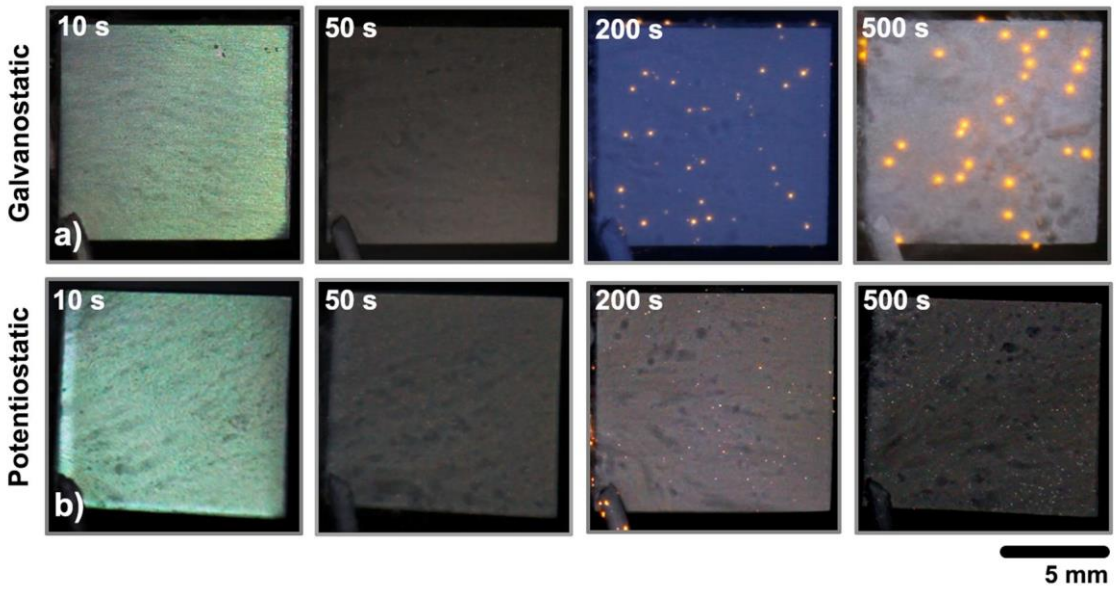

Figure 15. Micro - discharges appearance during anodizing on Ti6Al4V alloy at the following conditions: (a) galvanostatic coating formed at 50 mA cm^{-2} in Al - Si solution, (b) potentiostatic coating formed at 400 V in Al - Si solution

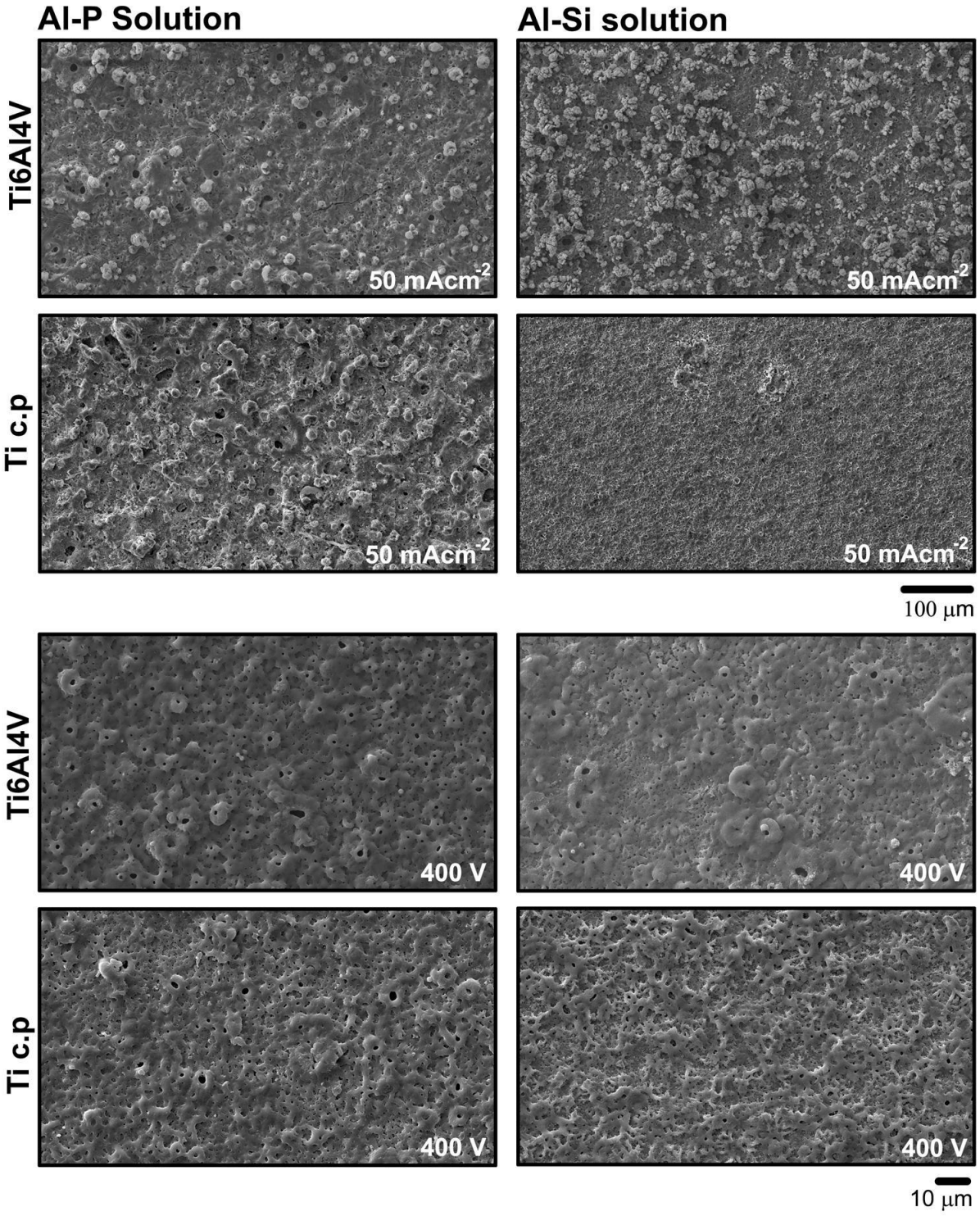

Figure 16. SEM micrographs of the coatings formed under the conditions listed in Table 4

The surface roughness of the coatings is shown in **Fig.** 17. The coatings formed in galvanostatic mode show higher roughness than the coatings obtained in potentiostatic mode, in agreement with the SEM observation due to the formation of volcano shaped pores (**Fig.** 16). The highest roughness occurred in the coating produced in the Al - Si solution on Ti6Al4V alloy, while the smoothest surface was formed in the Al - Si solution on Ti c.p. The coatings obtained under the potentiostatic mode exhibit similar topography roughnesses, regardless of both the solution composition and the substrate material.

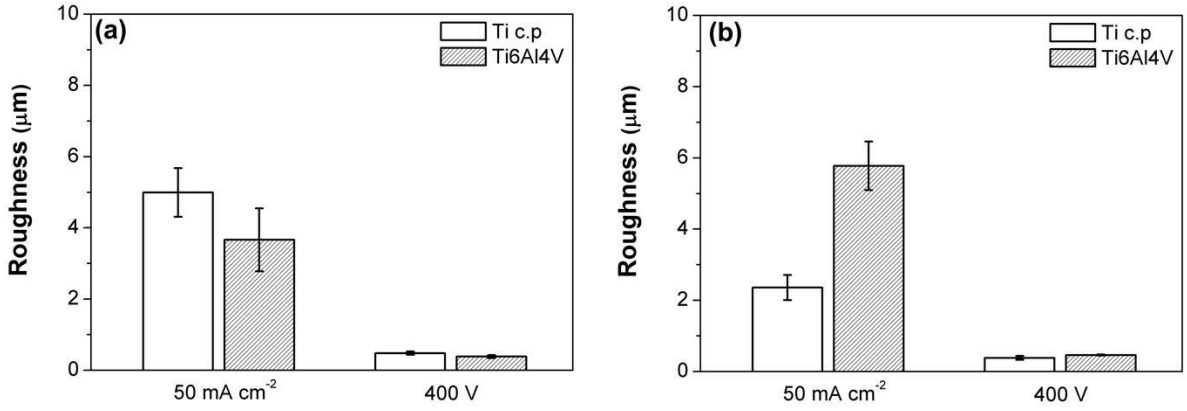

Figure 17. Average roughness determined by profilometry of the coatings obtained in the following solution (a) Al - P solution and (b) Al – Si solution

The cross-section micrographs of the anodic coatings obtained are shown in **Fig.** 18. The SEM images show changes for the coatings regarding porosity distribution through the coating, homogeneity and thickness. The potentiostatic coatings are thinner and denser than the galvanostatic coatings. Moreover, potentiostatic coatings are more homogeneous in thickness, because of the absence of large size pores. In the galvanostatic coatings, the

formation of a duplex structure is observed (an outer porous layer and a dense inner layer). The coatings obtained in Al - P solution reveal the formation of a higher density of voids and pores near the coating base. The coatings with much-reduced porosity are formed on Ti c.p in Al - Si solution due to the absence of formation of volcano-shaped pores.

Figure 19 shows the variation in thickness for all the coatings obtained. The coatings formed under the potentiostatic mode have similar thicknesses and these are much thinner than those produced under the galvanostatic mode. The thickness of the coatings formed under galvanostatic conditions varied with the solution composition and the substrate; the thinnest galvanostatic coating was formed in the Al - Si solution on Ti c.p, whose thickness is close those thickness of the potentiostatic coatings. The thickest coating was formed with the Al - P solution on Ti6Al4V alloy.

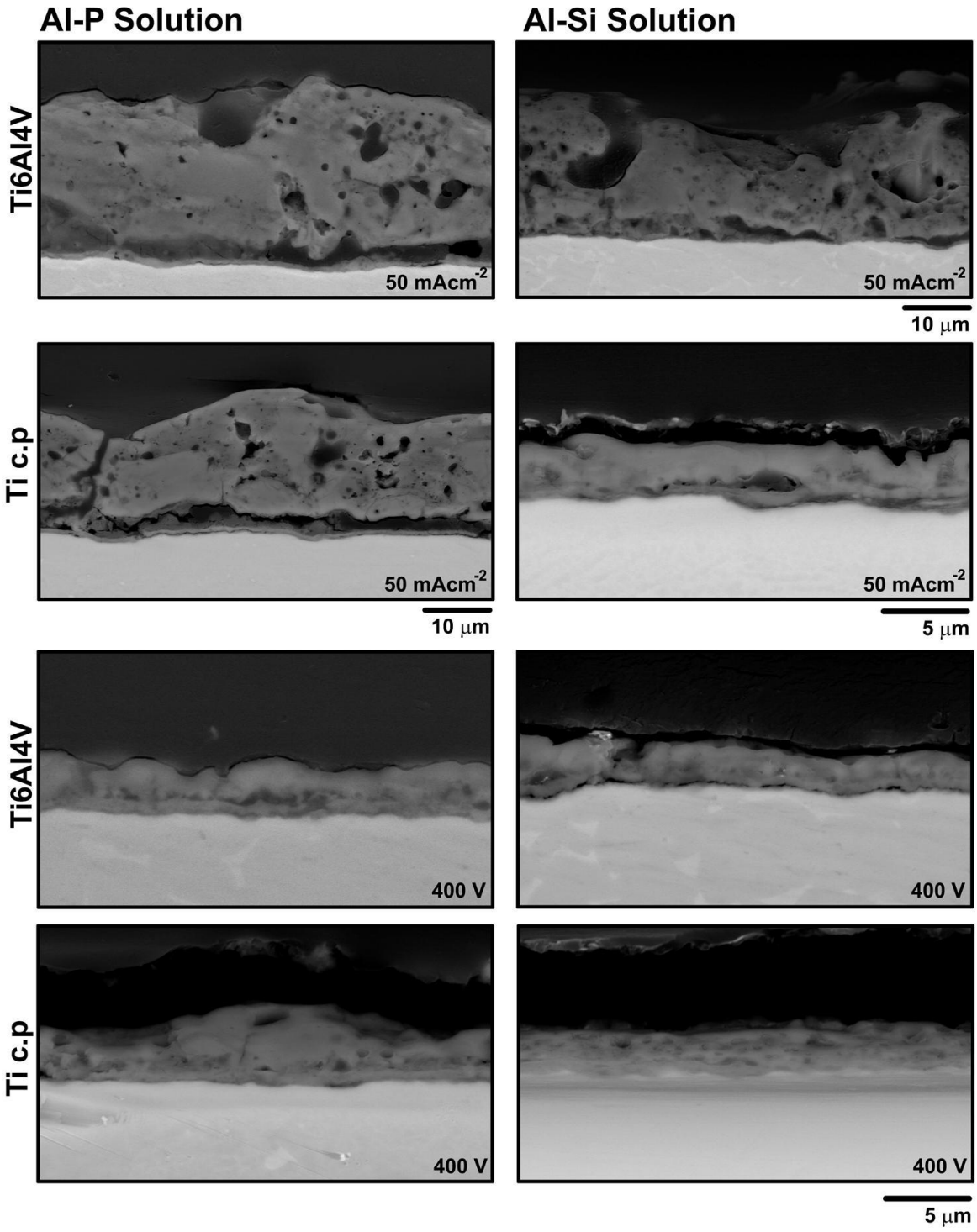

Figure 18. Cross-section SEM micrographs of the anodic coatings obtained under the conditions listed in Table 4

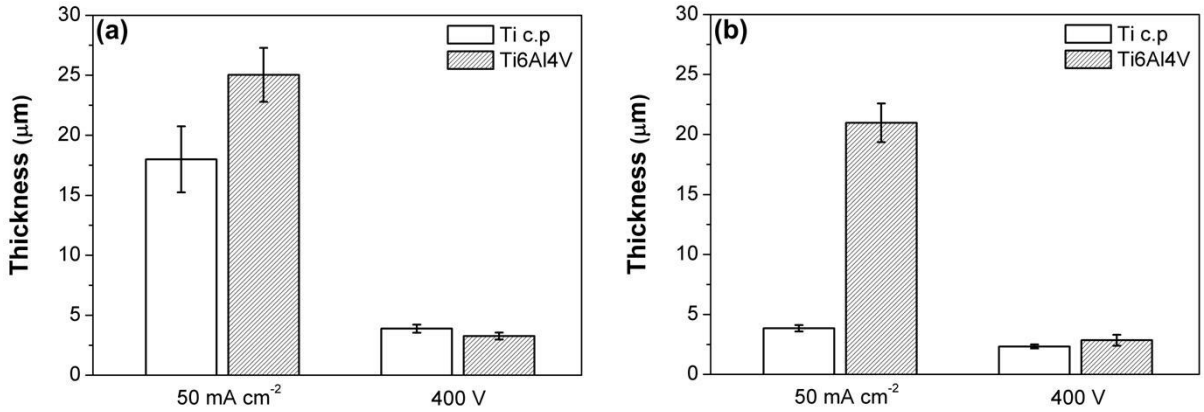

Figure 19. Average coating thickness of the coatings formed in (a) Al - P solution and (b) Al - Si solution

The composition of the surface coatings was assessed by EDS and summarized in **Table** 5. Aluminum, incorporated mainly from the solution, is the main element in the coating. Phosphorous, silicon, oxygen and sodium are also incorporated into the coatings, showing a higher concentration the coatings obtained under galvanostatic conditions. The coating contains titanium, derived from the alloy substrate, but the concentration is much lower than that of aluminum; vanadium is not evident into the coating. EDS elemental mapping shows the distribution of aluminum, phosphorous, oxygen, titanium and silicon in the coatings (**Fig.** 20). In all coatings, aluminum is mainly incorporated from the solution since it exhibits a much higher concentration in the coating than in the substrate, showing a homogeneous distribution through the film. Aluminum and oxygen are distributed homogeneously through the coating, while titanium is observed in small amounts near the coating base. In the coatings obtained with a NaH_2PO_2 addition (**Fig.** 20 a), phosphorous is observed, enriched near the coating base. For the coating obtained with a Na_2SiO_3 addition (Fig. 20 b), silicon is also observed in the coating, with a homogeneous distribution across. Sodium shows a

homogeneous distribution in the coating obtained in Al-Si solution (**Fig.** 20b), however, in the coating obtained in Al-P solution, sodium is not evidenced in the EDS elemental mapping due to its low concentration in the coating below 2 %.

Table 5. Chemical composition of the main components of the anodic coatings obtained

Solution ID	Electrical Parameter	Material	% Al	% O	% Ti	% P	% Si	% Na
Al – P	50 mA cm^{-2}	Ti c.p	27.56	60.50	4.67	4.46	---	2.81
		Ti6Al4V	29.32	64.36	2.84	2.45	---	1.04
	400 V	Ti c.p	20.65	62.49	14.54	1.83	---	0.49
		Ti6Al4V	23.45	64.81	10.10	1.06	---	0.59
Al - Si	50 mA cm^{-2}	Ti c.p	23.88	63.83	11.26	---	0.59	0.45
		Ti6Al4V	20.90	63.43	7.02	---	7.12	1.52
	400 V	Ti c.p	24.37	63.16	11.51	---	0.57	0.39
		Ti6Al4V	11.89	67.25	15.74	---	4.02	1.09

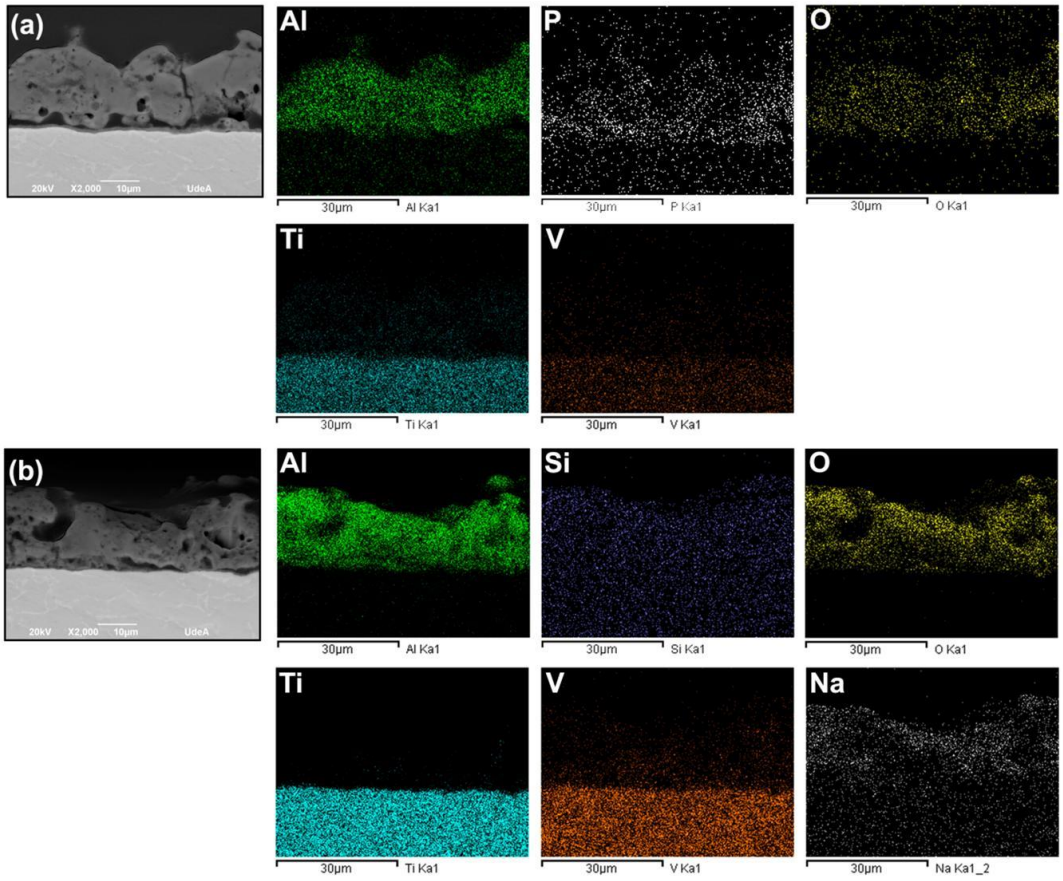

Figure 20. EDS elemental mapping for the coating obtained on Ti6Al4V alloy at 50 mA cm^{-2} in the following solution (a) Al - P solution and (b) Al - Si solution

The results of XRD (**Fig.** 21) for the galvanostatic coatings revealed the formation of γ - Al_2O_3, α - Al_2O_3 and Al_2TiO_5, except for the coatings obtained in Al - Si on Ti c.p, where the galvanostatic coating is composed mainly by γ - Al_2O_3 and Al_2TiO_5. Moreover, in the coatings obtained with the addition of NaH_2PO_2, small amounts of $Na_4Ti_5O_{12}$ was identified with the addition of 3 g l^{-1} of NaH_2PO_2 (**Fig.** 21 a,c) in both substrates. Mullite formation occurred for the coating obtained in the solution with 1 g l^{-1} Na_2SiO_3 under galvanostatic condition (**Fig.** 21d) only in the coating obtained on Ti6Al4V alloy. The potentiostatic coatings consisted of Al_2TiO_5 and γ-Al_2O_3 in minor proportion for all conditions.

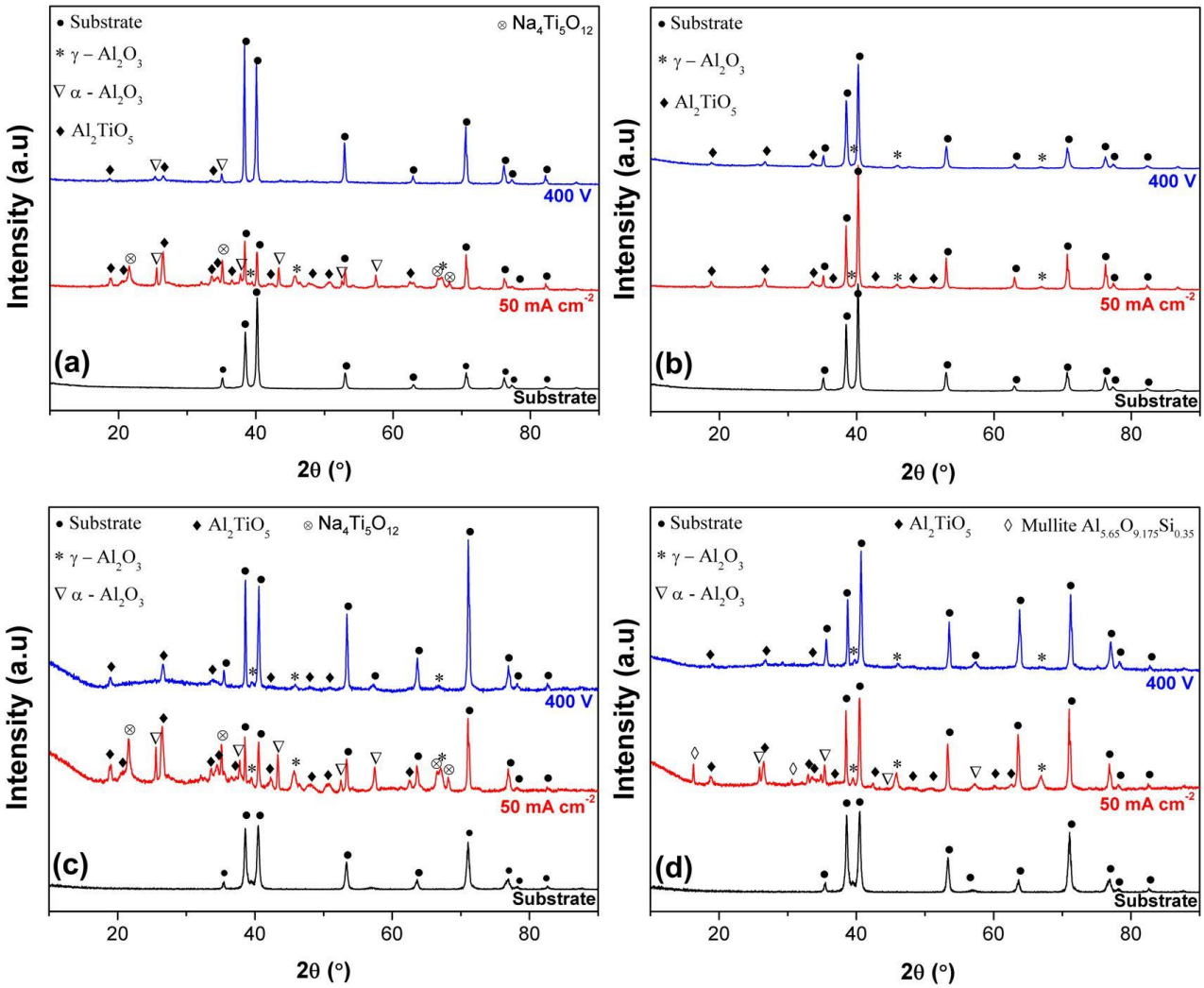

Figure 21. XRD patterns of coatings obtained on Ti c.p in (a) Al - P solution and (b) Al-Si solution and XRD patterns of the coatings obtained on Ti6Al4V alloy in (c) Al-P solution and (d) Al-Si solution

Figure 22 (a) presents typical results from friction measurements in the pin-on-disc tribological tests; the examples displayed are for coatings formed in the aluminate solution containing 3 g l^{-1} of NaH_2PO_2 using either the galvanostatic mode or the potentiostatic mode. The results are compared with the measurement of the friction coefficient for the

non-anodized alloy. All of the coatings in the present study revealed similar values of the friction coefficient, which were in the range 0.4 to 0.6, despite the differences in the coating roughness (**Fig.** 22b). The wear rates of the coatings obtained from the measurements of the weight losses of the samples following the wear tests are shown in **Fig.** 23. In general, the coatings formed under the potentiostatic conditions exhibited much lower wear rates than the respective coatings formed galvanostatically. The coatings grown in solutions with the addition of Na_2SiO_3 produced the lowest wear rate than those obtained in solutions with NaH_2PO_2 and coatings formed on Ti6Al4V alloy has lower wear rates than the coatings obtained on Ti c.p. All of the coatings revealed higher wear resistance than the bare substrate (wear rate of the substrate is 38.18 x 10^{-9} Kg/N.m for Ti6Al4V alloy and 41.08 x 10^{-9} Kg/N.m for Ti c.p under the same wear conditions), by factors between 2 to 100 times.

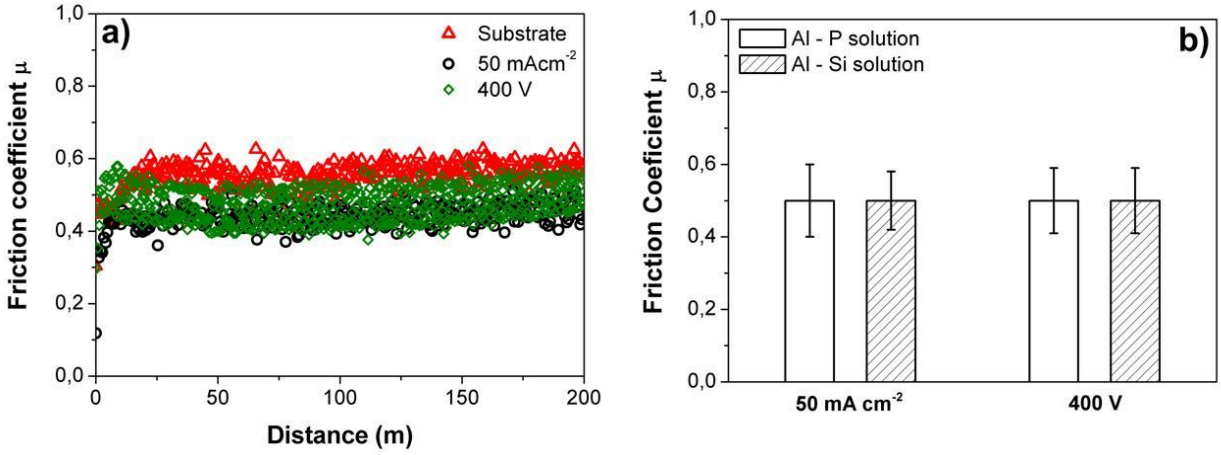

Figure 22. (a) Friction coefficient record for the coatings formed in the Al - P solution on Ti6Al4V alloy and (b) Average friction coefficient in the stable regime zone

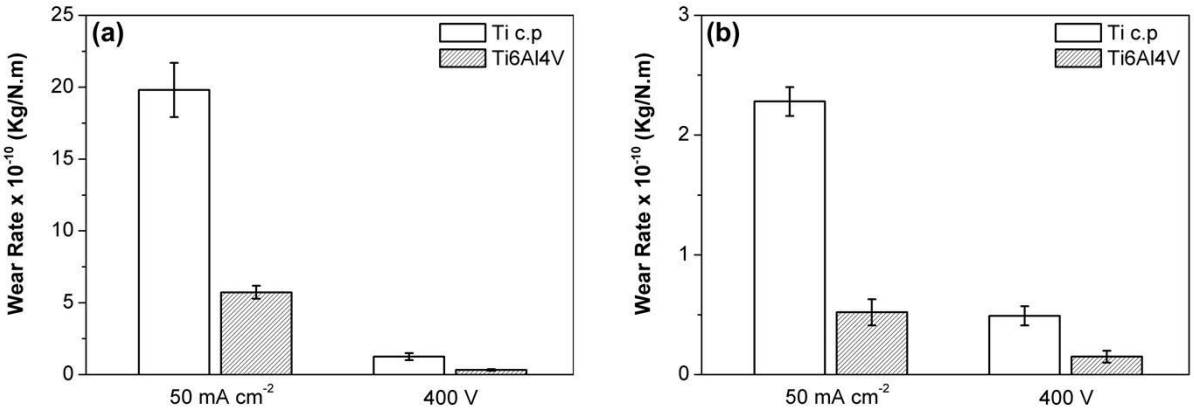

Figure 23. Wear rates of the coatings formed under the conditions listed in Table 4 in (a) Al - P solution and (b) Al - Si solution

SEM micrographs of the wear tracks after the wear tests are shown in **Fig.** 24. Adhesive wear and spalling are the main mechanisms of degradation for all the coatings. Among the coatings obtained under galvanostatic conditions, less surface damage occurs for the coating obtained in the solution with 1 gl^{-1} Na_2SiO_3 (**Figs.** 24 c-d) than in one with the additions with NaH_2PO_2 (**Figs.** 24 a-b). All of the coatings formed under the potentiostatic condition also show degradation due to adhesive wear and spalling, the surface damage is lower than for galvanostatically formed coatings; that especially true for those obtained in Al-Si solution (**Figs**. 24 e-f). Adhesion of particles from the counter-body was evidenced by EDS elemental mapping as shown in **Fig.** 24g, which shows the presence of iron in the wear track. Furthermore, the SEM images reveal that the tribological tests were stopped before reaching the substrate, indicating that the calculated wear rate is only for the coating. All the coatings obtained on Ti c.p exhibit the same wear mechanisms; therefore, the SEM images of the wear tracks on Ti6Al4V alloy are displayed as examples for all the coatings.

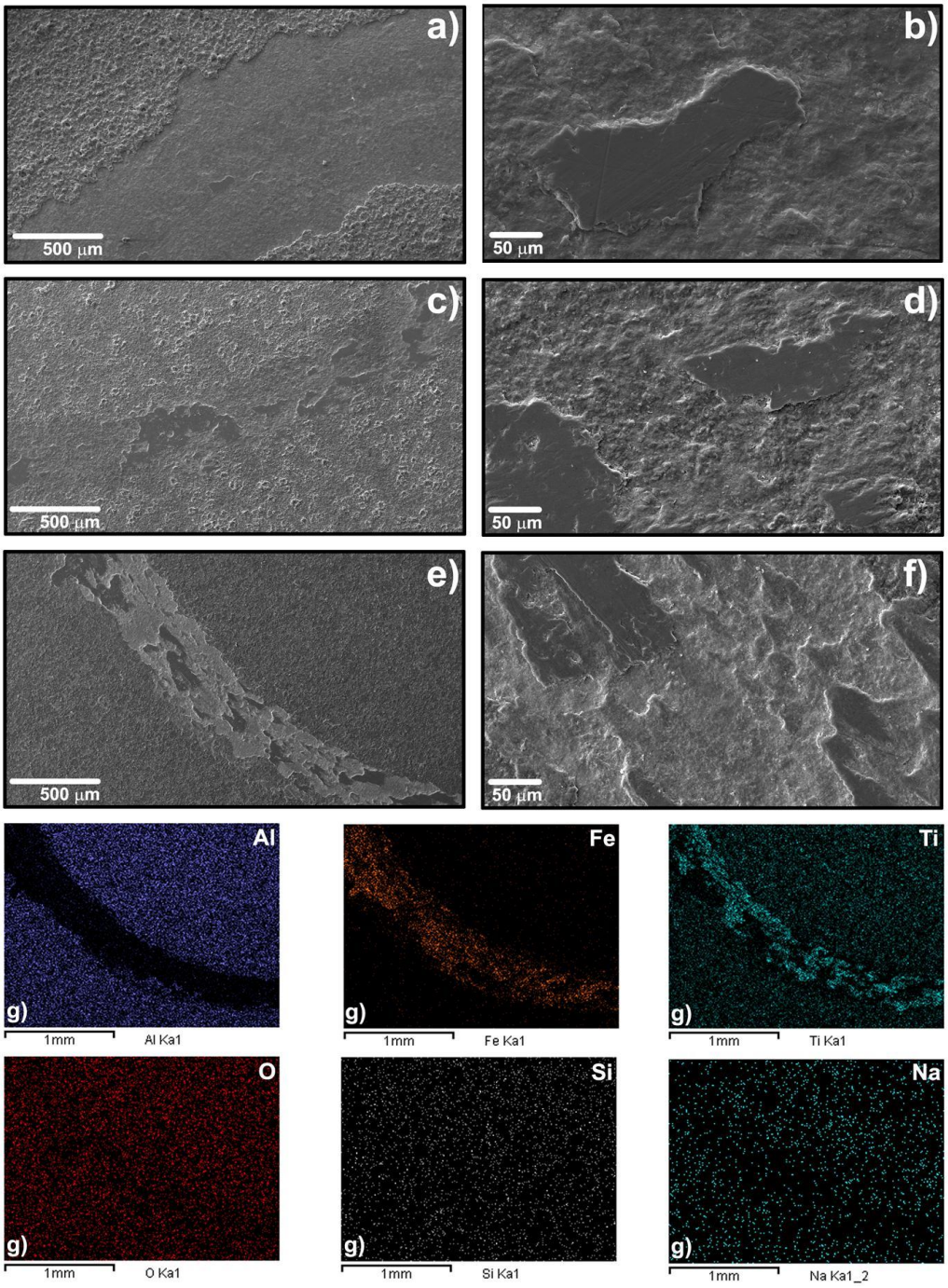

Figure 24. Wear tracks in the coatings obtained under the following conditions: a-b) at 50 mA cm^{-2} on Ti c.p in the Al - P solution, c-d) at 50 mA cm^{-2} on Ti6Al4V alloy in the Al - Si solution, e-f) at 400 V on Ti6Al4V alloy in Al - Si solution and g) EDS elemental mapping of the wear track of the coating formed at 400 V on Ti6Al4V alloy in Al - Si solution (Fig. 9e)

Bode diagrams obtained from EIS measurement are displayed in **Fig.** 25. Bode diagrams show two capacitive loops, indicating of a coating consisting of a dense inner layer and a porous outer layer as has been indicated in the SEM cross-sections and also by other authors [46], [135]. According to the literature reports, the first capacitive loop corresponds to the porous layer and the second to both the inner layer and the relaxation of the electrical double layer. The relaxation processes of both the inner layer and the electrical double layer have similar values of time constant so that only one capacitive loop at low frequencies appears in the impedance diagram [116]. Coatings obtained under potentiostatic conditions showed a slight increase in the real impedance values compared to the coatings under galvanostatic conditions, indicating a better corrosion protection. Similarly, coatings obtained in the Al - Si solution exhibited a higher resistance than the other coatings, especially the coatings obtained on Ti c.p (**Fig.** 25d). Bode diagrams exhibited changes mainly in the time constant related to the porous layers for the coatings obtained on Ti6Al4V alloy (**Figs.** 25 a-b), while for the coatings formed on Ti, there are changes in time constants of both the outer and the inner layer of the coating obtained in Al-P solution (**Fig.** 25c). For the coating obtained in Al-Si solution, the time constants do not show changes in the anodizing parameters evaluated (**Fig.** 25d). EIS results were analyzed using the equivalent circuit that has been described in the previous chapter. In the equivalent circuit, constant phase elements (CPE) were used for simulation of the experimental results. The effective capacitances were then calculated from the parameters of the CPE as reported by Hirschorn et al [68]. Results of the fitting are shown in **Table** 6; where R_p is the porous layer resistance, R_b is the inner layer resistance, R_{tc} is the charge transfer resistance, C_p is the capacitance of the porous layer, C_b is the capacitance of the inner layer, C_{dc} is the capacitance of the electrical double layer and n is one of the

parameters of the CPE. Bode diagrams in **Fig.** 25 show a good correlation between experimental and simulated data (see goodness of fit values in Table 6). In general, higher layer resistances and lower capacitances were observed for coatings formed under the potentiostatic mode and for coatings obtained on Ti c.p in the solution with addition of Na_2SiO_3.

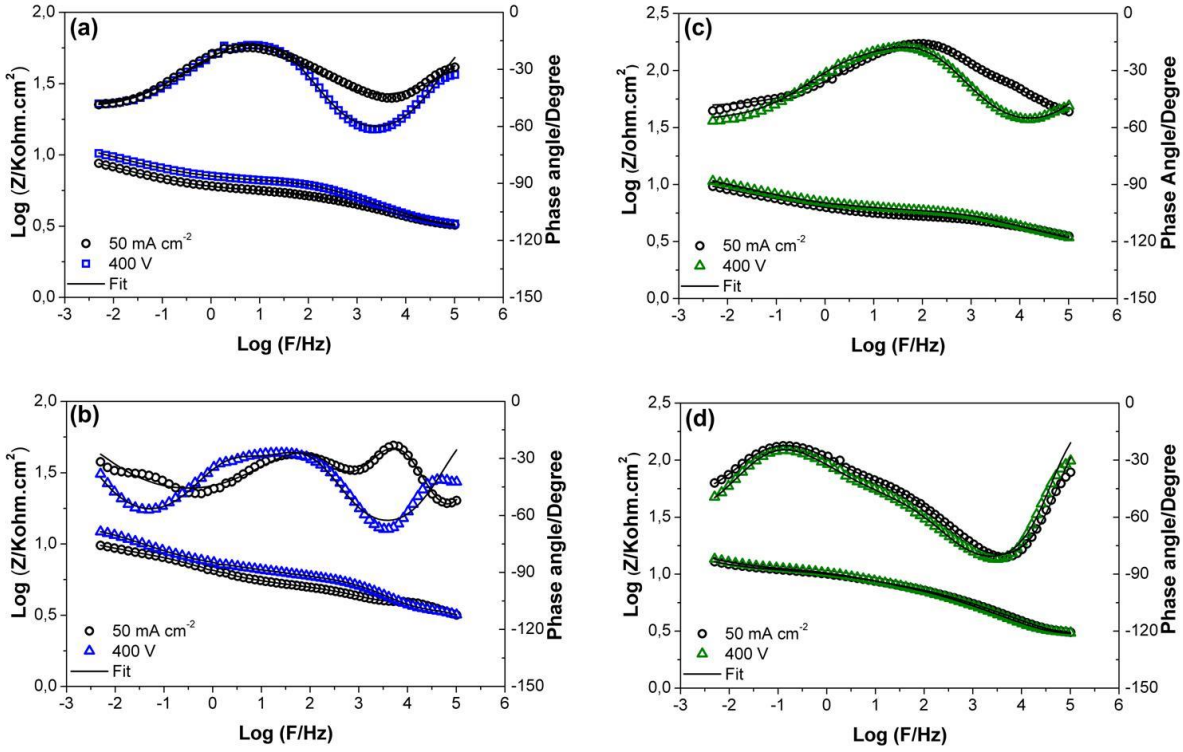

Figure 25. Bode spectra for the coatings obtained on Ti6Al4V alloy in (a) Al-P solution and (b) Al-Si solution and Bode spectra for the coatings obtained on Ti c.p in (c) Al-P solution and (d) Al-Si solution

Table 6. Electrical parameters of the coatings obtained by the fitting of the EIS experimental results

Solution ID	Electrical parameter	Material	Electrical parameter provided by the EIS fitting									
			R_p (KΩ cm^2)	R_b (MΩ cm^2)	R_{tc} (MΩ cm^2)	C_p (μF cm^{-2})	n_p	C_b (μF cm^{-2})	n_b	C_{dc} (μF cm^{-2})	$Z_{f=0.005}$ (KΩ cm^2)	Goodness of fit x 10^{-3}
Al - P	50 mA cm^{-2}	Ti c.p	0.80	2.51	0.46	0.08	0.98	5.46	0.93	18.34	205.05	1.93
		Ti6Al4V	4.90	1.22	0.21	0.07	0.78	6.17	0.74	22.54	121.75	1.29
	400 V	Ti c.p	17.81	31.86	4.50	0.07	0.83	0.04	0.73	7.33	800.15	5.92
		Ti6Al4V	20.79	26.10	3.67	0.05	0.78	3.54	0.74	16.52	329.64	1.29
Al - Si	50 mA cm^{-2}	Ti c.p	21.31	606.75	13.16	1.02	0.98	2.04	0.52	11.34	1011.90	0.99
		Ti6Al4V	5.41	15.63	15.10	3.05	0.77	13.97	0.70	21.18	223.86	0.23
	400 V	Ti c.p	25.29	764.52	42.56	0.02	0.98	0.02	0.51	6.58	1249.18	1.35
		Ti6Al4V	32.49	21.06	26.54	0.03	0.81	3.97	0.63	10.70	431.73	0.46

2.4. Discussion

The coatings obtained under the potentiostatic condition are denser, thinner and exhibit better tribological performance than those obtained under galvanostatic conditions. The coatings containing mullite and alumina revealed the best tribological performance for the coatings formed under galvanostatic mode (**Fig.** 23). The formation of Al_2O_3 and Al_2TiO_5 has been widely described for PEO of titanium in aluminate-based solutions [32], [61], [123], [136]. The addition of NaH_2PO_2 leads to the incorporation of phosphorous into the coating, mainly near the metal-oxide interface, suggesting that phosphorus species migrate to the inner layer through the breakdown channels under a high electric field [61]. Furthermore, sodium is incorporated into the coating and interacts with the TiO_2 formed in the coating, resulting in the formation of $Na_4Ti_5O_{12}$. This crystalline phase does not exist in the Na_2O-TiO_2 system but has been reported to be stabilized by doping at room temperature

[137], [138]. Despite the incorporation of phosphorous into the coating, the formation of phosphate species was not evidenced in any case (**Fig.** 21). Silicon incorporation into the coating leads the formation of SiO_2 [31], [56], which in the presence of Al_2O_3 results in the formation of mullite, which has a low thermal expansion and conductivity, suited to high-temperature applications [139].

The coatings obtained under galvanostatic conditions reveal the formation of a porous morphology due to the micro-discharges (**Fig.** 16). Morphological changes in the coatings are disclosed by EIS with the inner layer exhibiting a higher resistance than the outer layer; hence, the corrosion resistance of the coatings depends mainly on the inner layer [1], [78], [80]. A decreasing of porosity (**Figs.** 16,18) increases the resistance of both coating layers (Table 6) and decreases the capacitance of each layer as observed from the electrical parameters of the coatings obtained in Al-Si in both materials. In the coatings obtained on Ti c.p in Al-P solution, a higher density of voids and pores is evidenced near the coating base, which reduces the adhesion of the coating and, therefore the tribological properties in comparison with Ti6Al4V alloy. The highest resistance was obtained in the coatings formed in the Al - Si solution on Ti c.p due to the low porosity of these coatings. Formation of coatings using a solution containing metasilicate with good corrosion protection has been also reported by other authors [18], [90], [132]. In the coating obtained on Ti6Al4V alloy, mullite can increase the fracture toughness of the alumina matrix, and a better tribological performance is observed for the coatings obtained under galvanostatic conditions (**Fig.** 23) [1]. Some researchers also have shown that the formation of mullite improves the wear performance of PEO coatings [77], [128], [129]. The CPE parameter (n) of the porous layer

is about 0.7-0.9, indicating that the porosity distribution is more or less homogenous for all the coatings. Regarding the inner layer, the CPE parameter is lower for the coating formed in the Al - Si solution given the formation of a metal-oxide interface with high roughness. The addition of Na_2SiO_3, especially on Ti c.p, increases both the time at which sparking commences and the time at which the potential becomes constant (Fig. 14 b). These differences affect the growth rate, especially for the coating obtained on Ti c.p with Na_2SiO_3 addition, which has the lowest growth rate (Fig. 19b). The increase of gas evolution during the early stages of the anodizing process also contributes to the decrease of the efficiency of the process [1].

Coatings obtained under the potentiostatic condition reveal the formation of dense coatings and exhibit low roughness, important aspects for the tribological performance, with a lower porosity than the coatings formed under the galvanostatic mode (**Figs.** 18,16). The potentiostatic mode modifies the micro-discharge size decreasing the coating porosity as well as the thickness (Fig. 15). All the potentiostatic coatings have similar thickness, despite the different charge density applied in forming the coatings; the higher charge density used was for the coatings obtained in Al - Si solution. As for coatings formed under the galvanostatic mode, a reduction in the growth rate is observed due to either the addition of Na_2SiO_3 or the substrate, which is associated with an increase on gas evolution as well as the time to initiate discharges. The formation of dense coatings under potentiostatic control improves the wear performance of these coatings with respect to the coatings obtained under galvanostatic conditions (Fig. 23). The small micro-discharges formed in this condition, do not have the enough energy to generate the temperature required to synthesize $Na_4Ti_5O_{12}$ and

mullite phases. For that reason, the chemical composition is similar for all potentiostatic coatings despite the solution composition differences and accordingly, the wear behavior is also similar in all cases. In the coatings obtained under galvanostatic conditions, the outer porous layer influences the high roughness, features that contribute obtaining high wear rates, except for the coating formed on Ti6Al4V alloy in the solution containing Na_2SiO_3 due to the mullite formation. Concerning the wear mechanisms, all coatings have the same wear mechanisms; nevertheless, in the coatings obtained under galvanostatic conditions a higher material removal occurs given that the outer porous layer wears more easily soon after the test initiates. The better corrosion resistance of the potentiostatic coatings is due to the low porosity relative to the coatings formed under galvanostatic control. However, the corrosion resistance is dependence on the solution composition for both potentiostatic and galvanostatic coatings. The inner layer resistance is higher than that of the porous layer, suggesting the corrosion resistance of the coating depends on mainly on the inner layer.

2.5. Conclusions

The conclusions of the chapter are as follows:

1. Anodic coatings were obtained using different additives and electrical parameters. The additives induce changes in the coatings such as chemical and phase composition, porosity and thickness, especially for the coatings obtained under galvanostatic condition.
2. The formation of mullite reduces the wear rate significantly in the galvanostatic coating obtained on Ti6Al4V alloy; this compound could be useful in applications at high temperature due to its thermal barrier properties. Coatings formed under potentiostatic conditions are denser than the coatings obtained under galvanostatic conditions, exhibiting a better wear behavior.
3. The crystalline phase composition of these potentiostatic coatings is mainly Al_2O_3 and Al_2TiO_5, which results from the small size and low energy of the PEO micro-discharges.
4. The addition of Na_2SiO_3 allows the formation of coatings with better corrosion resistance in comparison with the coatings obtained with the addition of NaH_2PO_2.
5. The selection of the anodizing electrical parameters allows controlling the morphological characteristics of the coatings, which in turn influence their final technological properties. It was observed for all cases that the morphological changes into the coatings are related to the electrical parameter calculated by fitting of the EIS experimental results. This was evidenced comparing the changes in thickness and porosity observed in the SEM images of the coatings with their corresponding electrical parameter.

3. Chapter 3

Effect of the anodizing parameters on the morphology and the corrosion and wear properties of the anodic coatings

Abstract: The effect of the anodizing parameters both on the coating formation as well as on the tribological properties and the corrosion resistance was studied. For the coatings obtained under galvanostatic conditions, the increase of the current density generates a decrease in the mechanical and tribological properties due to the decrease of the inner layer thickness. A higher current density increases the intensity and size of the micro-discharges, generating rougher surfaces and thicker coatings. In the coatings obtained under potentiostatic conditions, it was evidenced that the initial current density applied has a significant effect on the tribological properties. Higher current densities lead to the formation of voids and pores near the coating base that reduces the corrosion resistance and the tribological performance, as was evidenced in the EIS analysis and the pin-on-disc test. Finally, the composition of the solution has an effect on the PEO characteristics and the electrical properties of the coating. The size

and intensity of the micro-discharges are influenced by the capacitance and the growth mechanism of the coating. However, more research is necessary in order to obtain a good relationship between the anodizing parameters and the coating characteristics.

Keywords: Anodizing parameters, voltage, time, temperature, current density, growth coating, wear and mechanical properties, corrosion resistance

3.1. Introduction

Different studies carried out for determining the relationship between the anodizing process conditions and the characteristics of the anodic coating have demonstrated the critical influence of the electrochemical parameters on the surface properties of the coating [78], [80]. Both intrinsic factors (solution compositions and pH) and extrinsic factors (electrical parameters, and solution temperature) affect the formation and microstructure of PEO coatings. The composition and concentration of the solution and the electrical parameters used during the process play a crucial role in obtaining the desired coatings with particular phase components and microstructure [36], [57], [66]. In summary, the coating growth generates systemic changes in the superficial topography, which gives the possibility of obtaining different morphologies and surface finishing. Anionic incorporation into the layer alters both the chemical composition and the crystalline structure of the oxide [25], [31]. The potential and the current density applied modifies the size and energy of the micro-discharges, which in turn affect the chemical composition, the coating porosity and the

growth kinetic of the coating. Finally, it is important to consider that an adequate combination of the anodizing parameters allows obtaining the required coating properties according to its final application [11], [12], [69]. Besides, the composition, structure and thickness of the titanium oxide film are strongly dependent on these electrochemical variables; these factors largely determine the chemical and mechanical stability of the coating [1], [36], [78], [80].

In this chapter, the effect of some anodizing parameters on the coating properties is observed. The analysis was carried out in a specific anodizing solution. The same behavior is evidenced in all the solutions and substrates evaluated; nevertheless, a specific condition is shown here in order to illustrate the phenomenon. Results shown in Chapter 1 and 2 are the anodizing conditions with better corrosion and wear performance obtained, but different electrical conditions were evaluated for each solution and substrate.

3.2. Effect of the current density on the tribological and corrosion properties of titanium alloy obtained by PEO

3.2.1. Introduction

As mentioned above, the coating properties are strongly influenced by the morphological characteristics and the chemical composition of the coating obtained. The coating characteristics can be modified according to its final application by the control of the electrical parameters during the anodizing process, indicating that an adequate selection of the anodizing parameters is an important to obtain the desired coating [140]–[142]. Between the modes of PEO coating formation, the galvanostatic conditions mode allows the formation of a wide range of crystalline species depending on the solution used due to the formation of micro-discharges with higher energy and size as was evidenced in previous chapters. However, the formation of micro-discharges with larger size and higher energy induces the formation of higher porosity and the formation of channels through the coating that leads to lower hardness, and thus worse mechanical performance. On the other hand, the increase of the current density rises the growth rate, allowing the formation of thick coatings, whose efficiency is affected mainly by the increase of gas evolution and the dissolution of substrate elements with the current increase [1], [41], [110], [136], [143]–[145]. In this section, the effect of the current density on the tribological and corrosion properties of coatings obtained under galvanostatic conditions in a sodium hypophosphite-based solution was studied; these solutions were selected as the resulting coatings show a good wear performance and the incorporation of Ca and P benefits the biocompatibility properties.

3.2.2. Experimental

The coatings were obtained on Ti c.p in a solution composed by $NaH_2PO_2.H_2O$ 10 g L^{-1}, $EDTANa_2$ 7.44 g L^{-1}, $(CH_3COO)_2Ca$ 1.78 g L^{-1} and NaOH 3 g L^{-1} with a pH of 13.2 and a conductivity of 17.2 mS cm^{-1}. The coatings were obtained under galvanostatic conditions at a constant current. The current density is applied during 600 s and the potential response is recorded. The current densities evaluated were 50 and 100 mA cm^{-2}, which were higher than needed to obtain sparking.

The anodizing process and the characterization of the coatings were carried out under the same conditions as mentioned in Chapter 1.

3.2.3. Results

The kinetics of the anodic layer formation depends on the electrochemical parameters and the nature of the electrolytic solution [48], [60]. **Fig.** 26 shows the response of potential with time for the anodic coatings obtained at constant current. The potential vs. time curves show typical stages for the plasma electrolytic oxidation [13], [146]. The curve shows three different regions. In region I, potential linearly increases with time from 0 to ~150 V, corresponding to the traditional anodizing stage, where an insulating thin film is formed on the surface. In region II, the slope of the curve decreases and the potential continues ascending to a critical potential value. In this region, the formation of sparks and gas evolution on the coating surface begins. In region III, the potential remains stable until the end of the process and a large number of fine sparks continuously appear on the surface; this stage is known as the micro-arc stage. At the end of the process, the sparks grow in size and

evolution of oxygen continues. The slope of the curve at initial stages (region I) increases as the current density gets higher and the potential reached at the end of the process is higher for a higher current density.

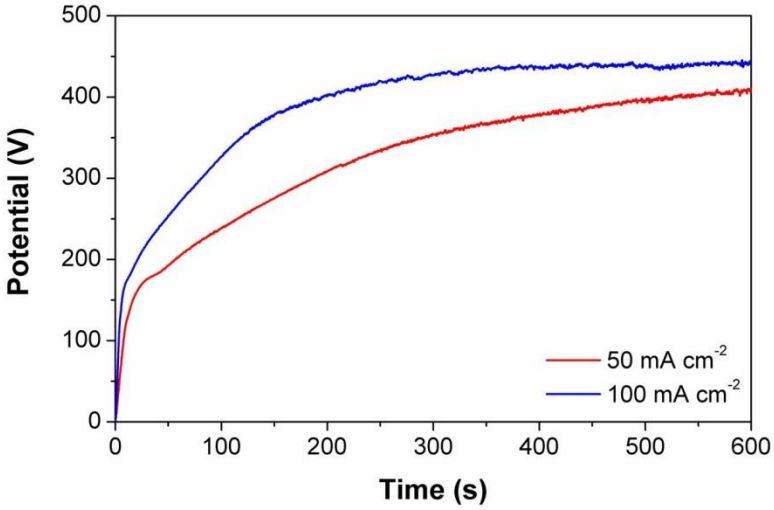

Figure 26. Current-time responses of the anodic coatings obtained on Ti c.p in P solution at room temperature

Figure 27 shows SEM micrographs of the anodic films obtained galvanostatically at different current densities; surface morphologies of the anodic films are shown in **Fig.** 27(a,b) and coating cross-sections are shown in **Fig.** 27(c,d). The surface morphology shows that the anodic films have a porous structure with a homogeneous distribution on the surface. Circular pores are observed in both conditions with some volcano shaped pores. A decrease in the surface porosity is observed when the current density gets higher. The roughness values for the coatings are 976.45 ± 76.54 nm for the coating obtained at 50 mA cm^{-2} and 1629.03 ± 264.52 nm for the coating obtained at 100 mA cm^{-2}. Cross-section views (Fig 27 c,d) show the porosity distribution through the coating. An increase in the thickness of the

coating is evidenced with the current density. For the coating obtained at 50 mA cm^{-2} the thickness is ~ 9.21 ± 0.76 µm and for the coating formed at 100 mA cm^{-2} is ~ 16.62 ± 2.01 µm. The cross-section shows that the anodic films have an interconnected porous structure and the formation of pores and voids close the coating base is evidenced in both conditions.

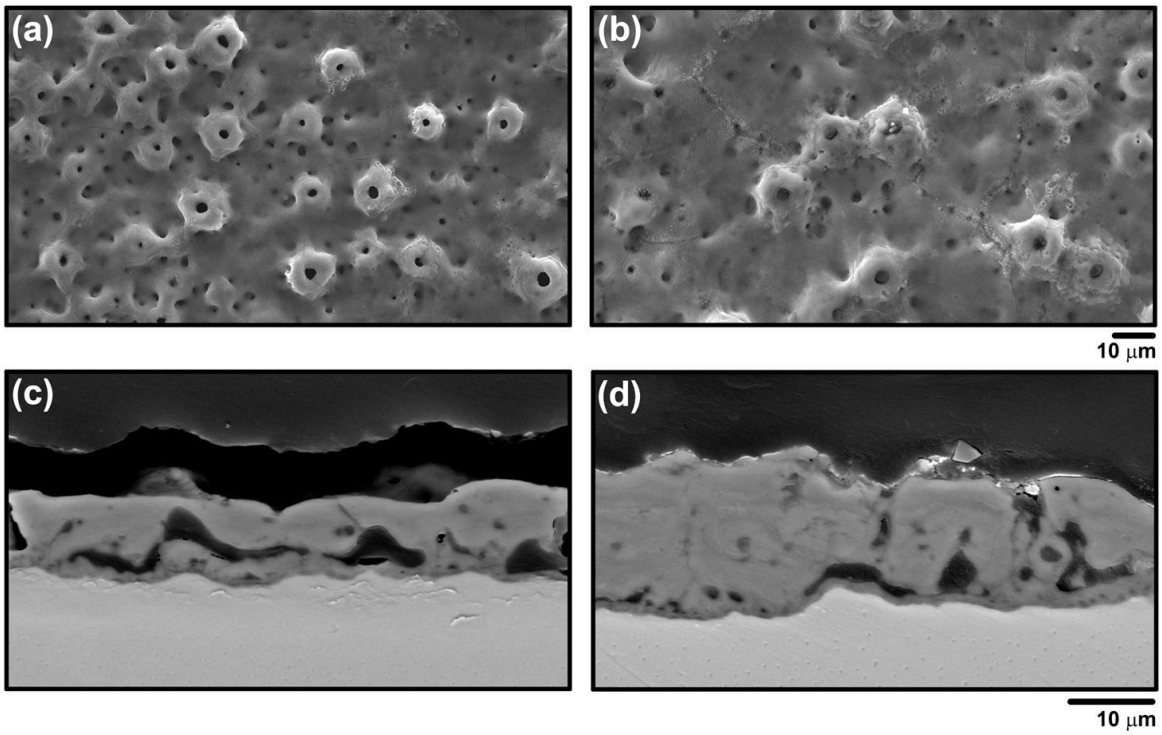

Figure 27. SEM images (SE) of top views of the coatings obtained in P solution at (a) 50 mA cm^{-2} and (b) 100 mA cm^{-2} and SEM images (BSE) of the cross-section views of the coatings obtained at (a) 50 mA cm^{-2} and (b) 100 mA cm^{-2}. The anodizing solution temperature is 20 ºC

The composition of the coatings was assessed by EDS and summarized in **Table** 7. Phosphorus, sodium, calcium and oxygen are incorporated into the coatings from the solution, showing higher concentrations for the coatings obtained at a higher current density. The coating contains titanium, derived from the alloy substrate. The results of XRD (Fig. 28)

for the galvanostatic coatings revealed that the coating obtained at 50 mA cm^{-2} is composed mainly of anatase, while the coating obtained at higher current density (100 mA cm^{-2}), in addition to the anatase phase, also contains rutile, but in a minor proportion.

Table 7. Chemical composition of the anodic coatings formed by anodizing on Ti c.p in P solution

Electrical Parameter	% O	% Ti	% P	% Na	% Ca
50 mA cm^{-2}	68.58	20.46	7.45	0.48	2.52
100 mA cm^{-2}	70.08	18.13	7.96	0.67	3.66

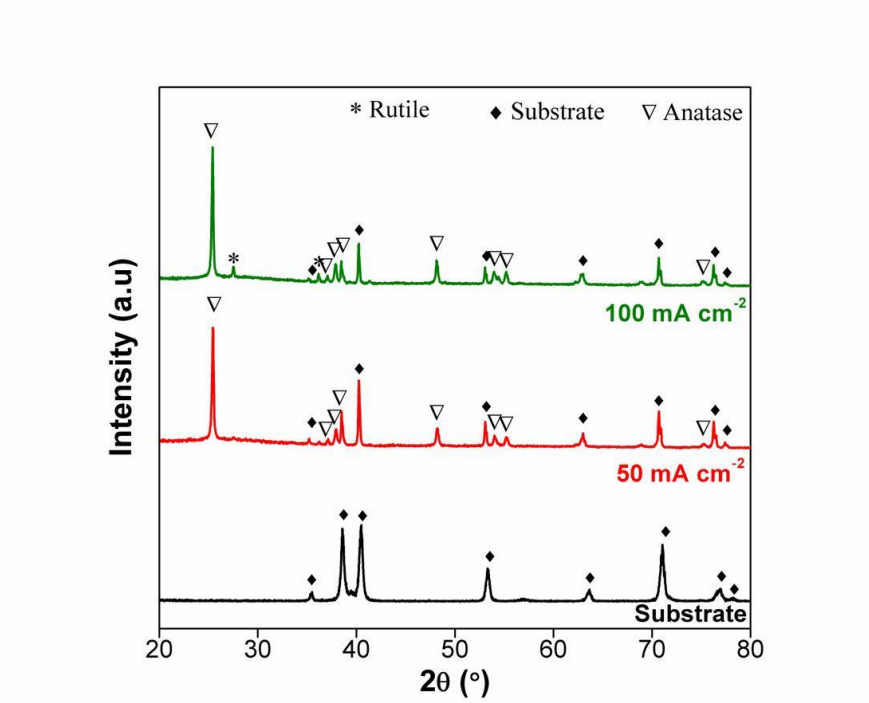

Figure 28. XRD spectra of the anodic coatings obtained on Ti c.p in P solution under galvanostatic condition

The tribological performance of the coatings depends on the electrochemical parameters

used for their formation. **Fig.** 29 shows dry sliding friction coefficient and wear rates of the coated specimens. Friction coefficients for the anodic coatings obtained are shown in **Fig.** 29a. Both coatings show a stable friction coefficient during the test and the friction coefficient values are similar for all the coatings, despite having different surface roughnesses. The coating obtained at lower current density reveals a better tribological performance as observed in **Fig**. 29b. The wear rate of the bare substrate under the same wear test condition is as high as 18.7 x 10^{-9} kg/N.m, indicating that the anodic coatings improve the wear resistance by 12 - 26 times. The substrate has a friction coefficient higher than the coatings about 0.5.

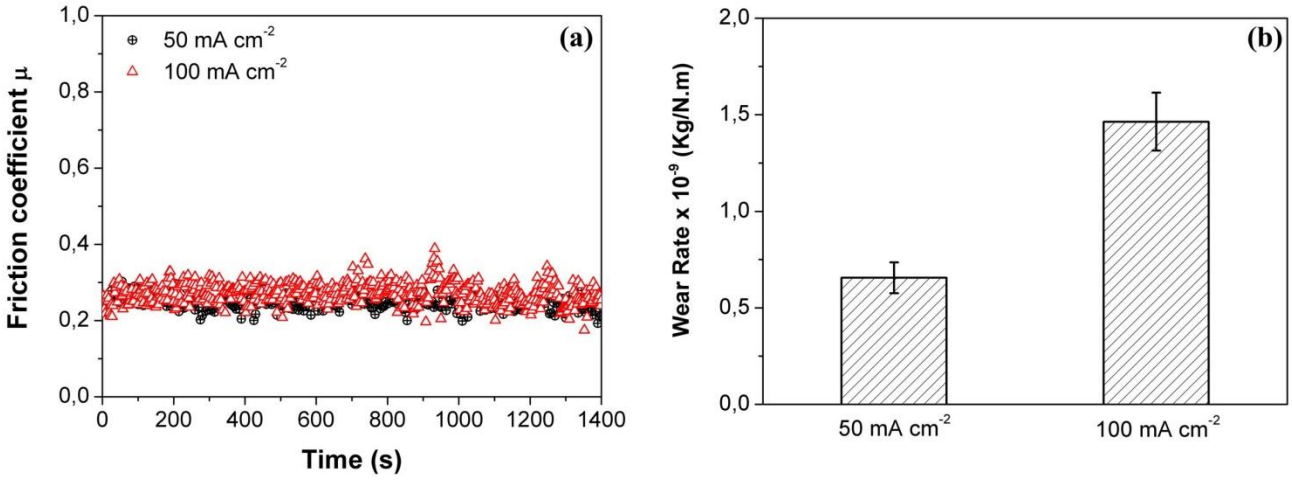

Figure 29. (a) Friction coefficient-time response for the coatings obtained in P solution and (b) wear rate of the coatings formed in P solution on Ti c.p

The appearance of the wear paths on the coatings after the tribological tests is shown in **Fig.** 30. Adhesion of material from the counter-body on the coated surface and spalling are the main wear mechanisms for the coatings obtained at 50 mA cm^{-2}. In the coating

obtained at 100 mA cm^{-2}, it also is observed adhesion as wear mechanism and fatigue due to the presence of cracks on the wear track (Fig. 30d), indicating a worse wear behavior. **Fig.** 30e shows the presence of iron on the wear path due to the adhesion of the counter-body on the coating. On the other hand, the SEM images evidence that the tribological tests were stopped before reaching the substrate, indicating that the wear rate calculated is only for the coating.

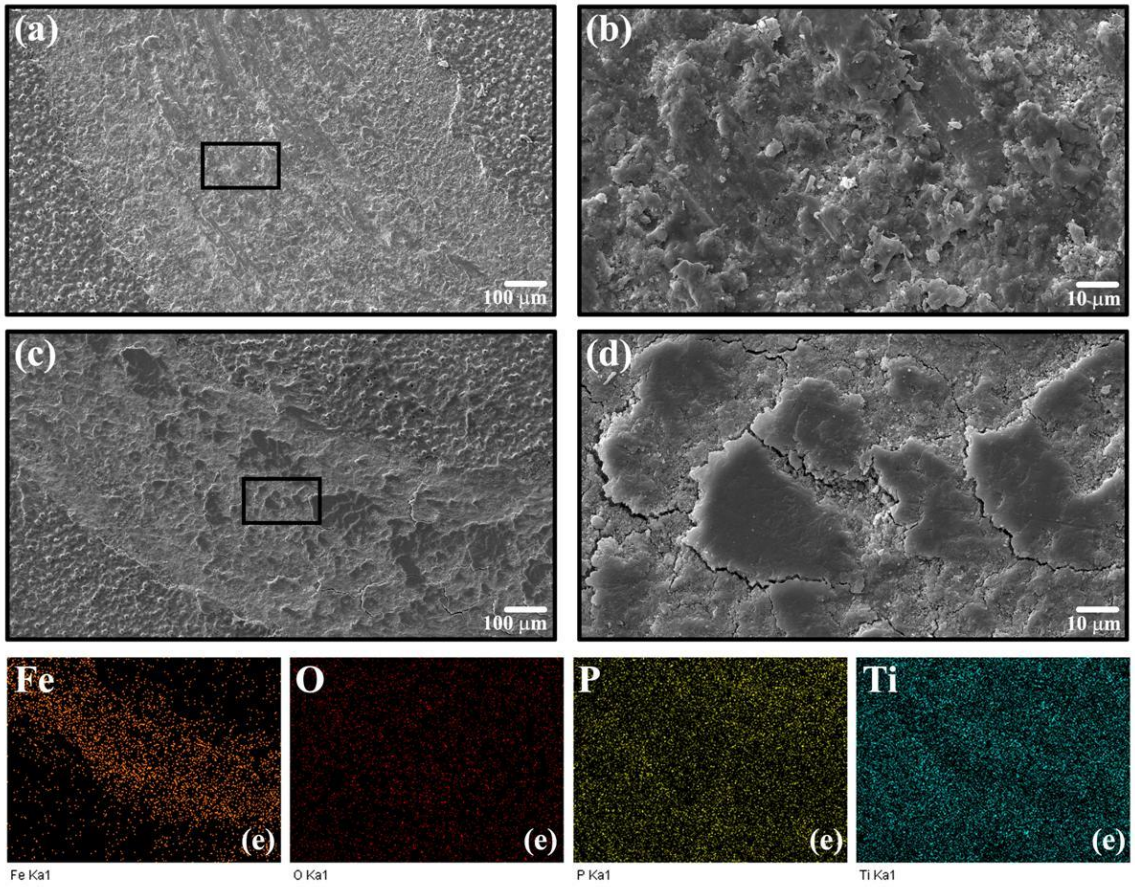

Figure 30. Wear tracks of the coatings obtained on Ti c.p after wear test for the coating obtained at (a,b) 50 mA cm^{-2} and (c,d) 100 mA cm^{-2} and EDS elemental mapping of the wear track of the coating obtained at 100 mA cm^{-2} (Fig. 30e)

Figure 31 shows both Nyquist and Bode diagrams of electrochemical impedance for the anodic films obtained. In the Bode diagram, two time constants are observed, corresponding to the formation of a duplex coating (a dense inner layer and a porous outer layer) as was mentioned in previous chapters. This duplex structure is also observed in Nyquist diagrams. The Nyquist diagram shows two capacitive arcs, the first arc corresponds to the porous layer and the second arc correspond both to the inner layer and the relaxation of the electrical double layer. **Figure** 31(b) shows the Bode curves of the anodic films obtained galvanostatically, where an increase is observed in the impedance module of the anodic layer as the current density applied increases. Likewise, both capacitive arcs for the anodic films obtained show slight changes in frequency, indicating variations in the dielectric properties of the coatings. EIS results were analyzed using the equivalent circuit that has been described in the previous chapter. In the equivalent circuit, constant phase elements (CPE) were used for simulation of the experimental results. The effective capacitances were then calculated from the parameters of the CPE as reported by Hirschorn et al [68]. Results of the fitting are shown in Table 8; where R_p is the porous layer resistance, R_b is the inner layer resistance, R_{tc} is the charge transfer resistance, C_p is the capacitance of the porous layer, C_b is the capacitance of the inner layer, C_{dc} is the capacitance of the electrical double layer and n is one of the parameters of the CPE. Bode diagrams in **Fig.** 31(b) show a good correlation between experimental and simulated data (see goodness of fit values in **Table** 8).

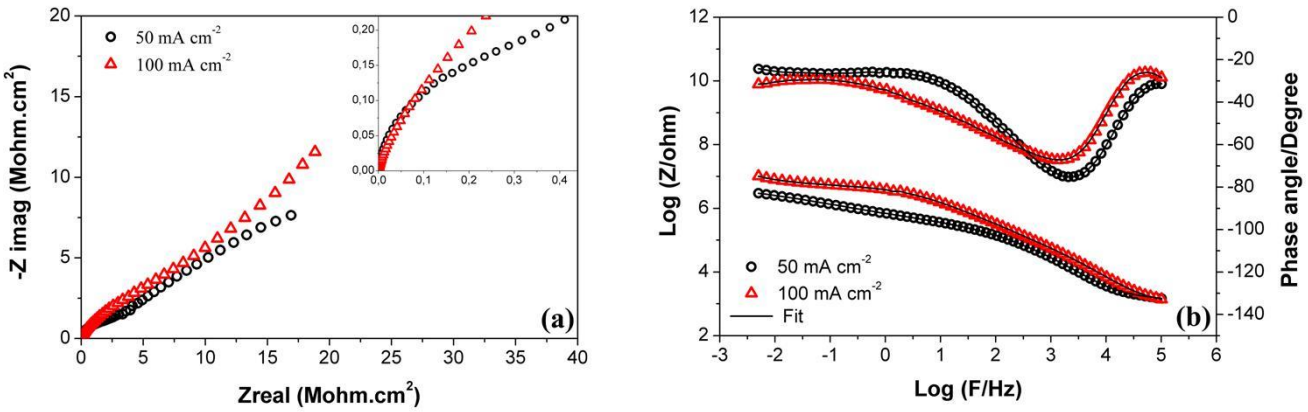

Figure 31. (a) Nyquist and (b) bode diagrams of the coatings obtained on Ti c.p in P solution under galvanostatic conditions

Table 8. Electrical parameters of the coatings obtained on Ti c.p by the fitting of the EIS experimental results

Anodizing condition	Electrical parameter provided by the EIS fitting									
	R_p	R_b	R_{tc}	C_p	n_p	C_b	n_b	C_{dc}	$Z_{f=0.005}$	Goodness of
	(KΩ cm^2)	(MΩ cm^2)	(MΩ cm^2)	(μF cm^2)		(μFcm^{-2})		(μF cm^{-2})	(MΩ cm^2)	fit x 10^{-4}
50 mA cm^{-2}	18.61	3.98	29.01	0.065	0.52	0.041	0.91	0.15	430.29	3.19
100 mA cm^{-2}	23.86	0.138	17.94	0.025	0.73	0.161	0.75	29.24	479.58	4.49

3.2.4. Discussion

SEM micrographs of the anodic films obtained evidenced the formation of porous layers. The porosity of the coatings produced by the anodizing technique is due to the formation of sparks during the formation process of the coating. It is well known that during plasma electrolytic oxidation, sparks instantaneously increase the temperature causing local melting of the coating. Some researches by OES have been found that sparks have different local temperatures [14], [147], [148]. The inner region has a higher temperature than the outer

region and the size of the sparks changes according to the process parameters. After the sparks are formed, the coating is cooled by the electrolytic solution which leads to the formation of a porous structure [14], [149]–[153]. Different researchers have reported duplex structures composed of a dense inner layer and a porous outer layer [57], [63], [114]. This duplex structure was evidenced both in EIS and SEM analysis. Moreover, the thickness of the inner layer depends on the intensity of the micro-discharges. A higher intensity of the micro-discharges generates deeper pores (type B) than micro-discharges with low intensity (type A, C), according to the micro-discharges model proposed by Hussein et al [117]. The coatings obtained at low current density have an inner layer thicker than that of coatings obtained at higher current density due to the changes in the micro-discharges intensity. The XRD analysis shows that anatase phase is the only crystalline structure present on the coatings obtained at 50 mA cm^{-2}. Nevertheless, the increase of the current density leads to the formation of minor proportions of rutile phase into the coating due to the formation of sparks with higher intensity and size (**Fig.** 28). The increase in the characteristic bands of the anatase phase by increasing current density is clearly related to the increase in the coating thickness (**Fig.** 27). However, there are not crystalline species different to titanium dioxide, despite that EDS analysis showed the incorporation of phosphorus ions on the coating from the anodizing solution. Other researchers found by XPS the incorporation of phosphate ion species ($H2PO^{-}_{4}$, HPO^{-2}_{4}, PO^{-3}_{4}) into the coating from the solution [154], [155].

SEM micrographs show that pore diameter increases as current density increases. These changes in pore size are related to the increase of sparks size as the cell potential increase, which has been evidenced by other authors [154], [156]. Cross-section SEM micrographs

show that coating thickness increases when current density gets higher, both in the inner layer and the porous layer (**Fig.** 27). Increase in the curve slope in the region I (**Fig.** 26) and the increase in the time necessary to reach a constant value (region III), indicate a rise in the kinetics of the anodizing process. For this reason, the anodic coatings obtained at higher current density are thicker. This behavior has been also reported when using other electrolytic solutions [149], [157]. Analysis by EIS of the galvanostatic coatings evidenced the structural changes of the coating. In **Table** 8, it was observed that R_b is higher than R_p, indicating that the resistance of the coating mainly depends on the inner layer, as has been noted in previous chapters. Regarding the porous layer, the increase of R_p is due to the increase of the coating thickness when the current density is increased (**Fig.** 27). For the same reason, the capacitance of the porous layer (C_p) decreases with current density. With respect to the inner layer, it is observed that R_b decreases when the current density gets higher; indicating a decrease in the thickness of the inner layer, which also explains the ascending behavior of C_b. In the cross-section images the decrease in the thickness of the inner layer is evidenced, which affects the tribological behavior. The formation of voids near the coating or the formation of a thin inner layer reduced the adhesion of the coating and therefore the mechanical and wear properties, as was evidenced in the pin-on-disc tests (**Fig.** 29). The charge transfer resistance represents the inner layer blocking of electron transfer. A similar behavior is shown by R_{tc} and C_{dc}. Finally, the impedance module increases when current density gets higher, due to the increase of coating thickness. Moreover, the frequency changes in the time constants reflect the changes on the coatings dielectric properties. The parameter n_p of the CPE could be related to the heterogeneity of the porous layer across the thickness of the coating. **Table** 8 shows that n_p exhibit significant changes, indicating that the

heterogeneity of the porous layer is similar for the galvanostatic coatings. Likewise, n_b is similar for all the coatings obtained at galvanostatic conditions, which could indicate that the roughness in the metal-oxide interface increases with the current density. The increase of intensity and size of the sparks due to the increase of the current density is not beneficial for the inner layer due to the formation of deep pores which increases the roughness of the metal-oxide interface, as has been widely reported [78], [116]. Finally, the increase in the current density decreases the wear rate of the coatings due to the formation of voids and pores near the coating base. When the current density increases, the formation of sparks with higher intensity and size reduces the inner layer thickness and affects the metal-oxide interface, increasing the roughness in the interface. These facts affect the mechanical and tribological properties of the coatings due to the adhesion of the coating depends on the inner layer and the chemical composition of the coatings. The morphology changes can be related to changes in size, frequency and the intensity of the sparks during the anodizing process, and these spark characteristics depend on the anodizing parameters used to obtain the coating.

3.2.5. Conclusions

Anodic films homogeneously distributed were obtained on titanium c.p, which presents a duplex structure, with an outer porous layer and a compact inner layer. Anatase is the crystalline phase found in the coatings, while the presence of rutile in minor proportions is evidenced at a high current density. Phosphorous and other species from the anodizing solution was evidenced from the EDS analysis, nonetheless, only the formation of titanium oxide was observed. Circular pores are observed in the anodic films obtained, which exhibit surface morphological changes depending on the applied current. The inner layer has a greater influence on the resistance of the coatings as well as on the tribological performance of the coatings, showing an increase in the wear rate when the current density gets higher.

3.3. Effect of pre-anodizing on the tribological and corrosion properties of titanium alloy following plasma electrolytic oxidation under potentiostatic conditions

3.3.1. Introduction

Alkaline solutions have been studied extensively on titanium alloys in order to obtain coatings with good wear resistance. Nevertheless, coatings obtained in alkaline solutions are generally thick coatings ≥ 10 μm [25], [61], [87], [125], [144], [158]. In some applications, the formation of thin coatings with good wear performance and corrosion are required, such as screws and pistons. Moreover, the formation of thin coatings allows reducing residual stress, improving the adhesion of the coatings to the substrate and the possibility to apply the anodizing process on parts where the over-sizing is not allowed. Of the modes for PEO coating formation, the coatings formed under potentiostatic conditions allow the growth of thin coatings due to a lower charge density applied, which also generates micro-discharges smaller than in the galvanostatic mode (**Fig.** 15). Smaller micro-discharges have low intensity and energy, which also allow controlling the thickness, the porosity and the formation of homogenous coatings, it also improves the corrosion protection of the coatings [78]. In previous chapters, it was found that coatings obtained under potentiostatic conditions exhibit better tribological performance and corrosion resistance than coatings obtained under galvanostatic conditions. To obtain a coating under potentiostatic conditions a short galvanostatic stage is necessary as the first stage of anodizing before reaching the definite potential. In literature reports, the effect of this pre-anodizing stage on the tribological and corrosion properties for the potentiostatic coatings has not been studied widely. The aim of

this section is to evaluate the effect of the initial current density applied in coatings formed under potentiostatic conditions, especially on the coating wear and corrosion properties. Coatings obtained with a lower current density at the initial stages of anodizing exhibit a better wear and corrosion resistance due to the low-density of voids and pores near the coating base.

3.3.2. Experimental

The coatings were obtained on Ti6Al4V alloy in a solution composed by $NaAlO_2$ 12.24 g l^{-1} and $Na_2SiO_3.9H_2O$ 1g l^{-1} with a pH of 13.74 and a conductivity of 12.32 mS cm^{-1}. The coatings were obtained under potentiostatic conditions at a constant potential of 400 V. A short galvanostatic stage is necessary before to reach the specified potential value; then, the potentiostatic control anodizing is carried out. In this research, three current densities were applied during the short galvanostatic stage as a pre-anodizing process before changing to the potentiostatic mode. The current densities evaluated were 100, 150 and 200 mA cm^{-2}, which were higher than that needed to obtain sparking. The characterization of the coatings was carried out under the same conditions as mentioned in Chapter 2.

3.3.3. Results

Current-time and charge density-time curves for anodizing on Ti6Al4V alloy are shown in **Figs.** 32(a) and (b) respectively. The typical behavior of the PEO process is revealed in all conditions (**Fig.** 32a). The curves reveal three different regions during the anodizing process. First, a sudden rise of the current is observed until reaching the current density established (100, 150 or 200 mA cm^{-2}). Then, the current remains the same until the system reached 400

V and the potentiostatic control begins, followed for a sharp decreased of the current. In this stage, the higher the current density applied, the lower the necessary time to change to the potentiostatic control, being 120 s for the coating obtained with 100 mA cm^{-2}, 45 s for the coating formed with 150 mA cm^{-2} and 35 s for the coating obtained with 200 mA cm^{-2} as pre-anodizing process. Evolution of gas and formation of small micro-discharges on the metal surface were evident at ~ 300 V, which occurs in the first seconds of the process (~ 20 s). In the potentiostatic control, the current exhibits small variations until the end of the process and the density and size of micro-discharges remain constant. In all conditions, the charge density applied during the whole process showed similar values despite the different pre-anodizing processes before the potentiostatic control. For the coating obtained at 100 mA cm^{-2}, the charge density applied in the pre-anodizing stage is higher than in the other conditions; nevertheless, the charge applied to the other conditions is higher in the first seconds of the process (**Fig.** 32b). Potential time responses for the coatings obtained are observed in **Fig.** 32 c. First, the potential increases until reach 400 V and after this, the potential remains constant until the end of the process. The time to reach the constant potential is related to the time to change to potentiostatic mode after the short galvanostatic period as observed in **Fig.** 32a.

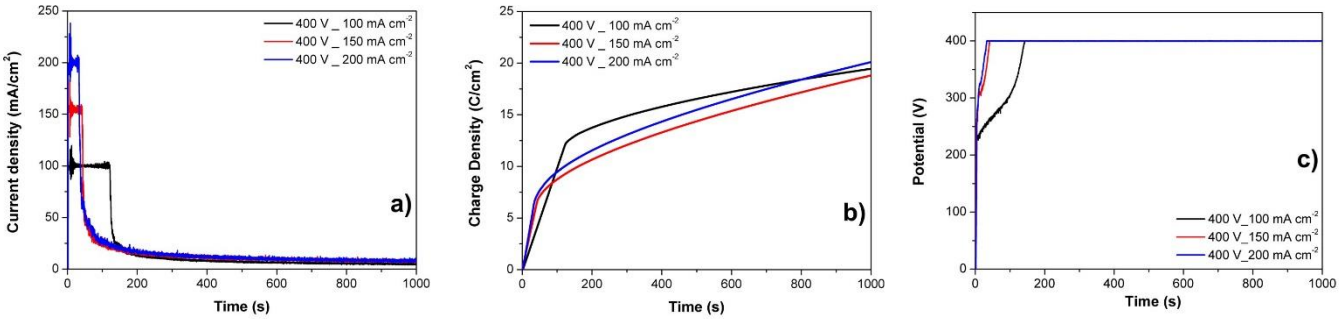

Figure 32. (a) Current-time and (a) charge density-time response for anodizing on Ti6Al4V alloy in Al-Si solution at 20 ºC degrees.

Top views of the coatings at different times of the process and cross-section views of the coatings on Ti6Al4V alloy are shown in **Fig.** 33. SEM images reveal the formation of a porous coating characteristic of the PEO process. Circular pores, homogeneously distributed, are observed in all the anodizing conditions. A lower surface porosity is observed in the coating formed at 100 mA cm^{-2}. The analysis of the morphology with anodizing time shows that the topography and morphology of the coatings do not change significantly. Nevertheless, a homogenization of the structure and the formation of some coalescent pores are observed (The first SEM image corresponds to the time at which potentiostatic control begins). The changes in the coating porosity with the pre-anodizing process are evidenced in the cross-section views for the coatings obtained during 1000 s. The formation of voids and pores near the coating base is evident for the coatings formed at higher current density (200 mA cm^{-2}), while a dense coating was formed under the condition of 100 mA cm^{-2} as pre-anodizing process. All the coatings show a similar roughness value of ~ 398.55 nm as was assessed by profilometry.

The thickness of the coatings formed is shown in **Fig.** 34. The coating thickness at 100 mA cm^{-2} at different times assessed by eddy current is shown in **Fig.** 34a. A similar behavior

is observed for the other conditions. During the pre-anodizing, the coating grows at a higher rate than in the potentiostatic control. In the potentiostatic mode, the coating thickness exhibits a linear increase with time until the end of the process. In all anodizing conditions, the coating thicknesses show similar values despite the different pre-anodizing processes (**Fig.** 34b).

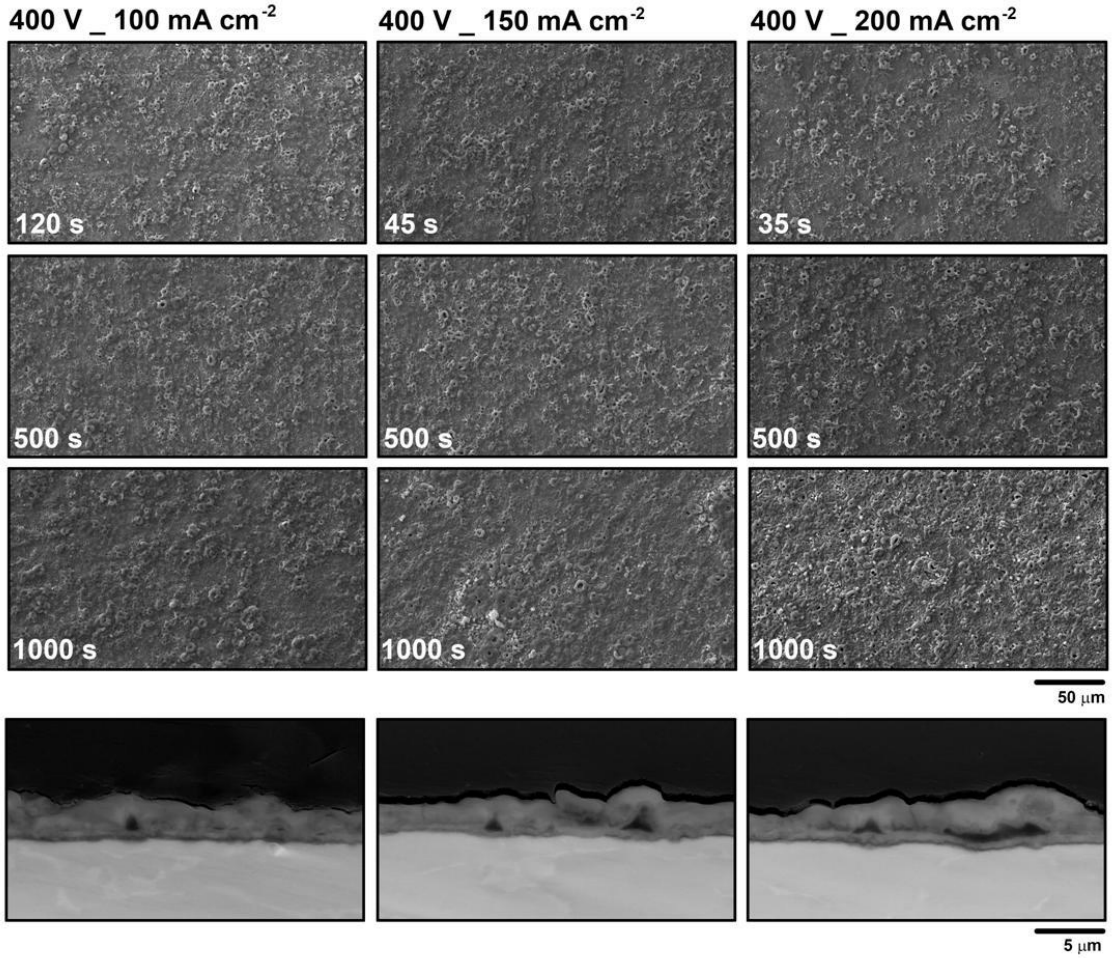

Figure 33. Top and cross-section views of the coatings obtained on Ti6Al4V alloy in Al-Si solution

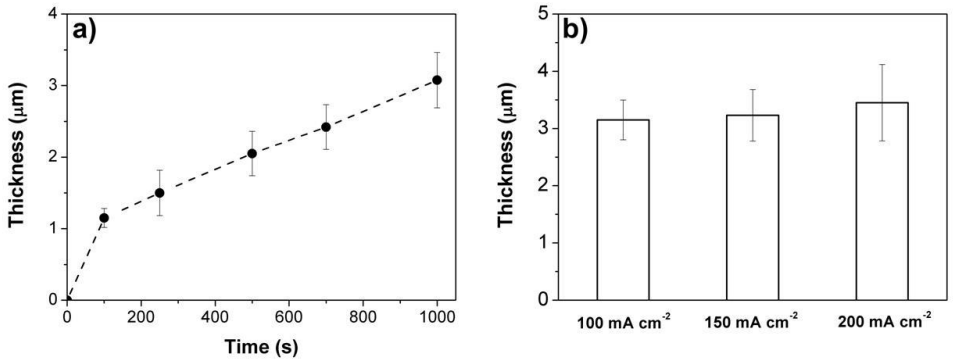

Figure 34. (a) Thickness of the coating on time for the coating obtained at 400 V with a current density of 100 $mAcm^{-2}$ applied as a pre-anodizing process and (b) thickness of the coatings formed assessed from the cross-section images

The crystalline phases in the coatings characterized by XRD are shown in **Fig.** 35. The chemical composition of the coatings is mainly γ-Al_2O_3, α-Al_2O_3 and Al_2TiO_5. All the coatings have the same chemical composition despite the different galvanostatic pre-anodizing processes. The XRD spectra in different times of anodizing do not show changes in the chemical composition of the coatings and the same behavior is observed for all anodizing conditions. It is evidenced that the coatings are crystalline from the first stages of the process (between 35 to 120 s).

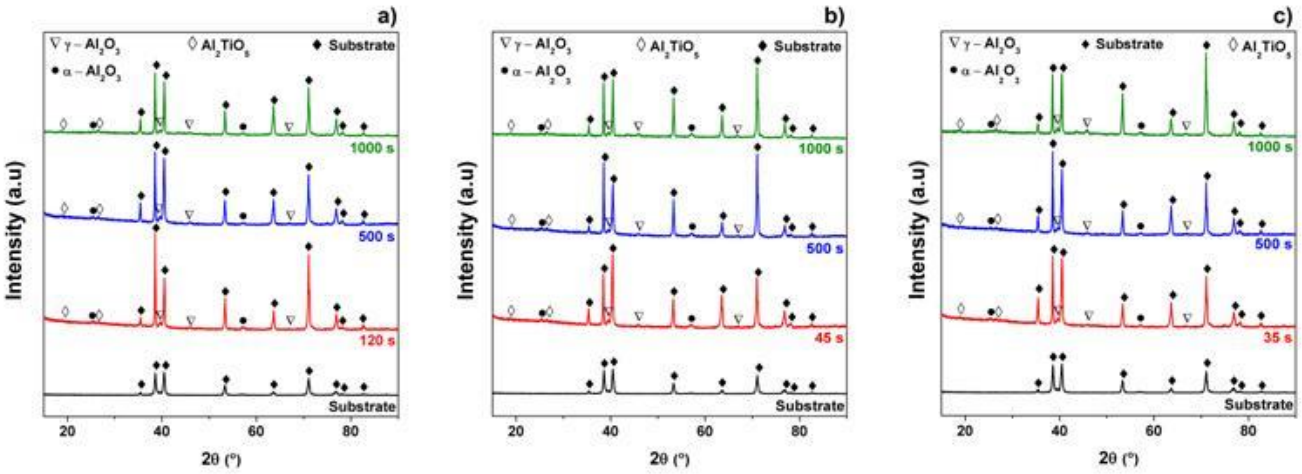

Figure 35. XRD spectra of the coatings obtained at 400 V on Ti6Al4V alloy under the followings pre-anodizing condition (a) 100 mA cm^{-2}, (b) 150 mA cm^{-2} and (c) 200 mA cm^{-2}

The friction-distance responses for all anodizing conditions are shown in **Fig.** 36. In all anodizing conditions, an initial increase of the friction coefficient up to 0.5 is observed and then the friction coefficient increases gradually until the end of the test. In this test, the effect on the wear resistance of the different galvanostatic pre-anodizing processes was evaluated; therefore, the test was stopped at the moment at which a friction coefficient change was observed; sudden changes in the friction coefficient are related to the coating failure. However, SEM images before and after the coating failure were taken in order to confirm the above statement as observed in **Fig.** 37. Pin-on-disc tests reveal that pre-anodizing at 100 mA cm^{-2} gives a better wear performance, with the coating failing at longer sliding distances ~ 215 m (**Fig.** 36a) and decreases with the increase of the current density applied at initial stages (**Figs.** 36 b-c). Wear rate was calculated for the sliding distance before coating failure and are summarized in **Table** 9. Nevertheless, for the coating formed at 200 mA cm^{-2}, the

wear rate was not calculated given that the coating failure was observed in the first minutes of the test. The appearance of the wear track before the coating failure is observed in the SEM image in **Fig.** 36d and the optical image shows the appearance of the counter-body after the wear test, where abrasion wear is observed (**Fig.** 36e).

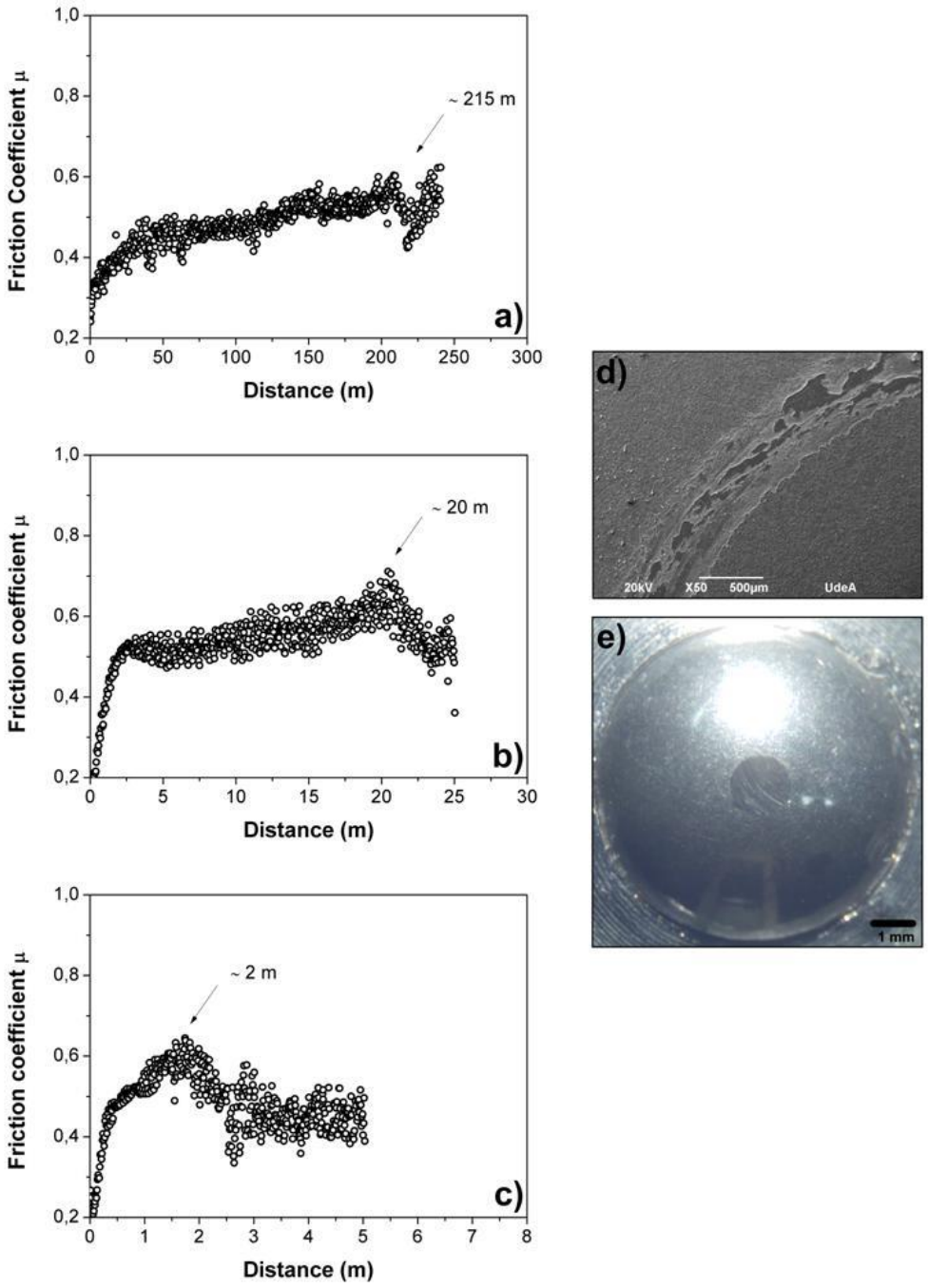

Figure 36. Friction-time response for the coating obtained under the following pre-anodizing condition (a) 100 mA cm^{-2}, (b) 150 mA cm^{-2}, (c) 200 mA cm^{-2}, (d) The appearance of the wear track before the coating failure and (e) optical image of the counter-body after the wear test.

SEM images of the wear tracks after the tribological tests are shown in **Fig.** 37 and the summary of the wear properties are listed in **Table** 9. The lowest wear rate is for the coating obtained when pre-anodizing at 100 mA cm^{-2} due to a longer sliding distance before the coating failure occurs (**Table** 9). In all the anodizing conditions, the main wear mechanisms of the coatings are fatigue and adhesion (**Figs.** 37 a, e). After the coating failure, abrasion is observed as a wear mechanism, which is characteristic of the substrate. The SEM images confirm that the sudden changes in the friction coefficient are related to the coating failure. Adhesion of the counter-body particles was confirmed by elemental mapping (**Fig.** 37d) on the wear track of the coating obtained with a pre-anodizing of 100 mA cm^{-2} (**Fig.** 37a). In the elemental mapping, the aluminum signal is reduced due to the presence of iron on the wear track, while the oxygen signal shows a homogenous distribution, indicating that the wear test does not reach the substrate.

Table 9. Summary of the wear properties of the coatings on Ti6Al4V alloy

Anodizing condition	Sliding distance	Wear rate (Kg/N.m)	Friction coefficient average	Wear mechanism
400 V _ 100 mA cm^{-2}	200 m	$6.75 \pm 1.06 \times 10^{-12}$	0.5	Fatigue Adhesion
400 V _ 150 mA cm^{-2}	15 m	$9.21 \pm 1.62 \times 10^{-7}$	0.5	Fatigue Adhesion
400 V _ 200 mA cm^{-2}	---	---	~ 0.5	---

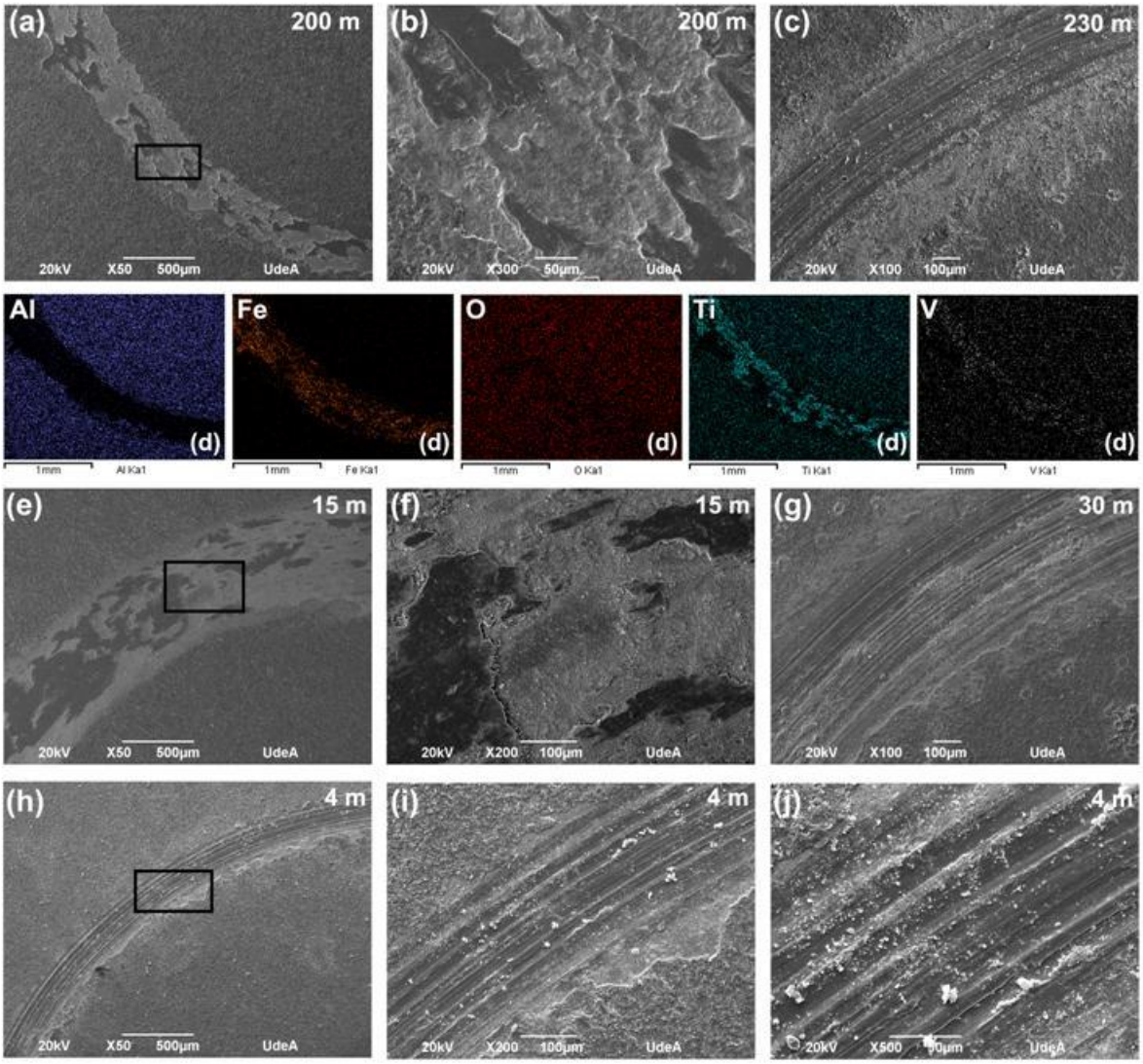

Figure 37. Wear tracks of the coating formed applying 100 $mAcm^{-2}$ as pre-anodizing process (a,b) before and (c) after the coating failure. (d) EDS elemental mapping of the coating obtained at 100 $mAcm^{-2}$ (Fig. 6a). Wear tracks of the coating formed applying 150 $mAcm^{-2}$ as pre-anodizing process (e,f) before and (g) after the coating failure. (h,i,j) Wear tracks of the coating obtained applying 200 $mAcm^{-2}$ as a pre-anodizing process after the failure coating.

Nyquist and bode diagrams of the coatings obtained on Ti6Al4V alloy are observed in **Fig.** 38. Bode diagrams show two capacitive arcs due to the formation of a coating with a dual structure (an outer porous layer and a dense inner layer). The literature reports that the

first capacitive arc is related to the porous layer (**Fig.** 38a inset) and the second capacitive arc relates the inner layer and the relaxation of the electrical double layer. EIS analysis reveals that the anodic coating formed with a pre-anodizing process of 100 mA cm^{-2} exhibits a higher corrosion resistance than the other coatings, as evidenced in **Figs.** 38 a-b. Bode diagrams (**Fig.** 38b) show changes mainly in the time constant related to the inner layer, especially for the coating obtained at 100 mA cm^{-2} as pre-anodizing. EIS results were analyzed using the equivalent circuit that has been described in a previous chapter[80]. Constant phase elements (CPE) were used for simulation of the experimental results in the equivalent circuit. The effective capacitances were calculated from the parameters of the CPE according to the relationships reported by Hirschorn et al [68]. Results of the fitting are shown in **Table** 10; where, R_p is the porous layer resistance, R_b is the inner layer resistance, Rtc is the charge transfer resistance, C_p is the capacitance of the porous layer, C_b is the capacitance of the inner layer, C_{dc} is the capacitance of the electrical double layer and n is one of the parameters of the CPE. Bode diagrams in **Fig.** 38b show a good correlation between experimental and simulated data (see goodness of fit values in Table 10).

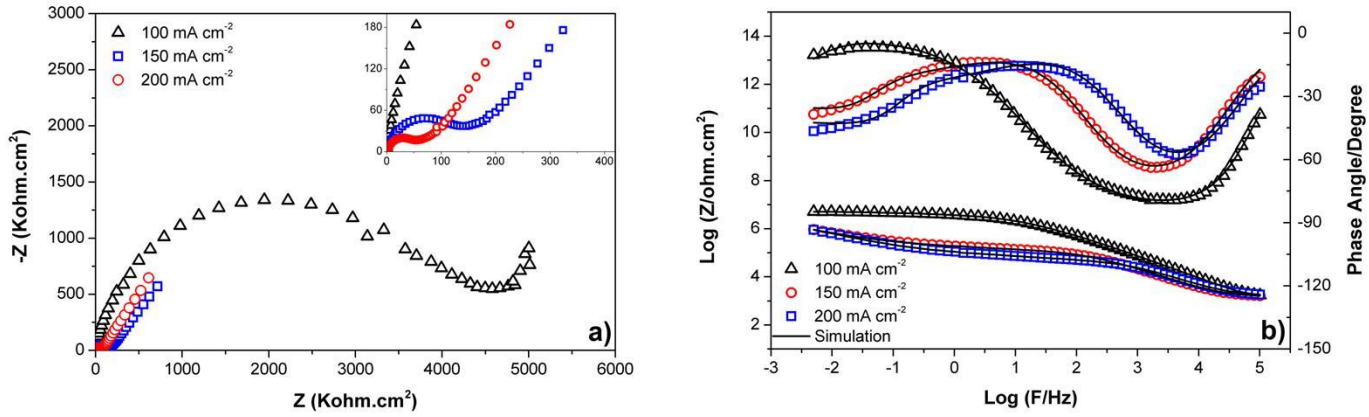

Figure 38. (a) Nyquist and (b) bode diagrams of the coatings obtained on Ti6Al4V alloy

Table 10. Electrical parameters of the coatings obtained on Ti6Al4V alloy by the fitting of the EIS experimental results using an equivalent circuit

Pre - anodizing condition	Electrical parameter provided by the EIS fitting									
	R_p ($K\Omega\ cm^2$)	R_b ($M\Omega\ cm^2$)	R_{tc} ($M\Omega\ cm^2$)	C_p ($\mu F\ cm^{-2}$)	n_p	C_b ($\mu F\ cm^{-2}$)	n_b	C_{dc} ($\mu F\ cm^{-2}$)	$Z_{f=0.005}$ ($M\Omega\ cm^2$)	Goodness of fit x 10^{-4}
100 mA cm^{-2}	32.49	21.06	26.54	0.030	0.81	3.97	0.47	10.70	431.73	0.46
150 mA cm^{-2}	18.93	0.12	0.39	0.050	0.83	13.25	0.44	24.41	0.72	4.26
200 mA cm^{-2}	8.05	0.06	0.18	0.069	0.82	14.03	0.46	17.87	0.61	8.62

3.3.4. Discussion

Thin coatings with good wear-resistance and corrosion protection were formed under a pre-anodizing of 100 mA cm^{-2} due to the formation of dense coatings. The coatings are composed of Al_2TiO_5, γ - Al_2O_3 and α - Al_2O_3. Despite the different pre-anodizing process, the charge density applied is similar in all the coatings, which leads to the formation of coatings with similar composition and thickness. Al_2O_3 is formed into the coating due to the incorporation of aluminum and the high temperatures developed during the PEO process. The eutectic reaction between Al_2O_3 and TiO_2 leads to the formation of the Al_2TiO_5 phase, as has been described in the growth mechanisms of coatings formed in aluminate solutions [1], [29], [89], [126]. The formation of micro-discharges at early stages of anodizing allow the crystallizing of the coating in the first stages of the process (**Fig.** 35). Nevertheless, after the potentiostatic control starts, neither the size nor the intensity of the micro-discharges changes

significantly; so the composition of the coatings is the same during all the process, given that the low energy of the micro-discharges does not lead to the formation of new crystalline phases. The coating thickness growth rate is higher during pre-anodizing (**Fig.** 34) since a high percentage of the charge density is applied during this stage of the process (**Fig.** 32). After this, a linear growth in both the charge and the thickness is revealed.

The pre-anodizing process has an important effect on the corrosion protection and wear due to the control of the porosity. The increase of the current density in the first galvanostatic stage leads the formation of voids and pores near the coating base due to the formation of larger micro-discharges in this stage (**Fig.** 33). Large micro-discharges contribute to the formation of deep pores, increasing the porosity through the coating. Dense coatings have a better behavior against corrosion (**Fig.** 38) and wear (**Fig.** 36) as was evidenced in this work, in agreement with other researches [61], [116], [122]. The formation of voids and pores near the coating base reduce the adhesion of the coating, affecting its tribological performance as well as its corrosion protection. The protection against corrosion by the anodic coatings depends mainly on the dense inner layer, as observed in the electrical parameters of the coatings (**Table** 10) [57], [63], [114]. The internal changes into the coatings are also evidenced in the electrical parameters calculated by fitting the EIS results. R_b and R_p are higher for the coating obtained at 100 mA cm^{-2} and decreases with the current density applied, consequently causing the increase of C_b and C_p, due to the increase in the porosity with the current density. Rtc represents the inner layer blocking the electron transfer. Therefore, R_{tc} and C_{dc} show a similar behavior than R_b and C_b. The parameters of the CPE n_b and n_p have similar values for all the coatings, indicating a homogenous distribution of the porosity

through the coating (n_p) and the formation of a rough surface in the metal-oxide interface (n_b). In the present work, it has been found that a pre-anodizing at 100 mA cm^{-2} during the formation of coatings under potentiostatic condition allows the formation of dense coatings that exhibit a better performance against corrosion and wear. At higher current densities, at the first stages, micro-discharges of higher size are formed, inducing the formation of voids and pores near the coating base, which influences the final properties of the coatings.

3.3.5. Conclusions

Anodic coatings were obtained on Ti6Al4V alloy under potentiostatic conditions using different pre-anodizing conditions. The pre-anodizing process has a significant effect on the corrosion protection and wear due to the change in the porosity distribution in the coating. The formation of coatings at low current densities allows the formation of dense coatings, which exhibit a better corrosion protection and wear resistance. The increase in current density leads the formation of voids and pores near the metal-oxide interface, which affects their final properties. The coatings are mainly composed by Al_2O_3 and Al_2TiO_5 due to the incorporation of aluminum and the high temperature obtained during the spark anodizing. The anodizing under potentiostatic conditions does not generate micro-discharges with high intensity and temperature, therefore, the chemical composition of the coatings does not change significantly during the anodizing time. Nevertheless, an increase in the coating thickness and homogenization of the morphology was observed during the time of anodizing. The porosity changes in the coating are correlated with changes in the electrical parameters of the coating, which were calculated by fitting the EIS experimental results.

3.4. Effect of the anodizing solution on the micro-discharges behavior during PEO process

3.4.1. Introduction

PEO involves anodizing at potentials above the dielectric breakdown of the coating. During the process, short-lived micro-discharges are generated on the surface of the material, accompanied by gas evolution. Local heating and internal compressive stresses generate crystallization of the anodic coating, whilst ionic incorporation alters both chemical composition and crystalline structure of the oxide [128], [159]. According to literature reports, the formation mechanism, the morphological changes and some properties of the coatings are influenced by the characteristics and distribution of the micro-discharges during the anodizing process. In addition to the electrical parameters, the anodizing solution has a significant effect on the size and the energy of the micro-discharges during PEO anodizing given that the species in the solution could be dissociated and interact in plasma reactions modifying the plasma characteristics [78], [142], [151], [157], [160]. In this section, the plasma characteristics in different solutions are compared with the electrical parameters of the coatings obtained.

3.4.2. Experimental

The coatings were obtained on Ti6Al4V alloy under the conditions listed in Table 11. The coatings were obtained under galvanostatic conditions at a constant current of 50 mA cm^{-2}. The current density evaluated was higher than that needed to obtain sparking during the

process. The characterization of the coatings was reported in Chapters 1 and 2. The total capacitance of the coating is the sum ($C_T = C_p + C_b$) of the inner layer capacitance and the outer layer capacitance given that these capacitances are in parallel. The inner layer capacitance is higher than the outer layer capacitance, therefore, the total capacitance of the coating is approximately the inner layer capacitance. A thicker and denser inner layer obtained in the coating obtained in P-Si solution generates a low capacitance in the coating. For the coating obtained in Al-Si solution, the high capacitance value is due to the formation of a thin inner layer, although this coating is thicker.

Table 11. Solution concentrations and electrical parameters used to obtain the anodic coatings on Ti6Al4V alloy

Solution ID	Solution concentration (g L^{-1})	pH	Conductivity (mS cm^{-1})	Charge Applied (C cm^{-2})	Total coating capacitance (F/cm^2)
P	NaH_2PO_2 : 10 $EDTANa_2$: 7.4 $(CH_3COO)_2Ca$: 1.8 NaOH : 4.0	14	22.3	30	1.73 x 10^{-6}
P - Si	NaH_2PO_2: 10.0 Na_2SiO_3: 5.0	13.7	10.77	50	1.42 x 10^{-11}
Al - Si	$NaAlO_2$: 12.2 $Na_2SiO_3.9H_2O$: 1.0	13.74	12.32	50	1.70 x 10^{-5}

3.4.3. Results

Figure 39 shows the micro-discharges appearance for the conditions listed in **Table** 11. The size and shape of the micro-discharges are related to the species in the solution. In P

solution, the size of the micro-discharges is smaller than in the other solutions; in addition, shows a white color, while in the P-Si solution, the formation of micro-discharges with a yellow color and a larger size is evident. Like in the P-Si solution, in the PEO process in aluminate-based solutions, the micro-discharges are bigger than in the P solution; besides, has a circular shape and a yellow color. The coating capacitance, obtained from the electrical parameters by the fitting of the experimental EIS results, (**Tables** 3 and 6), evidences a relationship with the PEO behavior. The coating capacitance depends on the chemical composition, structure, and the coating thickness, for that reason the coating capacitances changes as a function of the solution composition (**Table** 11). Consequently, the differences in the coatings capacitance could induce differences in the intensity and duration of plasma sparks (Fig. 39). In the coating obtained in the aluminate-based solution, the formation of sparks with large size is due to the formation of thick coatings given that when the thickness increases, the voltage value increases and the number of sparks reduce. However, the intensity of the spark is increased due to the higher energy required for the rupture of the thick coating [1][61]. Nevertheless, in the coatings obtained in P-Si solution, a high density and intensity of the sparks were evidenced experimentally (see **Fig.** 39). The high density and intensity of the sparks could be related to the release of energy due to the low capacitance values. For that reason, in this solution, the coatings obtained reveals low porosity. The more compact and thicker the inner layer (low capacitance values), the lesser energy is required to electrically charge the coating and higher energy will be released during the plasma process through formation of sparks. Experimentally was found that the thickness of the coatings depends on the solution composition (**Fig**. 40).

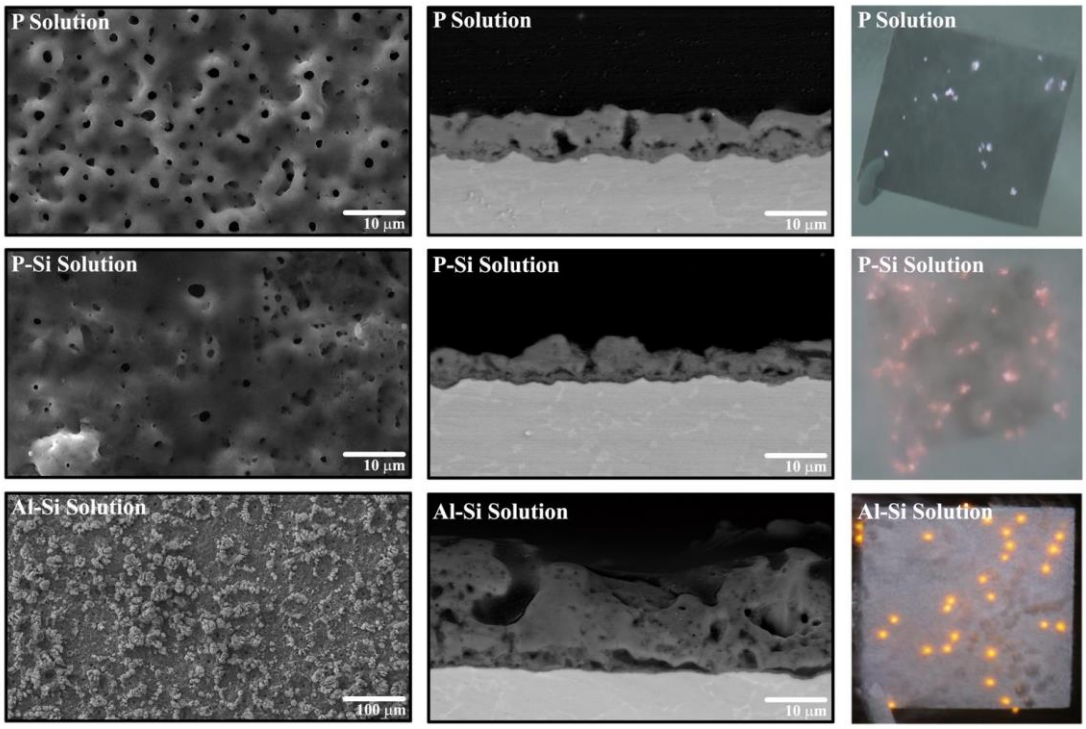

Figure 39. Top and cross-section views of the coatings obtained in different alkaline solutions at 50 mA cm^{-2} and the micro-discharge appearance for each solution respectively

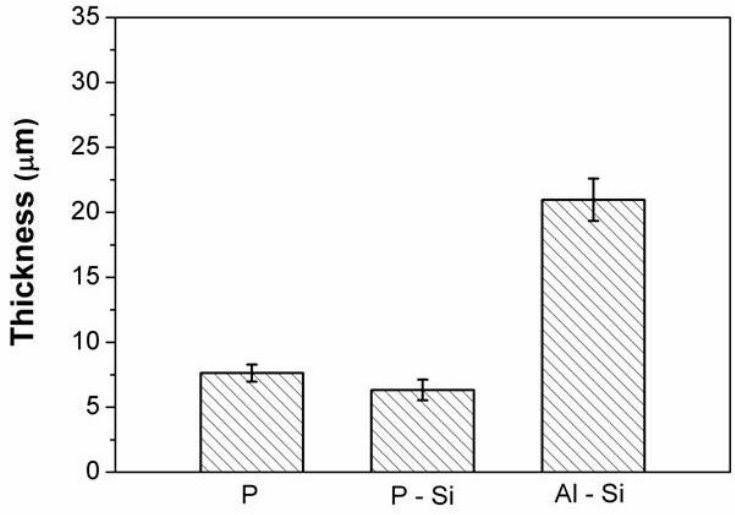

Figure 40. Thickness of the coatings obtained in different alkaline solutions

3.4.4. Conclusions

In PEO process, the size and intensity of the sparks influence the morphological characteristics of the coatings during the formation process. The plasma characteristics are influenced for the coating capacitance, which depends on the chemical composition of the coating, the thickness, and the coating structure. The incorporation of species into the coating modifies the coating capacitance modifying the PEO behavior (**Table** 11). In the coatings obtained in aluminate-based solution, the formation of large micro-discharges due to the higher energy required for the rupture of the coating that reduces the number of sparks on the surface but increases the intensity and size. Coatings with low capacitance (P-Si coating) generate the formation of sparks with high density and intensity given that the energy required for coating charging will be significantly lower, forcing the system to release a greater amount of energy by plasma formation, generating the formation of a dense coating. Although in this work a relationship between the electrical properties of the coatings and the plasma behavior is proposed, additional works are required in order to establish a better relationship between the plasma features and the coating characteristics, allowing a better control of the coating properties.

4. Chapter 4

Formation mechanism of the anodic coatings obtained in alkaline solutions by PEO

Abstract: The growth mechanism of coatings obtained by PEO in alkaline solutions was studied by means of SEM, EDS and XRD. Anodic coatings were obtained both on Ti c.p and Ti6Al4V alloy. In the solution based on sodium hypophosphite, the growth mechanism for the coating obtained in both substrates has a similar behavior. On the other hand, the coatings obtained in a sodium aluminate-based solution with the addition of sodium metasilicate have a different growth rate due to the abundant gas evolution produced in the anodizing process on Ti c.p. Thicker coatings were obtained on Ti6Al4V alloy, and EDS analysis reveals the incorporation of elements from the solution into the coating, showing an increase in the concentration with the time of process. The anodizing process under potentiostatic conditions allows controlling the size of the micro-discharges and the pore density of the coatings, however, the energy and intensity of small

micro-discharges do not allow the formation of crystalline phases which require high energy and temperature.

Keywords: PEO, titanium alloys, growth mechanism, anodic coatings, growth mechanism

4.1. Introduction

At the beginning of the PEO process, the coating formation is a classical anodizing process resulting in growth of a layer of several hundreds of nanometers, generally with an amorphous structure. After the process reaches the breakdown potential, the formation of micro-discharges on the surface of the material is evidenced. In this growth stage, complicated physical-chemical reactions are carried out, which implies the reactions between the substrate elements and the species in the solution, the formation of short-lived micro discharges, surface-connected porosity in the coatings and individual discharges occurring in clusters [161]–[165]. When a high voltage is applied to a metal, a continuously moving micro-discharge occurs on the metallic surface and an excessive gas evolution compared with faradic oxidation processes. Meanwhile, the coating thickness increases continuously up to hundreds of microns. The coating growth can be divided into two keys processes: the micro-discharge mechanism and the coating growth mechanism [166]. Currently, three models of formation of the micro-discharges have been proposed which explains the formation of the sparking phenomenon during PEO anodizing. The first model regarded the micro-discharges as a local breakdown avalanche of a solid insulating coating [167], [168]. The second model considers that the initial discharge is first ignited in the gas bubbles between the coating and the solution and then it induced the breakdown of the dielectric barrier layers [169], [170]. The third model [166] considered each micro-discharge

as a gas discharge occurring in a micro-pore of the oxide film, which is believed to be induced by an initial dielectric breakdown of a barrier layer at the bottom of the micro-pore. Studying the micro-discharges mechanism require characterization techniques and equipment that helps to analyze the formation, composition and lifetime of the micro-discharges in order to correlate it to the coating formation. The analysis of micro-discharges is beyond the scope of this study.

In this section, the coatings growth mechanism was analyzed, studying the initiation, formation, and growth of the coatings at different times of the anodizing process. The morphology and compositional evolution of the coatings that showed better corrosion resistance and tribological performance by means SEM, XRD, OES were analyzed here.

4.2. Experimental

The anodizing process was carried out as was mentioned in Chapters 1 and 2. The anodizing solutions and the electrical parameters listed in **Table** 12, were the anodizing conditions that exhibited better corrosion resistance and tribological performance. Two electrochemical conditions were used to obtain the coatings, namely galvanostatic mode and potentiostatic mode as was described in previous chapters.

XRD, SEM and EDS characterization was carried out using the same conditions mentioned in previous chapters. Light emission of the discharges was collected using an optical emission spectroscope (USB4000 Ocean Optics), with an optical fibre immersed in the solution, and located a few centimeters from the specimen surface in order to optimize the collected light intensity and to reduce absorption from the bath. The solarization-resistant optical fibre (ZFQ-9596, Ocean Optics) with PVDF sleeving and a PEEK ferrule (1/4 in. in diameter and 3″ in length) was of 1000 μm diameter, with a numerical aperture of 0.22±0.02. Emission spectra were studied in the wavelength range 200–900 nm with a spectral resolution of 1 nm.

Table 12. Solution concentrations and electrical parameters used to obtain the anodic coatings.

Solution ID	Solution concentration (g L^{-1})	Conductivity (mS cm^{-1})	Substrate	Anodizing parameters	Charge density (C cm^{-2})	Thickness (µm)	Growth rate (µm min^{-1})
P - Si	NaH_2PO_2: 10.0 $Na_2SiO_3.9H_2O$: 5.0	10.7	Ti c.p	50 mA cm^{-2}	20.83 C cm^{-2}	5.42	0.36
			Ti6Al4V			8.13	0.54
			Ti c.p	400 V	15.83 C cm^{-2}	3.72	0.25
			Ti6Al4V			5.18	0.35
Al - Si	NaAlO2 : 12.2 $Na_2SiO_3.9H_2O$: 1.0	17.2	Ti c.p	50 mA cm^{-2}	20.83 C cm^{-2}	3.84	0.26
			Ti6Al4V			20.97	1.40
			Ti c.p	400 V	44.58 C cm^{-2}	2.33	0.16
			Ti6Al4V		19.41 C cm^{-2}	2.84	0.19

4.3. Results

Figure 41 shows the potential-time and current density-time curves for the coatings obtained under the conditions listed in **Table** 12. The curves were described in previous chapters; nevertheless, some important facts are mentioned in this section. The curves indicate the times at which the morphology and compositional evolution were studied. The times selected are the moments where a change in the slope of the curve is observed or a significant change in the anodizing process occurs. The first morphological analysis was carried out at high potentials (> 190 V) in order to analyze the chemical composition changes during the coating growth. Anodic coatings obtained during the conventional anodizing stage are very thin and have an amorphous structure; therefore, the study was initiated at potentials near the breakdown potential. The anodizing process in the P - Si solution has a similar behavior for both substrates as well as the electrical parameters applied (**Fig.** 41 a,b). For the

coatings obtained in Al - Si solution, the anodizing process in both substrates is different, the abundant gas evolution for the coatings obtained on Ti c.p modifies the potential-time responses and the micro-discharges intensity and size (**Fig**. 41c), which reduces the efficiency of this process.

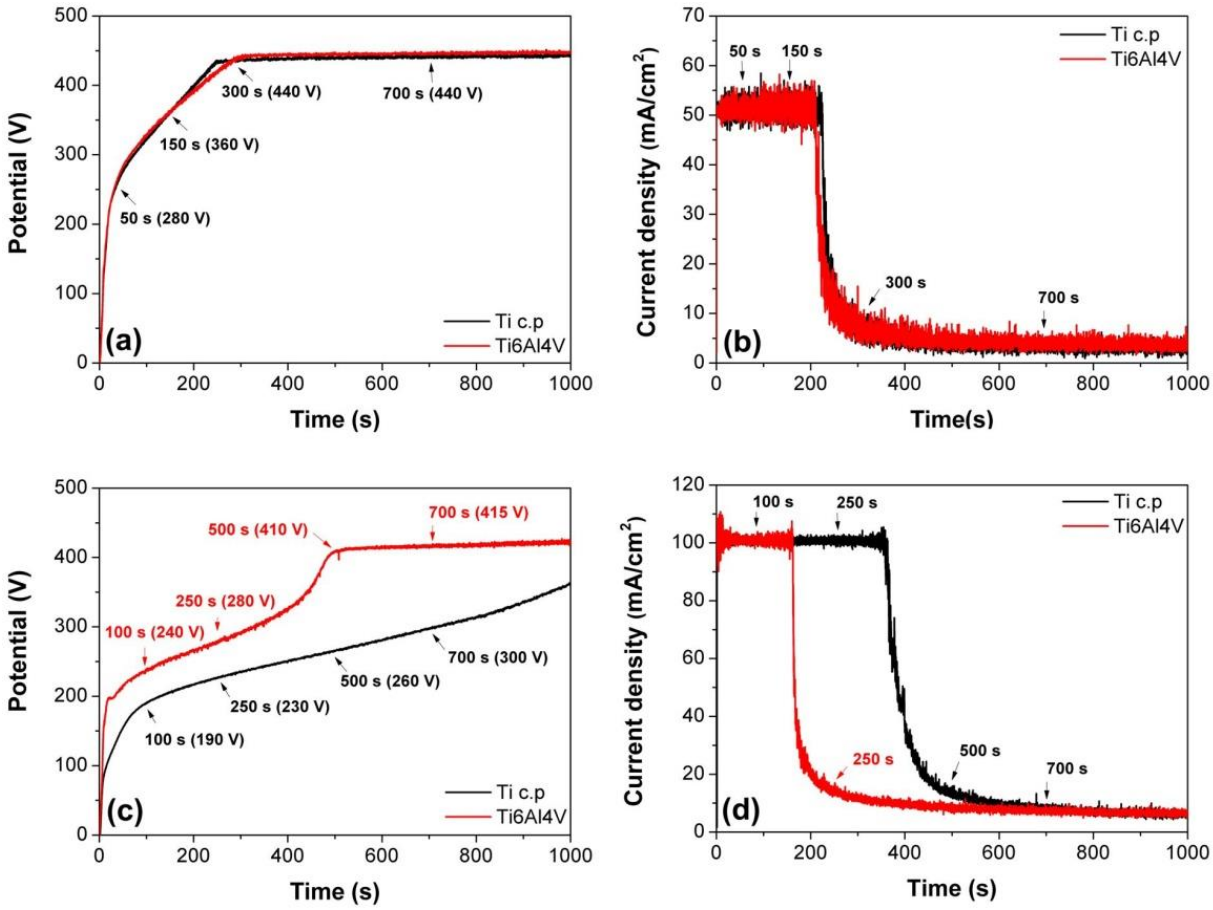

Figure 41. Potential-time responses for the coatings obtained in (a) P-Si solution and (c) Al-Si solution and Current-time responses for the coatings obtained in (b) P-Si solution and (d) Al-Si solution.

Figure 42 shows the micro-discharges appearance for the coatings obtained under galvanostatic conditions. The micro-discharges generated in the coatings obtained in P-Si

solution have similar appearance in both substrates during all anodizing process **(Fig.** 42a). At 300 s, the size of the micro-discharges increases significantly, at this time the potential becomes stable until the end of the process (Fig. 41a). For the coatings obtained in the Al-Si solution, a difference in the appearance of the micro-discharge is evidenced. In the coatings obtained on Ti c.p, the size of the micro-discharges is smaller than in the coatings obtained on Ti6Al4V alloy and it stays the same until the end of the process (**Fig.** 42b). In the coating obtained on Ti6Al4V alloy, the size of the sparks increase significantly at 500 s (**Fig.** 42c), time when the potential response reaches stability as observed in **Fig.** 41 c. For the coatings obtained under potentiostatic conditions, the size of the micro-discharges is controlled and it is smaller than in the galvanostatic coatings as it was evidenced in **Fig.** 15.

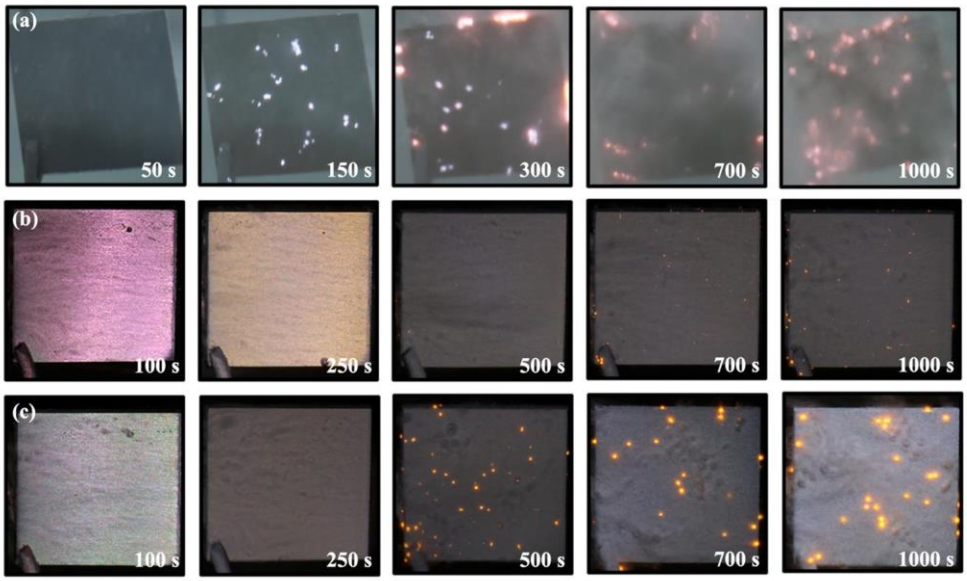

Figure 42. Micro-discharges appearance for the coatings obtained under galvanostatic conditions in (a) P-Si solution, (b) Al-Si solution on Ti c.p and (c) Al-Si solution on Ti6Al4V alloy.

Comparison of emission spectra for the PEO coatings obtained under galvanostatic conditions is shown in Fig. 43. The low intensity of the micro-discharges obtained under potentiostatic conditions did not allow obtaining emission spectra. Using NIST's atomic spectra database [171], each peak was assigned to a characteristic atomic transition, taking into account the transition probability (**Table** 13). The atomic species identified by OES were Ti, O, Al, Si, Na, H, P. Therefore, the results indicated the participation of species from both the metal electrode and the solution during PEO treatment. On the other hand, emission spectra for the coatings obtained in P-Si solution have a similar behavior. Nevertheless, the coatings obtained in Al-Si on Ti6Al4V alloy shows higher intensity in the emission spectrum and the intensity of the Si peak is higher as well.

Table 13. Spectroscopic data of emission lines detected during the PEO anodizing for the coatings obtained under galvanostatic conditions, where A_{ki} is the transition probability for the transition from the upper atomic energy level k to lower level i.

Ion	Observed wavelength (nm)	Aki (s^{-1})
Ti I	394.77683	9.6×10^6
Ti II	324.071	3.7×10^7
Al I	315.0753	1.59×10^7
Si II	566.956	5.00×10^7
Na I	819.4824	5.14×10^7
H I	656.272	2.24×10^7
P I	255.4911	3.00×10^7

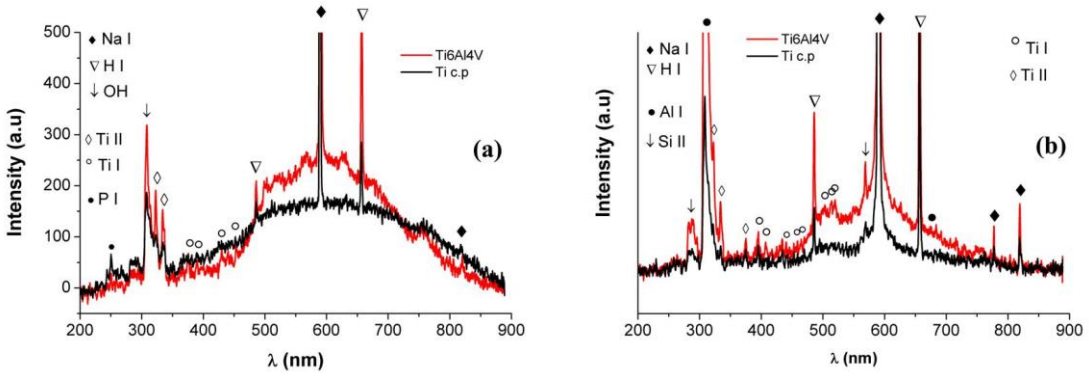

Figure 43. Emission spectra of the coatings obtained by PEO at final stages in (a) P-Si solution at 50 mA cm^{-2} and (b) Al-Si solution at 50 mA cm^{-2}

4.4. Morphological development and compositional evolution of the coatings obtained in P-Si solution

Figure 44 shows the morphological evolution of the coatings obtained on Ti c.p and Ti6Al4V alloy under galvanostatic conditions in P - Si solution. At early stages of the process (50 s), the formation of a dense layer and small pores distributed in some zones of the surface are evidenced. Moreover, the lines generated by polishing are still observed on the surface, indicating the formation of thin coatings (**Figs.** 44 a,b). At 150 s of the process, the formation of a homogeneous structure is observed in both substrates with the formation of circular pores and some coalescent pores (**Figs.** 44 c,d). On Ti c.p., from 300 s, the formation of volcano-shaped pores is observed until the end of the process, showing a homogeneous distribution on the surface without appreciable changes in the pore diameter (**Figs.** 44 e,g,i). Nonetheless, on Ti6Al4V alloy, between the 300 to 700 s of the process the morphology does not change significantly, and a decrease in the surface porosity is observed at the end of the process (**Figs.** 44 f,h,j). Additionally, the cross-sections images show that the coating

obtained on Ti6Al4V alloy has a low porosity through the coating as was shown in a previous chapter (**Fig.** 5). The morphological evolution of the coatings obtained under potentiostatic conditions in both substrates is shown in **Fig.** 45. The surface topography of the coatings during the first stages (50 and 150 s) is similar to the galvanostatic coatings given that in the potentiostatic mode, a short galvanostatic process is necessary to reach the defined potential, which takes approx. 200 s. Therefore, the coatings growth during the first 200 s is similar in both modes due to the same current density applied (Fig. 41b). In the coatings obtained on Ti c.p., the morphology obtained has a similar appearance compared with the coatings obtained under galvanostatic conditions, where the formation of volcano-shaped pores is evidenced until the end of the process (Figs. 45 e,g,i). Nevertheless, the density and the pore diameter in the coatings obtained in galvanostatic mode is higher than in the coatings formed at potentiostatic mode since the micro-discharges size in the galvanostatic mode is higher (**Fig.** 15). In the coatings obtained on Ti6Al4V alloy, a difference in the final morphology of the coatings is observed for both modes of coating formation. The morphology at the end of the process for the potentiostatic coating has a similar appearance to the coating obtained at galvanostatic mode between 300 to 700 s (Figs. 45 f,h,j). The morphologies obtained are the typical topography obtained in these materials in phosphate solutions [70], [96], [97]; however, the control of the characteristics of the coatings, especially the porosity distribution, has a significant effect on the coating properties. The coatings obtained under potentiostatic conditions are denser through the coating and therefore the mechanical and tribological properties and the corrosion resistance are superior to the properties of the galvanostatic coatings as was observed in Chapter 1.

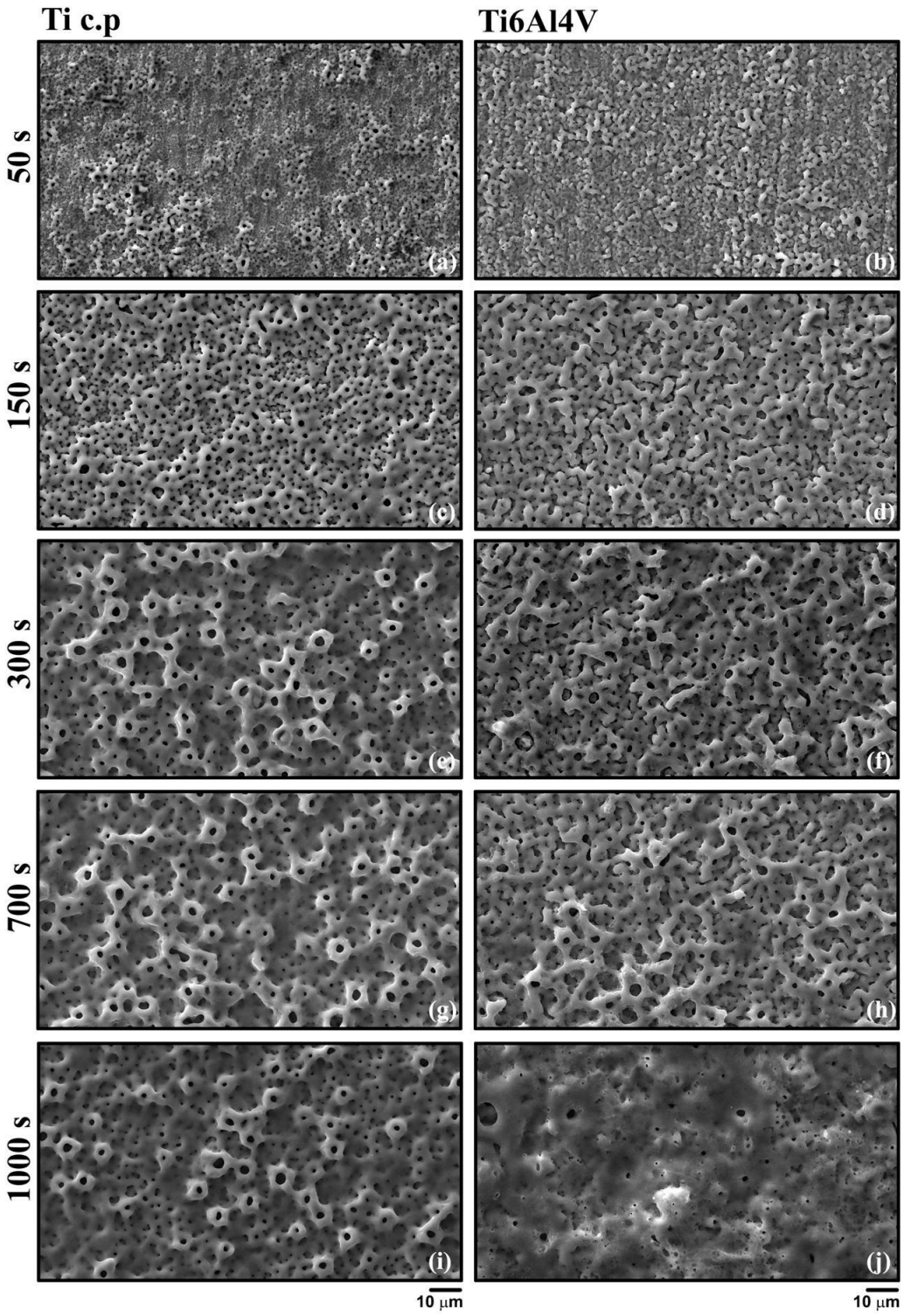

Figure 44. SEM images (SE) of the morphology evolution of the coatings obtained under galvanostatic conditions in P-Si solution at different times (a,b) 50 s, (c,d) 150s, (e,f) 300 s, (g,h) 700 s and (i,j) 1000 s.

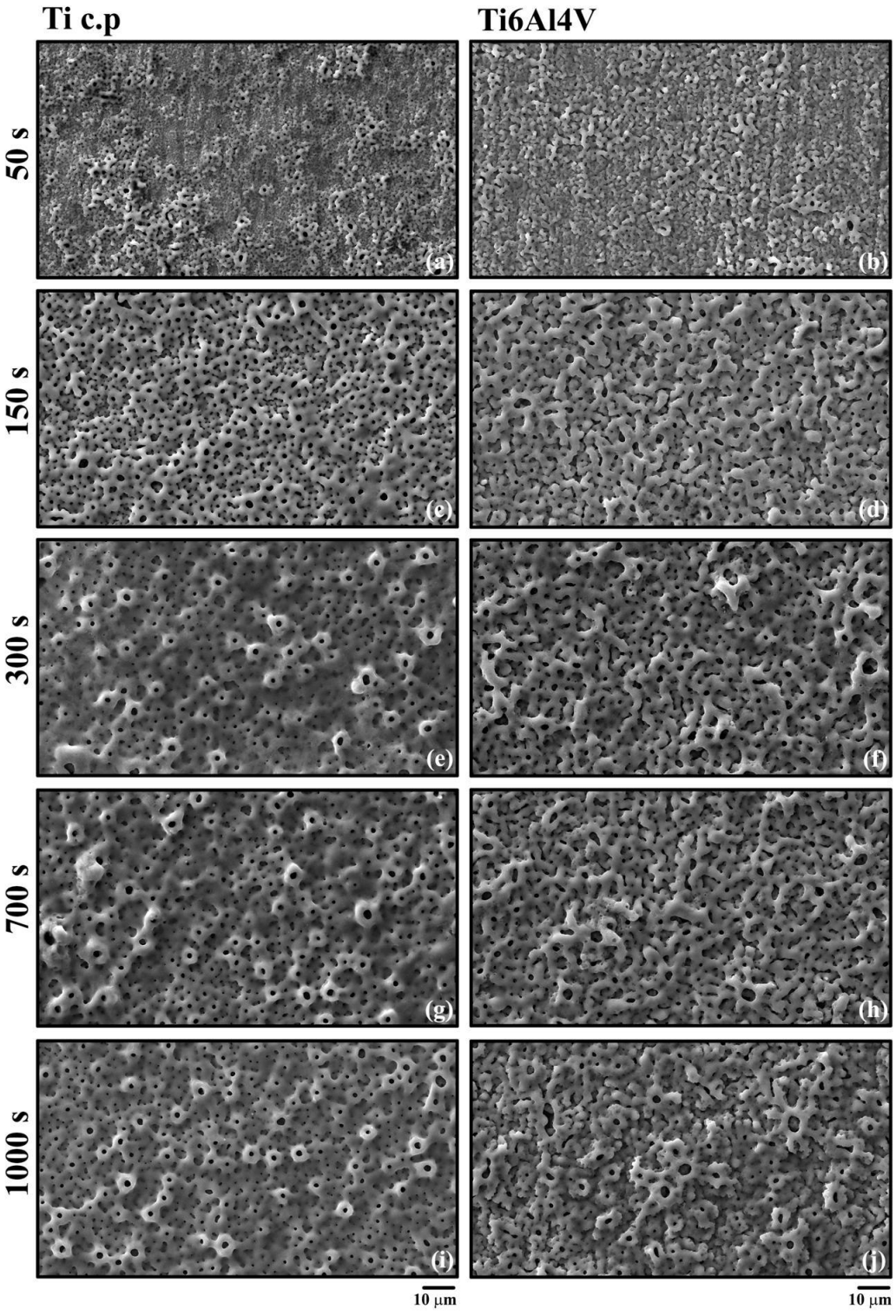

Figure 45. SEM images (SE) of the morphology evolution of the coatings obtained under potentiostatic conditions in P-Si solution at different times (a,b) 50 s, (c,d) 150s, (e,f) 300 s, (g,h) 700 s and (i,j) 1000 s.

Figure 46 shows the coating thickness at different times of the process for both modes of formation of the coatings. In both cases, the coatings obtained on Ti6Al4V alloy have higher thickness than the coatings obtained on Ti c.p. In the coatings obtained under galvanostatic conditions, the coating growth rate is higher at early stages due to the high efficiency in this stage and then a large number of micro-discharges is produced as a result of localized instability caused by breakdown and, at the same time, the process is accompanied by a large release of oxygen. The emergence of this large amount of oxygen is the main reason of lowering the current efficiency [1], [110]. At the end of the process, for the coating on Ti c.p, the coating thickness shows a slight increase, while in the coating obtained on Ti6Al4V alloy, the thickness increases until the end of the process at a lower rate than in early stages (**Fig.** 46a). In the coatings obtained under potentiostatic conditions, a similar behavior is observed; during the first 200 s, the growth rate of the coatings is higher corresponding to the short galvanostatic stage before reaching the potential defined. After this, the coating thickness shows a slight increase until the end of the process. Likewise, the coating obtained on Ti6Al4V alloy is thicker than the coating obtained on Ti c.p (**Fig.** 46b). In the potentiostatic process, the control of the size of the micro-discharges generates a low growth rate during the potentiostatic stage.

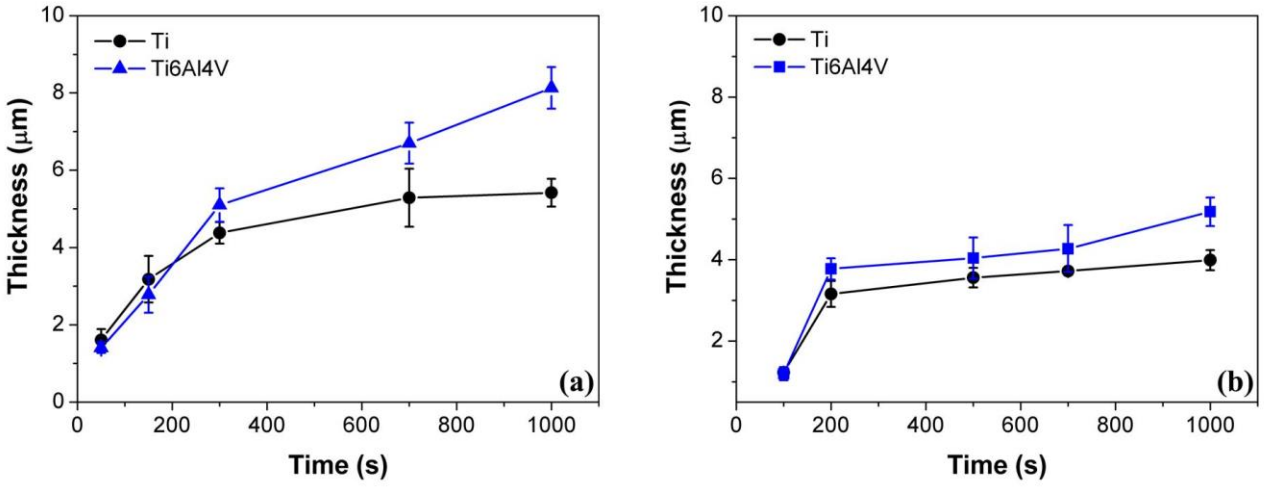

Figure 46. Average thickness measured from the cross-section images of the coatings obtained in P-Si solution at different times under (a) galvanostatic conditions and (b) potentiostatic conditions

The composition of the coatings was assessed by EDS and summarized in **Table** 14 and 15 for the coatings obtained under galvanostatic and potentiostatic conditions respectively. The coatings are composed mainly of Ti, O and P and Si, which are incorporated from the solution into the coatings. The concentration of Si increases with the time; however, for the coatings obtained under potentiostatic conditions, the concentration between 300 to 1000 s is similar since both thickness and chemical composition of the coating are similar. P shows a decrease in the concentration with the time, given that it is incorporated near the coating base mainly and the intensity decreases due to the increase of the coating thickness. In the coating obtained under potentiostatic mode, the concentration of P is similar from 300 to 1000 s.

Table 14. Concentration of the main components of the coatings obtained under galvanostatic conditions in P-Si solution

Time	% O		% Si		% P		% Ti	
	Ti	Ti6Al4V	Ti	Ti6Al4V	Ti	Ti6Al4V	Ti	Ti6Al4V
50 s	66.66	66.31	090	1.00	4.57	4.08	27.86	25.25
150 s	68.22	68.13	2.44	3.65	6.53	6.14	22.81	19.56
300 s	73.51	69.70	2.65	4.64	5.07	5.65	18.77	17.75
700 s	71.26	70.07	2.69	5.52	5.09	5.38	20.96	16.98
1000 s	71.30	70.48	3.24	7.74	5.33	5.21	20.13	14.75

X-ray diffraction patterns showing the structural evolution of the coatings obtained in P-Si solution are shown in **Fig.** 47. **Figs.** 47 a,b show the XRD spectra for the coatings obtained on Ti c.p. The anatase phase (TiO_2) is the main crystalline phase in the coatings; small amounts of the rutile phase are evidenced only in the coating obtained under galvanostatic conditions after 700 s of the process (**Fig.** 47a). The structural evolution shows that the coatings are crystalline from the early stages of the process (50 s), even before the appearance of visible micro-discharges on the surface of the material. The chemical composition of the coatings obtained under potentiostatic conditions is similar during all process due to the size of the micro-discharges under this mode does not change significantly. For the coatings obtained on Ti6Al4V alloy (**Figs.** 47 c,d), the formation of higher amounts of rutile phase is revealed both in the galvanostatic and potentiostatic mode compared to the coatings obtained on Ti c.p. Only at 50 s, the anatase phase is the main crystalline phase in any of the coatings, after this time the amount of the rutile phase increases with the time, showing a higher rutile/anatase ratio the coatings obtained under galvanostatic conditions.

All the spectra also show the characteristics peaks of the substrate.

Table 15. Concentration of the main components of the coatings obtained under potentiostatic conditions in P-Si solution

Time	% O		% Si		% P		% Ti	
	Ti	Ti6Al4V	Ti	Ti6Al4V	Ti	Ti6Al4V	Ti	Ti6Al4V
50 s	69.15	66.93	1.59	2.17	5.09	5.90	24.16	22.16
150 s	71.55	67.92	2.29	3.24	5.12	6.05	21.04	20.10
300 s	71.10	68.47	2.84	4.42	5.25	5.67	20.81	18.97
700 s	70.12	68.68	2.74	4.43	5.57	5.64	21.57	18.89
1000 s	69.53	68.88	2.85	4.42	5.55	5.72	22.08	18.75

In the literature, it is well known that coating formation in this solution is carried out under the following chemical reactions [1]:

$$Ti^{4+} + 2O^{-2} \longrightarrow TiO_2$$

$$Ti^{4+} + xOH^{-} \longrightarrow [Ti(OH)_n]^{n-}_{gel}$$

$$[Ti(OH)_n]^{n-}_{gel} \longrightarrow Ti(OH)_4 + (X-4)OH^{-}$$

$$Ti(OH)_4 \longrightarrow TiO_2 + 2H_2O$$

For the coatings obtained under sparking conditions, during the micro-discharge, the substrate metal evolves into the discharge channel by dissolution, melting or sputtering. The high temperature generated during the sparking phenomenon leads to the formation of crystalline phases. The sparking phenomenon produces porous structures and formation of a

dual coating (inner dense layer and outer porous layer). After the micro-discharge ends, the rapid cooling of the coating by the solution generates in the metal-oxide interface the solidification of a nano-crystalline layer with small uniform nano-grains. These nano-grains are subject to gradual growth under the metallurgical process caused by the repeated discharge [172]. It is believed that formation of the very thin nano-crystalline layer is an universal characteristic of the PEO process, regardless of the substrate species. The nano-crystalline layer is constantly produced by 'eating' the substrate and moves towards the substrate; this is also considered as the main inner growth mechanism. The substrate species and the solution have a significant effect on the nano-crystalline layer. In solutions that contain phosphates or silicates, it has been found that the TiO_2 coating formed in the metal-oxide interface consist mainly of a nano-crystalline structure, combined with small amounts of an amorphous phase [173]. During the plasma reactions that form the outer porous layer, the elements in the solution are incorporated into the coating. The mechanism to the incorporation of the different elements depends on the species and the solution conditions (pH). In phosphates solutions, the PO_4^{-3} ions migrate to the proximity of the substrate-coating interface (Fig. 7) through the discharge channel rather than by a diffusion phenomenon. Phosphorous species does not easily form a gel, compared with Si and therefore it is more easily dragged to the region of the coating–metal interface through the discharge channel under the high electric field effect. Si species form an H_2SiO_3 gel and generally are deposited near the coating surface (Fig. 7). However, the formation of crystalline Si-based in the coatings was not evidenced in this work (Fig. 8) [32], [90], [142].

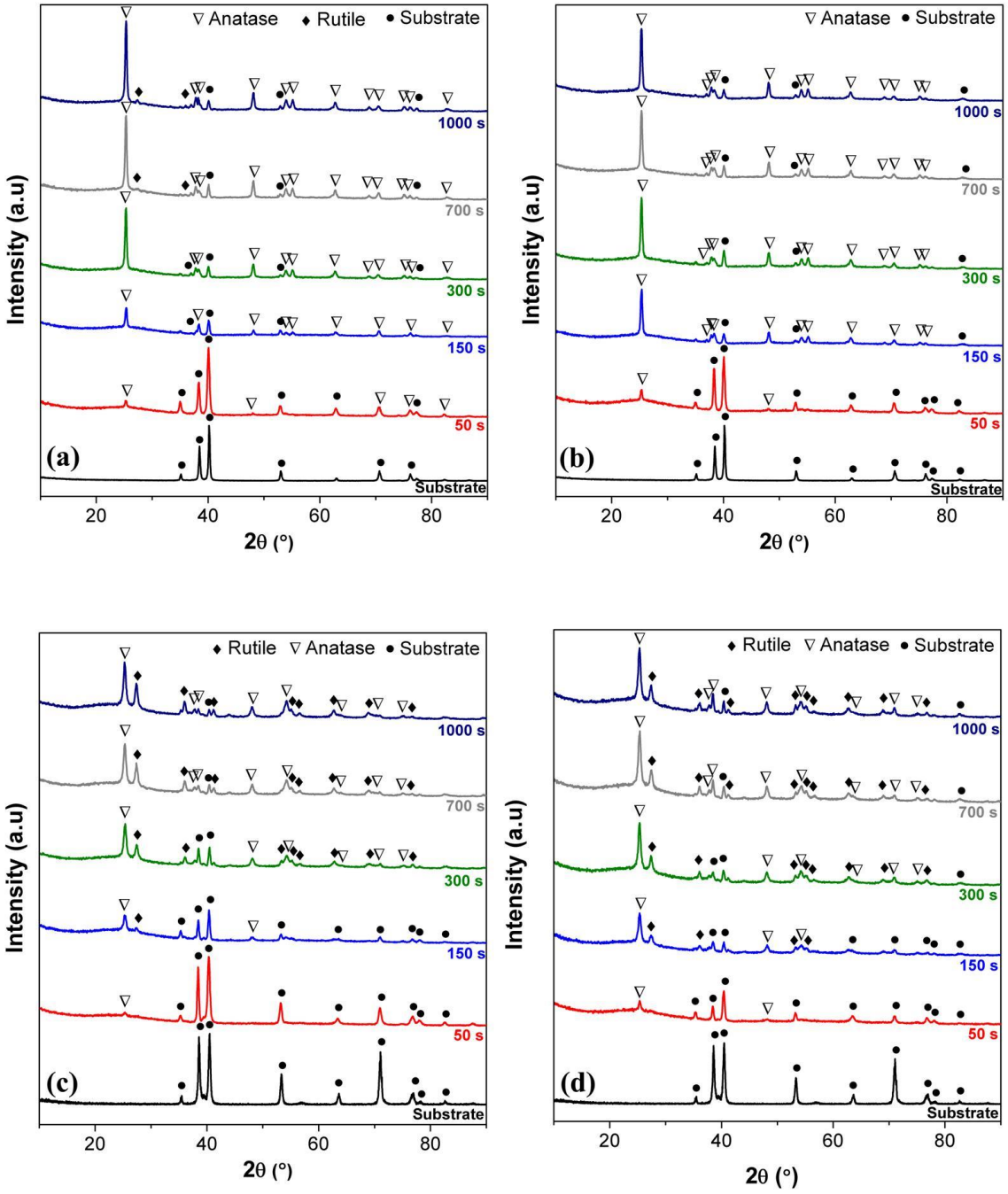

Figure 47. XRD spectra of the coatings obtained under galvanostatic conditions in P-Si solution on (a) Ti c.p and (c) Ti6Al4V alloy and XRD spectra of the coatings obtained under potentiostatic conditions in P-Si solution on (b) Ti c.p and (d) Ti6Al4V alloy

4.5. Morphological development and compositional evolution of the coatings obtained in Al-Si solution

Figure 48 shows the morphological evolution of the coatings obtained on Ti c.p and Ti6Al4V alloy under galvanostatic conditions in Al - Si solution. In this solution, significant changes are observed in both substrates due to the differences during the anodizing process. A higher gas evolution is generated on Ti c.p and therefore changes in the potential are observed (**Fig**. 41c). At early stages of the process (100 s), the formation of a dense layer is observed in both materials, nevertheless, on Ti6Al4V alloy, there are already zones of initial formation of pores which are related to the higher coating growth rate for this material. Lines generated by polishing are still observed on the surface indicating the formation of a thin coating (**Figs**. 48 a,b). At 250 s of the process, the surface morphology of both materials is completely different. On Ti c.p, the formation of a dense layer with some circular zones protruding the surface are evidenced whereas on Ti6Al4V alloy, circular pores are distributed homogeneously on the surface material (**Figs.** 48 c,d). At 500 s of the process, on Ti c.p a surface morphology similar to obtained on Ti6Al4V alloy at 250 s is evidenced composed by small circular pores. On Ti6Al4V alloy, the size and diameter of the pores have increased significantly (**Figs.** 48 e,f). From 700 to 1000 seconds, the morphology of the coatings does not change significantly. Nevertheless, the topography in both substrates is different. On Ti c.p, the formation of a porous structure composed of circular pores homogeneously distributed on the surface, while on Ti6Al4V alloy, volcano-shaped pores are formed and the number of pores increases with time (**Figs.** 48 g-j). The formation of the volcano-shaped pores increases the roughness of the sample significantly (**Fig.** 17). The formation of

volcano-shaped pores on Ti6Al4V alloy is due to the formation of micro-discharges with higher size than the micro-discharges formed on Ti c.p (**Fig.** 42). The morphology evolution of the coatings obtained under potentiostatic conditions is shown in Fig. 49. At early stages (100 s), a similar morphology than the coatings obtained under galvanostatic conditions is observed, which corresponds to the formation of dense coatings. This is explained as a first galvanostatic stage takes place before reaching the defined potential, resulting in a similar morphology during first seconds in both modes of coating formation. On Ti c.p, from 250 to 1000 s (**Figs.** 49 e,g,i), the surface morphology remains more or less the same and it resembles the morphology the appearance of the coating obtained under galvanostatic conditions on the same substrate. For the coating formed on Ti6Al4V alloy, the morphology obtained between 250 to 1000 s shows the formation of circular pores and this surface porosity decreases with time, especially at 1000 s, this morphology has somehow similar appearance than the coating obtained under galvanostatic conditions during at 500 s (**Figs**. 49 f,h,j).

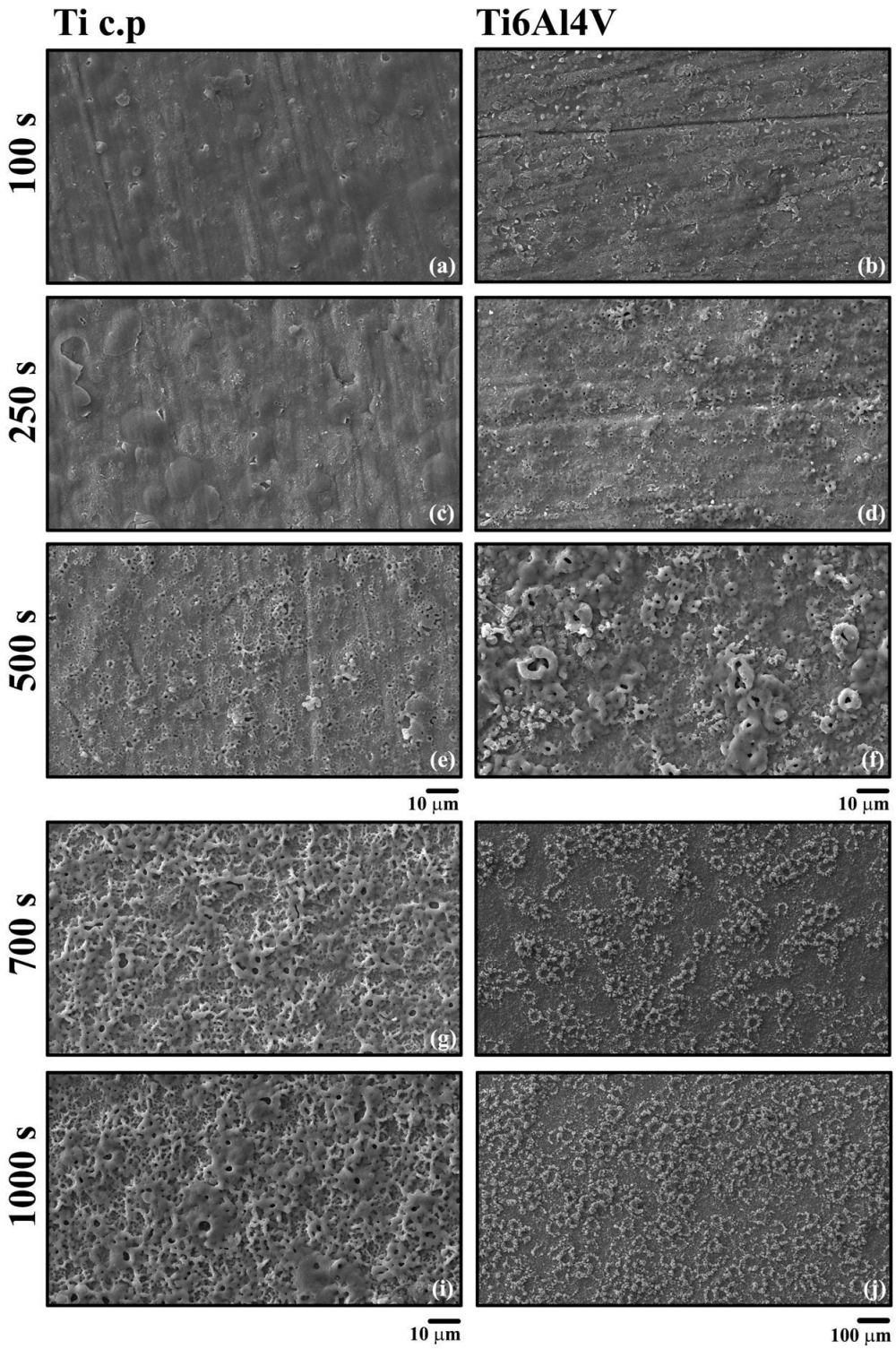

Figure 48. SEM images (SE) of the morphology evolution of the coatings obtained under galvanostatic conditions in Al-Si solution at different times (a,b) 100 s, (c,d) 250s, (e,f) 500 s, (g,h) 700 s and (i,j) 1000 s

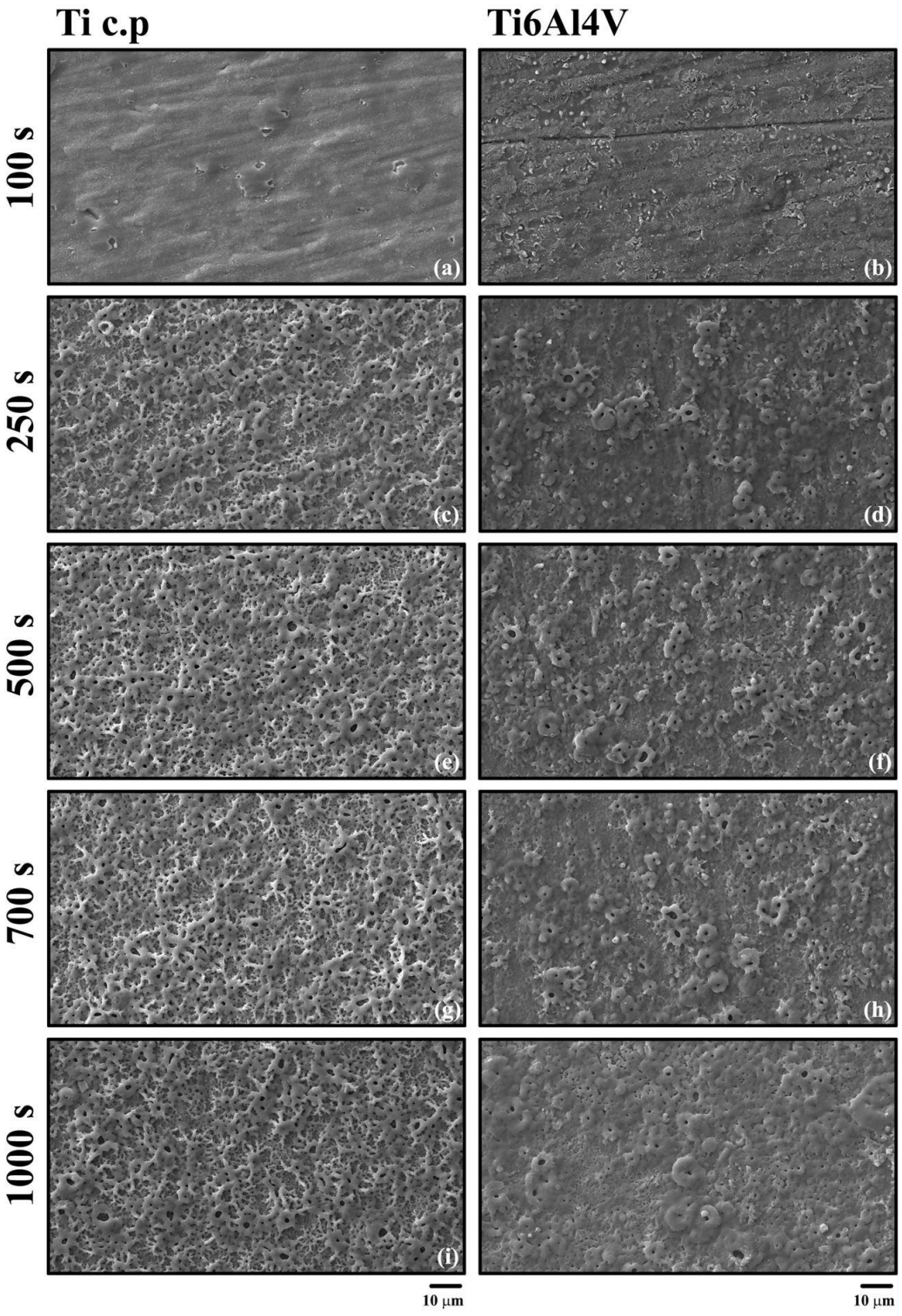

Figure 49. SEM images (secondary electrons) of the morphology evolution of the coatings obtained under potentiostatic conditions in Al-Si solution at different times (a,b) 100 s, (c,d) 250s, (e,f) 500 s, (g,h) 700 s and (i,j) 1000 s

Figure 50 shows the coating thickness at different times of the process. In all conditions, the coatings obtained on Ti6Al4V alloy are thicker than coatings obtained on Ti c.p. In the coatings obtained under galvanostatic conditions during the early stages (between 0 to 250 s) the growth rate is similar. Then, after 500 s, a significant difference in the coating growth rate is evidenced for both substrates. For the coating formed on Ti c.p a slight increase is observed until the end of the process, while for the coating obtained on Ti6Al4V alloy, the coating growth rate increases significantly until the end of the process. In this stage, the formation of bigger micro-discharges was evidenced coinciding with the higher coating growth rate as has been reported by other authors [1], [126]. In the coatings obtained under potentiostatic conditions, a similar behavior is observed; during the first 200 s, the growth rate of the coatings is higher and after this, the coating thickness shows a slight increase until the end of the process. In the potentiostatic process, the control of the size of the micro-discharges generates a low growth rate during the potentiostatic process and the formation of dense coatings as observed in previous chapters. On the coating obtained on Ti c.p, the charge density applied is approximately two times the charge applied on Ti6Al4V alloy (**Table** 12); however, the abundant gas evolution on the Ti c.p process decreases the efficiency of the process, generating a coating with similar thickness than the coating obtained on Ti6Al4V alloy.

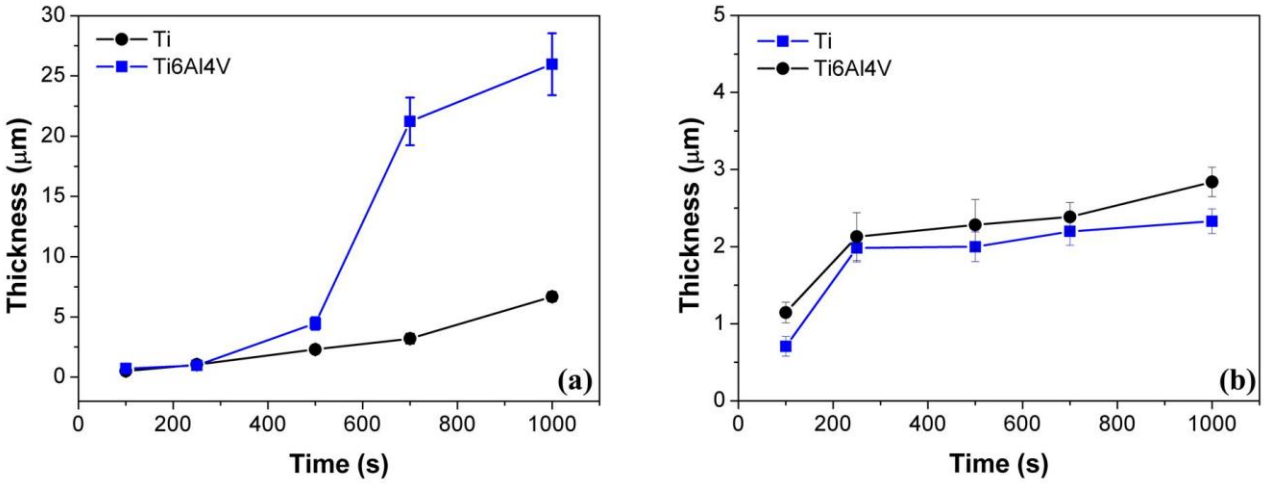

Figure 50. Average thickness measured from the cross-section images of the coatings obtained in Al-Si solution at different times under (a) galvanostatic conditions and (b) potentiostatic conditions

The composition of the coatings was assessed by EDS and summarized in **Table** 16 and 17 for the coatings obtained under galvanostatic and potentiostatic conditions respectively. The coatings are composed mainly of Al, Ti, O and Si. Aluminum is mainly incorporated from the solution. In the coatings obtained under galvanostatic conditions, the concentration of Al and Si increases with time, especially the concentration of aluminum. The concentration of the components of the coatings obtained at galvanostatic mode is higher than in the potentiostatic coatings. In the coatings obtained under potentiostatic conditions, an increase in the amount of the main elements is observed until 500 s, then the concentrations stay constant due to the control of the micro-discharge size, keeping the composition of the coatings similar until the end of the process.

Table 16. Atomic percentage of main components of the coatings obtained under galvanostatic conditions in Al-Si solution

Time	% O		% Si		% Ti		% Al	
	Ti	Ti6Al4V	Ti	Ti6Al4V	Ti	Ti6Al4V	Ti	Ti6Al4V
100 s	60.94	64.09	0.27	0.25	36.51	28.84	2.28	5.99
250 s	64.90	69.80	0.35	0.29	32.30	17.32	2.45	11.55
500 s	70.28	67.92	0.53	0.59	21.13	5.88	8.07	23.93
700 s	69.65	65.21	0.57	0.80	11.47	0.45	18.31	31.05
1000 s	67.45	67.00	0.68	0.94	7.30	0.16	24.57	31.87

X-ray diffraction patterns showing the structural evolution of the coatings obtained in Al-Si solution are shown in **Fig.** 51. **Figs.** 51 a,b show the XRD spectra for the coatings obtained on Ti c.p. The coatings are composed mainly by α - Al_2O_3, γ - Al_2O_3 and Al_2TiO_5. There are few changes for the coatings obtained in both modes. For the coating obtained under galvanostatic conditions, the formation of α - Al_2O_3 is evidenced during the first seconds of the process (between 100 to 250 s - Fig. 51a). Moreover, the coatings are crystalline from early stages of the anodizing process. After 500 s, the formation of Al_2TiO_5 and γ - Al_2O_3 is observed until the end of the process. Nevertheless, at 1000 s, the amount of α - Al_2O_3 decreases drastically whilst the intensity of the Al_2TiO_5 phase peaks largely increases. A similar behavior is observed in the coatings obtained under potentiostatic conditions. During the first seconds of the process, the formation of α - Al_2O_3 is observed into the coatings (100 s). After this, there are not changes in the composition of the coatings until the end of the process and the chemical composition of the coatings is mainly α - Al_2O_3 and γ - Al_2O_3 and Al_2TiO_5. For the coatings obtained on Ti6Al4V alloy, a significant

difference in the chemical composition is observed for both modes of coating formation (Fig. 51 c,d). For the coatings obtained under galvanostatic conditions, the formation of α - Al_2O_3 during the first stages of the process is observed (between 100 to 250 seconds), showing a similar behavior than the coating obtained on Ti c.p. Nonetheless, after 500 s, the chemical composition of the coating changes significantly and the coating is composed by γ - Al_2O_3, Al_2TiO_3 and mullite; moreover, the intensity of the peaks of the crystalline phases increases with the time, especially for the mullite phase, due to the increase in the incorporation of Si (**Table** 16). For the coating obtained under potentiostatic conditions, the chemical composition of the coating does not change during the process and is composed mainly by γ - Al_2O_3, α - Al_2O_3 and Al_2TiO_5. All the spectra also show the characteristic peaks of the substrate. The crystalline phases obtained on the coatings are due to the high incorporation of aluminum from the solution into the coating.

Table 17. Atomic percentage of main components of the coatings obtained under potentiostatic conditions in Al-Si solution

Time	% O		% Si		% Ti		% Al	
	Ti	Ti6Al4V	Ti	Ti6Al4V	Ti	Ti6Al4V	Ti	Ti6Al4V
100 s	64.68	69.46	0.44	0.48	32.41	9.92	2.47	19.10
250 s	68.96	69.35	0.60	0.54	10.76	10.02	19.38	19.13
500 s	50.63	68.89	0.62	0.51	9.96	9.81	20.84	19.61
700 s	68.93	69.17	0.63	0.47	9.39	9.51	21.05	19.90
1000 s	69.38	69.43	0.53	0.45	10.53	9.90	19.56	19.32

The formation of Al_2O_3 and Al_2TiO_5 has been widely described for PEO of titanium in

aluminate-based solutions and are described under the following reactions [126]:

$$Ti^{+4} + 4OH^{-} \longrightarrow TiO_2 + 2H_2O$$

$$Ti^{+4} + 4AlO_2^{-} \longrightarrow TiO_2 + Al_2O_3$$

$$Ti^{+4} + 4Al(OH)_4^{-} \longrightarrow TiO_2 + Al_2O_3 + 2Al(OH)_3 + 5H_2O$$

Due to the high thermal energy from the discharges, which can reach 6000–8000 K, sintering, and phase transformation of aluminates also occur as follows:

$$2Al(OH)_4^{-} \longrightarrow Al_2O_3 + 2OH^{-} + 3H_2O$$

$$Al_2O_3 + TiO_2 \longrightarrow Al_2TiO_5$$

According to the phase diagram of the TiO_2 - Al_2O_3, a condensation of the Al_2TiO_5 phase can be expected to occur at 2127 K, whereas the estimated temperatures usually developed in the discharge channels are substantially higher. Two eutectic reactions then follow:

$$Al_2TiO_5 + L \longrightarrow 3Al_2TiO_5 . Al_2O_3$$

(at an excess of Al)

$$Al_2TiO_5 + L \longrightarrow 3Al_2TiO_5 . TiO_2$$

(at an excess of Ti)

On the coatings obtained on Ti6Al4V alloy, the incorporation of Si leads to the formation of SiO_2, which reacts with the Al_2O_3 according to the eutectic reaction of the SiO_2-Al_2O_3

phase diagram:

$$SiO_2 + Al_2O_3 \longrightarrow Mullite\ (Al_{4+2x}Si_{2-2x}O_{10-X})$$

As in the coatings obtained on the sodium hypophosphite-based solution, the formation a thin layer in the metal-oxide interface is evidenced. In the coatings obtained in solution with phosphates and metasilicates, that layer has been found to exhibit a nano-crystalline structure, however, in the coatings obtained in aluminate-based solutions, it shows a much larger grain size, generally at μm scale [30], [174]. Regarding the growth mechanism of coatings obtained in aluminate-based solutions on Al alloys, the formation of an amorphous layer near the coating base has been reported by many authors [74], [166]. The formation of this amorphous layer is due to an ionic migration process, which occurs at the metal-oxide interface for the high electric field generated during the anodizing process. In the coatings obtained on Ti alloys, a similar phenomenon is carried out since the thin inner layer is composed of a combination of amorphous and crystalline phases. In the coatings obtained under galvanostatic conditions on Ti6Al4V alloy, the formation of a broad peak is evidenced at 35º, indicating the presence of amorphous species into the coating, which could be due to the formation of SiO_2 amorphous into the coating, as has been evidenced by other authors [24], [142].

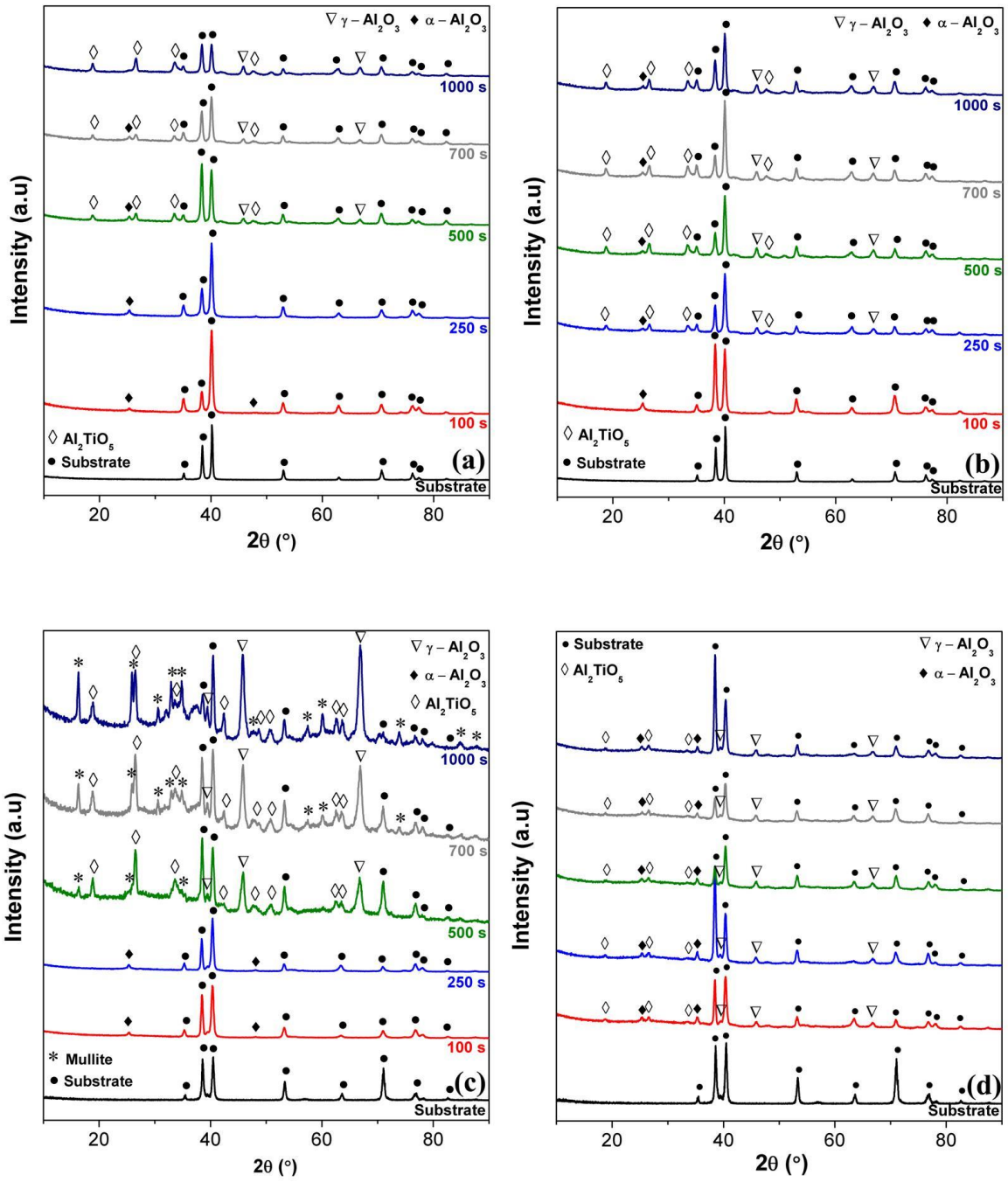

Figure 51. XRD spectra of the coatings obtained under galvanostatic conditions in Al-Si solution on (a) Ti c.p and (c) Ti6Al4V alloy and XRD spectra of the coatings obtained under potentiostatic conditions in Al-Si solution on (b) Ti c.p and (d) Ti6Al4V alloy

4.6. Discussion

Anodic coatings were obtained using different alkaline solutions and it was observed that the efficiency of the process is influenced both by the species in the solution and the substrate. The growth rate of the coatings formed on Ti6Al4V alloy is higher than in the coatings obtained on Ti c.p in agreement with the results reported by other authors [61]. In the coatings obtained on Ti c.p, especially in the Al-Si solution, the abundant gas evolution affects significantly the anodizing process, decreasing the efficiency of the process and the intensity of the micro-discharges. The high efficiency of the anodizing process during the early stages is reduced for the excessive oxygen gas evolution. It is estimated that the current efficiency of the oxide coating formation is generally as low as 10 - 30 %, while it can increase up to about 60 % depending on the solution additives [144], [175]. The formation of micro-discharges with low intensity and energy does not allow the crystallization of phases like mullite (that requires high temperature and energy), into the coatings, as was evidenced in the coatings obtained on Ti6Al4V alloy (Fig. 51). The formation of small micro-discharges allows controlling the porosity distribution, which is very important for the mechanical and tribological properties as was observed in previous chapters. However, the intensity and energy of the micro-discharges formed under potentiostatic conditions lead the formation of crystalline coatings, which confers good tribological properties. The OES spectra for the coating obtained on Ti6Al4V alloy evidenced the silicon peaks with higher intensity than in coating obtained on Ti c.p (Fig. 43) due to the high-intensity sparks, which allows the formation of mullite. In the coatings obtained in the P-Si solution, there are not significant differences in the coating formation in both substrates. In the coatings obtained in P-Si

solution on Ti6Al4V alloy, the formation of rutile phase is due to the higher temperature generated during the micro-discharges given that the Gibbs energy to transform from amorphous TiO_2 to rutile (10 kJ/mol) is higher that the energy required to transform amorphous TiO_2 to anatase (0.4 kJ/mol). Therefore, during the formation of PEO coatings, the anatase phase is formed from the first stages and with the increase of the energy and temperature, the formation of rutile takes places [176].

4.7. Conclusions

Anodic coatings were obtained using different alkaline solutions. The growth mechanism for both solutions changes significantly due to the plasma reactions generated with the species in the solution. In the coatings obtained in the P-Si solution, a similar growth mechanism is observed for both substrates. However, in the coatings obtained on Ti6Al4V alloy, the formation of rutile is evidenced due to a higher energy of the micro-discharges. In the coatings obtained in Al-Si solution, the coating obtained on Ti c.p has a lower efficiency of the process due to the abundant gas evolution during anodizing. The formation of micro-discharges with larger size on Ti6Al4V alloy leads to the crystallization of phases like mullite that provides a good wear performance, as evidenced in a previous chapter. The coatings obtained under potentiostatic conditions are crystalline in spite of the low energy of the micro-discharges. Potentiostatic coatings are dense coatings, which is important for corrosion protection and tribological performance; nevertheless, the formation of phases that required high energy cannot be formed under the potentiostatic mode.

5. Summary and Outlook

The work presented in this doctoral thesis showed the formation of coatings in alkaline solutions using different anodizing conditions. The composition of the solutions selected was optimized in order to obtain coatings with a homogeneous morphology. It was found that the coatings obtained under potentiostatic conditions have a better tribological performance and corrosion resistance than coatings obtained under galvanostatic conditions. The potentiostatic control allows the formation of small micro-discharges during anodizing, which allows the formation of crystalline coatings and low porosity through the coating. High size micro-discharges lead to the formation of voids and pores near the coating base, which affects the mechanical properties and the wear performance of the coatings. During the formation of the coatings obtained under potentiostatic conditions, the first stages have a significant effect on the final properties of the coating. In the potentiostatic mode, a short galvanostatic stage is carried out before reach the require potential. In this work, it was found

that this pre-anodizing stage is important to improve the wear and corrosion properties of the coatings, allowing the formation of thin coatings (1-2 μm) with good wear properties. High current densities applied in the first stages leads to the formation of voids and pores near the coating base, which affects its properties. The formation of thin coatings will be very useful for applications where no dimensional changes in the part is required like screws, pistons, among others.

In the coatings obtained under galvanostatic conditions, the formation of micro-discharges with high energy and intensity allows the formation of other crystalline phases into the coatings. It was found that the formation of mullite into the alumina matrix of the coatings obtained in sodium aluminate-based solution improved the wear properties significantly. These coatings could be used in applications at high temperature due to the thermal barrier properties of the mullite. The additives in the solution modify the structure and morphology of the coatings due to their effect on the anodizing process. Coatings obtained using sodium metasilicate as an additive in the solution, reveals the formation of low porosity through the coating, which benefits both the corrosion resistance and the wear properties. Coatings obtained on Ti6Al4V alloy are thicker and have better wear properties than coatings obtained on Ti due to the growing process is influenced by the substrate, this was observed more clearly in the coatings obtained in the solution composed by sodium aluminate with the addition of sodium metasilicate, where the abundant gas evolution during anodizing reduced the efficiency of the process and affected the micro-discharges intensity.

Even though new insights of the effect of the anodizing parameters on the structure,

morphology and composition of the coatings obtained by PEO and its relationship with the coating properties have been found in this doctoral thesis, more detailed studies are necessary in order to have a deeper knowledge of the effect of the solution on the structure of the coatings in order to have a control of the coating porosity. A better comprehension of the effect of the chemical species in the solution on the anodizing process, especially on the plasma characteristics is necessary, as well as a deeper study to understand the effect of the alloying elements in the growing process of the coatings, especially in coatings obtained in sodium aluminate-based solutions. Currently, in the PEO process, it is necessary to further study the fundamentals of the PEO technique to advance scientific understanding and to explore new functional PEO coatings for high-tech applications.

6. References

[1] H. Dong, *Surface Engineering of Light Alloys: Aluminium, Magnesium and Titanium Alloys*. UK: CRC Press, 2010.

[2] J. A. Disegi, "Anodizing Treatments for Titanium Implants."

[3] J. B. Park and J. D. Bronzino, *Biomaterials: Principles and Applications*. CRC Press, 2002.

[4] I. J. Polmear, "6 - Titanium alloys BT - Light Alloys (Fourth Edition)," Oxford: Butterworth-Heinemann, 2005, pp. 299–365.

[5] G. Lütjering and J. C. Williams, *Titanium*, 2nd ed. Heidelberg: Springer Berlin Heidelberg, 2007.

[6] M. Niinomi, "Mechanical properties of biomedical titanium alloys," *Mater. Sci. Eng. A*, vol. 243, pp. 231–236, 1998.

[7] M. Jackson and W. Ahmed, *Titanium Dioxide Coatings in Medical Device*

Applications. New York: Springer US, 2007.

[8] V. N. Moiseyev, *Titanium Alloys: Russian Aircraft and Aerospace Applications*. CRC Press, 2005.

[9] T. Akatsu, Y. Yamada, Y. Hoshikawa, T. Onoki, Y. Shinoda, and F. Wakai, "Multifunctional porous titanium oxide coating with apatite forming ability and photocatalytic activity on a titanium substrate formed by plasma electrolytic oxidation," *Mater. Sci. Eng. C*, vol. 33, no. 8, pp. 4871–4875, Dec. 2013.

[10] K. R. Shin, S. Il Yoon, Y. G. Ko, and D. H. Shin, "Deposition of hydroxyl-apatite on titanium subjected to electrochemical plasma coating," *Electrochim. Acta*, vol. 109, no. 0, pp. 173–180, Oct. 2013.

[11] M. Echeverry-Rendón, O. Galvis, D. Quintero Giraldo, J. Pavón, J. López-Lacomba, E. Jiménez-Piqué, M. Anglada, S. Robledo, J. Castaño, and F. Echeverría, "Osseointegration improvement by plasma electrolytic oxidation of modified titanium alloys surfaces," *J. Mater. Sci. Mater. Med.*, vol. 26, no. 2, pp. 1–18, 2015.

[12] X. Cui, H. M. Kim, M. Kawashita, L. Wang, T. Xiong, T. Kokubo, and T. Nakamura, "Preparation of bioactive titania films on titanium metal via anodic oxidation," *Dent. Mater.*, vol. 25, pp. 80–86, 2009.

[13] R. O. Hussein, D. O. Northwood, and X. Nie, "The effect of processing parameters and substrate composition on the corrosion resistance of plasma electrolytic oxidation (PEO) coated magnesium alloys," *Surf. Coatings Technol.*, vol. 237, pp. 357–368, 2013.

[14] J. Jovović, S. Stojadinović, N. M. Šišović, and N. Konjević, "Spectroscopic study of plasma during electrolytic oxidation of magnesium- and aluminium-alloy," *J. Quant.*

Spectrosc. Radiat. Transf., vol. 113, no. 15, pp. 1928–1937, Oct. 2012.

[15] T. S. N. Sankara Narayanan, I. S. Park, and M. H. Lee, "Strategies to improve the corrosion resistance of microarc oxidation (MAO) coated magnesium alloys for degradable implants: Prospects and challenges," *Prog. Mater. Sci.*, vol. 60, no. 1, pp. 1–71, 2014.

[16] F. ZHAO, A. LIAO, R. ZHANG, S. ZHANG, H. WANG, X. SHI, M. LI, and X. HE, "Effects of sodium tungstate on properties of micro-arc coatings on magnesium alloys," *Trans. Nonferrous Met. Soc. China*, vol. 20, Supple, pp. s683–s687, Jul. 2010.

[17] M. Tarakci, "Plasma electrolytic oxidation coating of synthetic Al–Mg binary alloys," *Mater. Charact.*, vol. 62, no. 12, pp. 1214–1221, Dec. 2011.

[18] A. L. Yerokhin, X. Nie, A. Leyland, and A. Matthews, "Characterisation of oxide films produced by plasma electrolytic oxidation of a Ti–6Al–4V alloy," *Surf. Coatings Technol.*, vol. 130, pp. 195–206, 2000.

[19] E. Matykina, F. Monfort, A. Berkani, P. Skeldon, G. E. Thompson, and J. Gough, "Characterization of Spark-Anodized Titanium for Biomedical Applications," *J. Electrochem. Soc.* , vol. 154, no. 6, pp. C279–C285, Jun. 2007.

[20] I. Cvijović-Alagić, Z. Cvijović, S. Mitrović, V. Panić, and M. Rakin, "Wear and corrosion behaviour of Ti–13Nb–13Zr and Ti–6Al–4V alloys in simulated physiological solution," *Corros. Sci.*, vol. 53, pp. 796–808, 2011.

[21] X. Sun, Z. Jiang, S. Xin, and Z. Yao, "Composition and mechanical properties of hard ceramic coating containing [alpha]-Al2O3 produced by microarc oxidation on Ti-6Al-4V alloy," *Thin Solid Films*, vol. 471, pp. 194–199, 2005.

[22] J. M. Wheeler, C. A. Collier, J. M. Paillard, and J. A. Curran, "Evaluation of

micromechanical behaviour of plasma electrolytic oxidation (PEO) coatings on Ti–6Al–4V," *Surf. Coatings Technol.*, vol. 204, pp. 3399–3409, 2010.

[23] A. F. Yetim, "Investigation of wear behavior of titanium oxide films, produced by anodic oxidation, on commercially pure titanium in vacuum conditions," *Surf. Coatings Technol.*, vol. 205, no. 6, pp. 1757–1763, 2010.

[24] Y. M. Wang, B. L. Jiang, T. Q. Lei, and L. X. Guo, "Microarc oxidation coatings formed on Ti6Al4V in Na2SiO3 system solution: Microstructure, mechanical and tribological properties," *Surf. Coatings Technol.*, vol. 201, pp. 82–89, 2006.

[25] M. Khorasanian, A. Dehghan, M. H. Shariat, M. E. Bahrololoom, and S. Javadpour, "Microstructure and wear resistance of oxide coatings on Ti–6Al–4V produced by plasma electrolytic oxidation in an inexpensive electrolyte," *Surf. Coatings Technol.*, vol. 206, pp. 1495–1502, 2011.

[26] M. Long and H. J. Rack, "Titanium alloys in total joint replacement—a materials science perspective," *Biomaterials*, vol. 19, pp. 1621–1639, 1998.

[27] C. Fei, Z. Hai, C. Chen, and X. Yangjian, "Study on the tribological performance of ceramic coatings on titanium alloy surfaces obtained through microarc oxidation," *Prog. Org. Coatings*, vol. 64, pp. 264–267, 2009.

[28] X. Liu, P. K. Chu, and C. Ding, "Surface modification of titanium, titanium alloys, and related materials for biomedical applications," *Mater. Sci. Eng. R Reports*, vol. 47, pp. 49–121, 2004.

[29] R. O. Hussein, X. Nie, and D. O. Northwood, "A spectroscopic and microstructural study of oxide coatings produced on a Ti–6Al–4V alloy by plasma electrolytic oxidation," *Mater. Chem. Phys.*, vol. 134, pp. 484–492, 2012.

[30] Y. M. Wang, B. L. Jiang, T. Q. Lei, and L. X. Guo, “Microarc oxidation and spraying graphite duplex coating formed on titanium alloy for antifriction purpose,” *Appl. Surf. Sci.*, vol. 246, pp. 214–221, 2005.

[31] Y. M. Wang, B. L. Jiang, T. Q. Lei, and L. X. Guo, “Microarc oxidation coatings formed on Ti6Al4V in Na2SiO3 system solution: Microstructure, mechanical and tribological properties,” *Surf. Coatings Technol.*, vol. 201, pp. 82–89, 2006.

[32] H. Habazaki, T. Onodera, K. Fushimi, H. Konno, and K. Toyotake, “Spark anodizing of β-Ti alloy for wear-resistant coating,” *Surf. Coatings Technol.*, vol. 201, pp. 8730–8737, 2007.

[33] L. Wu, B. C. Holloway, D. P. Beesabathina, C. Kalil, and D. M. Manos, “Analysis of diamond-like carbon and Ti/MoS2 coatings on Ti–6Al–4V substrates for applicability to turbine engine applications,” *Surf. Coatings Technol.*, vol. 130, pp. 207–217, 2000.

[34] F. Yildiz, A. F. Yetim, A. Alsaran, and A. Çelik, “Plasma nitriding behavior of Ti6Al4V orthopedic alloy,” *Surf. Coatings Technol.*, vol. 202, pp. 2471–2476, 2008.

[35] S. M. Johns, T. Bell, M. Samandi, and G. A. Collins, “Wear resistance of plasma immersion ion implanted Ti6Al4V,” *Surf. Coatings Technol.*, vol. 85, pp. 7–14, 1996.

[36] O. A. Galvis, D. Quintero, J. G. Castaño, H. Liu, G. E. Thompson, P. Skeldon, and F. Echeverría, “Formation of grooved and porous coatings on titanium by plasma electrolytic oxidation in H2SO4/H3PO4 electrolytes and effects of coating morphology on adhesive bonding,” *Surf. Coatings Technol.*, vol. 269, pp. 238–249, May 2015.

[37] S. Minagar, C. C. Berndt, J. Wang, E. Ivanova, and C. Wen, “A review of the application of anodization for the fabrication of nanotubes on metal implant surfaces,”

Acta Biomater., vol. 8, pp. 2875–2888, 2012.

[38] H. H. Park, I. S. Park, K. S. Kim, W. Y. Jeon, B. K. Park, H. S. Kim, T. S. Bae, and M. H. Lee, "Bioactive and electrochemical characterization of TiO2 nanotubes on titanium via anodic oxidation," *Electrochim. Acta*, vol. 55, pp. 6109–6114, 2010.

[39] J. M. Macak and P. Schmuki, "Anodic growth of self-organized anodic TiO2 nanotubes in viscous electrolytes," *Electrochim. Acta*, vol. 52, pp. 1258–1264, 2006.

[40] K. S. Raja, T. Gandhi, and M. Misra, "Effect of water content of ethylene glycol as electrolyte for synthesis of ordered titania nanotubes," *Electrochem. commun.*, vol. 9, pp. 1069–1076, 2007.

[41] D. V Bavykin, F. C. Walsh, P. O'Brien, H. Craighead, and H. Kroto, *Titanate and Titania Nanotubes*. The Royal Society of Chemistry, 2009.

[42] I. Eswaramoorthi and L.-P. Hwang, "Anodic titanium oxide: A new template for the synthesis of larger diameter multi-walled carbon nanotubes," *Diam. Relat. Mater.*, vol. 16, pp. 1571–1578, 2007.

[43] G. K. Mor, O. K. Varghese, M. Paulose, K. Shankar, and C. A. Grimes, "A review on highly ordered, vertically oriented TiO2 nanotube arrays: Fabrication, material properties, and solar energy applications," *Sol. Energy Mater. Sol. Cells*, vol. 90, pp. 2011–2075, 2006.

[44] Y. Yan, X. Zhang, Y. Huang, Q. Ding, and X. Pang, "Antibacterial and bioactivity of silver substituted hydroxyapatite/TiO2 nanotube composite coatings on titanium," *Appl. Surf. Sci.*, vol. 314, no. 0, pp. 348–357, Sep. 2014.

[45] A. Gomez Sanchez, W. Schreiner, G. Duffó, and S. Ceré, "Surface modification of titanium by anodic oxidation in phosphoric acid at low potentials. Part 1. Structure,

electronic properties and thickness of the anodic films," *Surf. Interface Anal.*, p. n/a-n/a, 2013.

[46] S. A. Fadl-allah and Q. Mohsen, "Characterization of native and anodic oxide films formed on commercial pure titanium using electrochemical properties and morphology techniques," *Appl. Surf. Sci.*, vol. 256, pp. 5849–5855, 2010.

[47] H. Habazaki, T. Ogasawara, H. Konno, K. Shimizu, S. Nagata, P. Skeldon, and G. E. Thompson, "Field crystallization of anodic niobia," *Corros. Sci.*, vol. 49, pp. 580–593, 2007.

[48] H.-J. Song, S.-H. Park, S.-H. Jeong, and Y.-J. Park, "Surface characteristics and bioactivity of oxide films formed by anodic spark oxidation on titanium in different electrolytes," *J. Mater. Process. Technol.*, vol. 209, pp. 864–870, 2009.

[49] Y.-T. Sul, C. B. Johansson, Y. Jeong, and T. Albrektsson, "The electrochemical oxide growth behaviour on titanium in acid and alkaline electrolytes," *Med. Eng. Phys.*, vol. 23, pp. 329–346, 2001.

[50] M. Lewandowska, M. Pisarek, K. Rożniatowski, M. Grądzka-Dahlke, M. Janik-Czachor, and K. J. Kurzydłowski, "Nanoscale characterization of anodic oxide films on Ti-6Al-4V alloy," *Thin Solid Films*, vol. 515, pp. 6460–6464, 2007.

[51] G. D. Sulka, J. Kapusta-Kolodziej, A. Brzózka, and M. Jaskula, "Fabrication of nanoporous TiO2 by electrochemical anodization," *Electrochim. Acta*, vol. 55, pp. 4359–4367, 2010.

[52] R. Narayanan, T.-Y. Kwon, and K.-H. Kim, "Anodic TiO2 from stirred Na2SO4/NaF electrolytes: Effect of applied voltage and stirring," *Mater. Lett.*, vol. 63, pp. 2003–2006, 2009.

[53] K. Scott and W. M. Taama, “An investigation of anode materials in the anodic oxidation of sulphur dioxide in sulphuric acid solutions,” *Electrochim. Acta*, vol. 44, pp. 3421–3427, 1999.

[54] A. F. Yetim, A. Alsaran, I. Efeoglu, and A. Çelik, “A comparative study: The effect of surface treatments on the tribological properties of Ti–6Al–4V alloy,” *Surf. Coatings Technol.*, vol. 202, pp. 2428–2432, 2008.

[55] X. Shi, Q. Wang, F. Wang, and S. Ge, “Effects of electrolytic concentration on properties of micro-arc film on Ti6Al4V alloy,” *Min. Sci. Technol.*, vol. 19, pp. 220–224, 2009.

[56] Y. M. Wang, D. C. Jia, L. X. Guo, T. Q. Lei, and B. L. Jiang, “Effect of discharge pulsating on microarc oxidation coatings formed on Ti6Al4V alloy,” *Mater. Chem. Phys.*, vol. 90, no. 1, pp. 128–133, 2005.

[57] X. L. Zhang, Z. H. Jiang, Z. P. Yao, and Z. D. Wu, “Electrochemical study of growth behaviour of plasma electrolytic oxidation coating on Ti6Al4V: Effects of the additive,” *Corros. Sci.*, vol. 52, pp. 3465–3473, 2010.

[58] H.-Y. Si, Z.-H. Sun, X. Kang, W.-W. Zi, and H.-L. Zhang, “Voltage-dependent morphology, wettability and photocurrent response of anodic porous titanium dioxide films,” *Microporous Mesoporous Mater.*, vol. 119, pp. 75–81, 2009.

[59] H.-J. Song, M.-K. Kim, G.-C. Jung, M.-S. Vang, and Y.-J. Park, “The effects of spark anodizing treatment of pure titanium metals and titanium alloys on corrosion characteristics,” *Surf. Coatings Technol.*, vol. 201, pp. 8738–8745, 2007.

[60] M. V. Diamanti, M. Ormellese, and M. Pedeferri, “Alternating current anodizing of titanium in halogen acids combined with Anodic Spark Deposition: Morphological

and structural variations," *Corros. Sci.*, vol. 52, pp. 1824–1829, 2010.

[61] M. Nakajima, Y. Miura, K. Fushimi, and H. Habazaki, "Spark anodizing behaviour of titanium and its alloys in alkaline aluminate electrolyte," *Corros. Sci.*, vol. 51, pp. 1534–1539, 2009.

[62] C. Sun, R. Hui, W. Qu, S. Yick, C. Sun, and W. Qian, "Effects of processing parameters on microstructures of TiO2 coatings formed on titanium by plasma electrolytic oxidation," *J. Mater. Sci.*, vol. 45, pp. 6235–6241, 2010.

[63] Q. Mohsen and S. A. Fadl-Allah, "Improvement in corrosion resistance of commercial pure titanium for the enhancement of its biocompatibility," *Mater. Corros.*, vol. 62, no. 4, pp. 310–319, 2001.

[64] J. Pouilleau, D. Devilliers, F. Garrido, S. Durand-Vidal, and E. Mahé, "Structure and composition of passive titanium oxide films," *Mater. Sci. Eng. B*, vol. 47, pp. 235–243, 1997.

[65] H. Ohmori, K. Katahira, M. Mizutani, and J. Komotori, "Investigation on Color-Finishing Process Conditions for Titanium Alloy applying a New Electrical Grinding Process," *CIRP Ann. - Manuf. Technol.*, vol. 53, pp. 455–458, 2004.

[66] D. Capek, M. P. Gigandet, M. Masmoudi, M. Wery, and O. Banakh, "Long-time anodisation of titanium in sulphuric acid," *Surf. Coatings Technol.*, vol. 202, pp. 1379–1384, 2008.

[67] K. Ajito, J. P. H. Sukamto, L. A. Nagahara, K. Hashimoto, and A. Fujishima, "Combined Raman and photoelectrochemical imaging system. Application to TiO2 films grown anodically on Ti□Ag alloy," *J. Electroanal. Chem.*, vol. 386, pp. 229–233, 1995.

[68] B. Hirschorn, M. E. Orazem, B. Tribollet, V. Vivier, I. Frateur, and M. Musiani, “Determination of effective capacitance and film thickness from constant-phase-element parameters,” *Electrochim. Acta*, vol. 55, pp. 6218–6227, 2010.

[69] X. Sun, Z. Jiang, S. Xin, and Z. Yao, “Composition and mechanical properties of hard ceramic coating containing α-Al2O3 produced by microarc oxidation on Ti–6Al–4V alloy,” *Thin Solid Films*, vol. 471, pp. 194–199, 2005.

[70] C. Martini, L. Ceschini, F. Tarterini, J. M. Paillard, and J. A. Curran, “PEO layers obtained from mixed aluminate–phosphate baths on Ti–6Al–4V: Dry sliding behaviour and influence of a PTFE topcoat,” *Wear*, vol. 269, pp. 747–756, 2010.

[71] A. Bloyce, P.-Y. Qi, H. Dong, and T. Bell, “Surface modification of titanium alloys for combined improvements in corrosion and wear resistance,” *Surf. Coatings Technol.*, vol. 107, no. 2–3, pp. 125–132, Sep. 1998.

[72] C.-T. Wu and F.-H. Lu, “Electrochemical deposition of barium titanate films using a wide electrolytic voltage range,” *Thin Solid Films*, vol. 398–399, pp. 621–625, Nov. 2001.

[73] F.-H. Lu, C.-T. Wu, and C.-Y. Hung, “Barium titanate films synthesized by an anodic oxidation-based electrochemical method,” *Surf. Coatings Technol.*, vol. 153, no. 2–3, pp. 276–283, Apr. 2002.

[74] J. A. Curran and T. W. Clyne, “The thermal conductivity of plasma electrolytic oxide coatings on aluminium and magnesium,” *Surf. Coatings Technol.*, vol. 199, no. 2–3, pp. 177–183, Sep. 2005.

[75] J. A. Curran, H. Kalkancı, Y. Magurova, and T. W. Clyne, “Mullite-rich plasma

electrolytic oxide coatings for thermal barrier applications," *Surf. Coatings Technol.*, vol. 201, no. 21, pp. 8683–8687, Aug. 2007.

[76] E. Medvedovski, "Alumina–mullite ceramics for structural applications," *Ceram. Int.*, vol. 32, no. 4, pp. 369–375, 2006.

[77] H. Kalkancı and S. C. Kurnaz, "The effect of process parameters on mullite-based plasma electrolytic oxide coatings," *Surf. Coatings Technol.*, vol. 203, no. 1–2, pp. 15–22, Oct. 2008.

[78] D. Quintero, O. Galvis, J. A. Calderón, M. A. Gómez, J. G. Castaño, F. Echeverría, and H. Habazaki, "Control of the physical properties of anodic coatings obtained by plasma electrolytic oxidation on Ti6Al4V alloy," *Surf. Coatings Technol.*, vol. 283, pp. 210–222, Dec. 2015.

[79] J. A. Curran and T. W. Clyne, "Porosity in plasma electrolytic oxide coatings," *Acta Mater.*, vol. 54, no. 7, pp. 1985–1993, Apr. 2006.

[80] D. Quintero, O. Galvis, J. A. Calderón, J. G. Castaño, and F. Echeverría, "Effect of electrochemical parameters on the formation of anodic films on commercially pure titanium by plasma electrolytic oxidation," *Surf. Coatings Technol.*, vol. 258, no. 0, pp. 1223–1231, Nov. 2014.

[81] K. M. Lee, B. U. Lee, S. Il Yoon, E. S. Lee, B. Yoo, and D. H. Shin, "Evaluation of plasma temperature during plasma oxidation processing of AZ91 Mg alloy through analysis of the melting behavior of incorporated particles," *Electrochim. Acta*, vol. 67, pp. 6–11, 2012.

[82] M. M. S. Al Bosta, K. J. Ma, and H. H. Chien, "Effect of Anodic Current Density on Characteristics and Low Temperature IR Emissivity of Ceramic Coating on

Aluminium 6061 Alloy Prepared by Microarc Oxidation," *J. Ceram.*, vol. 2013, pp. 1–14, 2013.

[83] S. K. Lazarouk, D. A. Sasinovich, O. V Kupreeva, T. I. Orehovskaia, N. Rochdi, F. A. d'Avitaya, and V. E. Borisenko, "Effect of the electrolyte temperature on the formation and structure of porous anodic titania film," *Thin Solid Films*, vol. 526, pp. 41–46, 2012.

[84] D. Krupa, J. Baszkiewicz, J. Zdunek, J. Smolik, Z. Słomka, and J. W. Sobczak, "Characterization of the surface layers formed on titanium by plasma electrolytic oxidation," *Surf. Coatings Technol.*, vol. 205, pp. 1743–1749, 2010.

[85] Y. Fu, N. L. Loh, J. Wei, B. Yan, and P. Hing, "Friction and wear behaviour of carbon nitride films deposited on plasma nitrided Ti–6Al–4V," *Wear*, vol. 237, pp. 12–19, 2000.

[86] W. Simka, "Preliminary investigations on the anodic oxidation of Ti–13Nb–13Zr alloy in a solution containing calcium and phosphorus," *Electrochim. Acta*, vol. 56, pp. 9831–9837, 2011.

[87] L. Ceschini, E. Lanzoni, C. Martini, D. Prandstraller, and G. Sambogna, "Comparison of dry sliding friction and wear of Ti6Al4V alloy treated by plasma electrolytic oxidation and PVD coating," *Wear*, vol. 264, pp. 86–95, 2008.

[88] T. Cheng, Y. Chen, and X. Nie, "Surface morphology manipulation and wear property of bioceramic oxide coatings on titanium alloy," *Surf. Coatings Technol.*, vol. 215, pp. 253–259, 2013.

[89] M. V. Diamanti, M. Sebastiani, V. Mangione, B. Del Curto, M. P. Pedeferri, E. Bemporad, A. Cigada, and F. Carassiti, "Multi-step anodizing on Ti6Al4V

components to improve tribomechanical performances," *Surf. Coatings Technol.*, vol. 227, pp. 19–27, 2013.

[90] S. Stojadinović, R. Vasilić, M. Petković, B. Kasalica, I. Belča, A. Žekić, and L. Zeković, "Characterization of the plasma electrolytic oxidation of titanium in sodium metasilicate," *Appl. Surf. Sci.*, vol. 265, pp. 226–233, 2013.

[91] C. Martini and L. Ceschini, "A comparative study of the tribological behaviour of PVD coatings on the Ti-6Al-4V alloy," *Tribol. Int.*, vol. 44, pp. 297–308, 2011.

[92] Y. S. Tian, C. Z. Chen, L. X. Chen, and Q. H. Huo, "Wear and oxidation resistance of composite coatings fabricated on Ti-6Al-4V by laser alloying with nitrogen and silicon," *J. Phys. D. Appl. Phys.*, vol. 38, pp. 4217–4221, 2005.

[93] B. G. Wendler and W. Pawlak, "Low friction and wear resistant coating systems on Ti6Al4V alloy," *J. Achiev. Mater. Manuf. Eng.*, vol. 26, pp. 207–210, 2008.

[94] H. Habazaki, S. Tsunekawa, E. Tsuji, and T. Nakayama, "Formation and characterization of wear-resistant PEO coatings formed on β-titanium alloy at different electrolyte temperatures," *Appl. Surf. Sci.*, vol. 259, pp. 711–718, 2012.

[95] W. K. Yeung, G. C. Reilly, A. Matthews, and A. Yerokhin, "In vitro biological response of plasma electrolytically oxidized and plasma-sprayed hydroxyapatite coatings on Ti – 6Al – 4V alloy," *J. Biomed. Mater. Res. Part B Appl. Biomater.*, pp. 939–949, 2013.

[96] S. Aliasghari, P. Skeldon, and G. E. Thompson, "Plasma electrolytic oxidation of titanium in a phosphate/silicate electrolyte and tribological performance of the coatings," *Appl. Surf. Sci.*, vol. 316, no. 0, pp. 463–476, Oct. 2014.

[97] R. Narayanan, S. K. Seshadri, T. Y. Kwon, and K. H. Kim, "Calcium phosphate-based

coatings on titanium and its alloys," *J. Biomed. Mater. Res. Part B Appl. Biomater.*, vol. 85B, pp. 279–299, 2008.

[98] S. Yang, Y. Aoki, P. Skeldon, G. E. Thompson, and H. Habazaki, "Growth of porous anodic alumina films in hot phosphate–glycerol electrolyte," *J. Solid State Electrochem.*, vol. 15, pp. 689–696, 2011.

[99] G. B. de Souza, G. G. de Lima, N. K. Kuromoto, P. Soares, C. M. Lepienski, C. E. Foerster, and A. Mikowski, "Tribo-mechanical characterization of rough, porous and bioactive Ti anodic layers," *J. Mech. Behav. Biomed. Mater.*, vol. 4, pp. 796–806, 2011.

[100] H.-Y. Wang, R.-F. Zhu, Y.-P. Lu, G.-Y. Xiao, X.-C. Zhao, K. He, Y. F. Yuan, Y. Li, and X.-N. Ma, "Preparation and properties of plasma electrolytic oxidation coating on sandblasted pure titanium by a combination treatment," *Mater. Sci. Eng. C*, vol. 42, no. 0, pp. 657–664, Sep. 2014.

[101] C. A. H. Laurindo, R. D. Torres, S. A. Mali, J. L. Gilbert, and P. Soares, "Incorporation of Ca and P on anodized titanium surface: Effect of high current density," *Mater. Sci. Eng. C*, vol. 37, no. 0, pp. 223–231, Apr. 2014.

[102] A. Krząkała, K. Służalska, G. Dercz, A. Maciej, A. Kazek, J. Szade, A. Winiarski, M. Dudek, J. Michalska, G. Tylko, A. M. Osyczka, and W. Simka, "Characterisation of bioactive films on Ti–6Al–4V alloy," *Electrochim. Acta*, vol. 104, no. 0, pp. 425–438, Aug. 2013.

[103] D. Wei, Y. Zhou, D. Jia, and Y. Wang, "Chemical treatment of TiO2-based coatings formed by plasma electrolytic oxidation in electrolyte containing nano-HA, calcium salts and phosphates for biomedical applications," *Appl. Surf. Sci.*, vol. 254, no. 6, pp.

1775–1782, Jan. 2008.

[104] A. Kazek-Kęsik, M. Krok-Borkowicz, E. Pamuła, and W. Simka, “Electrochemical and biological characterization of coatings formed on Ti–15Mo alloy by plasma electrolytic oxidation,” *Mater. Sci. Eng. C*, vol. 43, no. 0, pp. 172–181, Oct. 2014.

[105] J. R. Henstock, L. T. Canham, and S. I. Anderson, “Silicon: the evolution of its use in biomaterials.,” *Acta Biomater.*, vol. 11, pp. 17–26, Jan. 2015.

[106] S. Wang, X. Wang, F. G. Draenert, O. Albert, H. C. Schröder, V. Mailänder, G. Mitov, and W. E. G. Müller, “Bioactive and biodegradable silica biomaterial for bone regeneration.,” *Bone*, vol. 67, pp. 292–304, Oct. 2014.

[107] W. Zhang, K. Du, C. Yan, and F. Wang, “Preparation and characterization of a novel Si-incorporated ceramic film on pure titanium by plasma electrolytic oxidation,” *Appl. Surf. Sci.*, vol. 254, pp. 5216–5223, 2008.

[108] W. Simka, R. P. Socha, G. Dercz, J. Michalska, A. Maciej, and A. Krząkała, “Anodic oxidation of Ti–13Nb–13Zr alloy in silicate solutions,” *Appl. Surf. Sci.*, vol. 279, pp. 317–323, Aug. 2013.

[109] I. Han, J. H. Choi, B. H. Zhao, H. K. Baik, and I.-S. Lee, “Micro-arc oxidation in various concentration of KOH and structural change by different cut off potential,” *Curr. Appl. Phys.*, vol. 7, Supplem, pp. e23–e27, 2007.

[110] L. O. Snizhko, A. L. Yerokhin, N. L. Gurevina, V. A. Patalakha, and A. Matthews, “Excessive oxygen evolution during plasma electrolytic oxidation of aluminium,” *Thin Solid Films*, vol. 516, no. 2–4, pp. 460–464, Dec. 2007.

[111] P. Zhang, X. Nie, H. Hu, and Y. Liu, “TEM analysis and tribological properties of Plasma Electrolytic Oxidation (PEO) coatings on a magnesium engine AJ62 alloy,”

Surf. Coatings Technol., vol. 205, no. 5, pp. 1508–1514, 2010.

[112] J. Jovović, S. Stojadinović, N. M. M. Šišović, and N. Konjević, "Spectroscopic characterization of plasma during electrolytic oxidation (PEO) of aluminium," *Surf. Coatings Technol.*, vol. 206, no. 1, pp. 24–28, 2011.

[113] V. Dehnavi, B. L. Luan, D. W. Shoesmith, X. Y. Liu, and S. Rohani, "Effect of duty cycle and applied current frequency on plasma electrolytic oxidation (PEO) coating growth behavior," *Surf. Coatings Technol.*, vol. 226, pp. 100–107, 2013.

[114] S. Fadl-Allah, R. El-Sherief, and W. Badawy, "Electrochemical formation and characterization of porous titania (TiO2) films on Ti," *J. Appl. Electrochem.*, vol. 38, pp. 1459–1466, 2008.

[115] M. E. P. Souza, M. Ballester, and C. M. A. Freire, "EIS characterisation of Ti anodic oxide porous films formed using modulated potential," *Surf. Coatings Technol.*, vol. 201, pp. 7775–7780, 2007.

[116] X. Zhang, Z. Yao, Z. Jiang, Y. Zhang, and X. Liu, "Investigation of the plasma electrolytic oxidation of Ti6Al4V under single-pulse power supply," *Corros. Sci.*, vol. 53, no. 6, pp. 2253–2262, 2011.

[117] R. O. Hussein, X. Nie, D. O. Northwood, A. Yerokhin, and A. Matthews, "Spectroscopic study of electrolytic plasma and discharging behaviour during the plasma electrolytic oxidation (PEO) process," *J. Phys. D. Appl. Phys.*, vol. 43, no. 10, p. 105203, 2010.

[118] M. Fini, A. Cigada, G. Rondelli, R. Chiesa, R. Giardino, G. Giavaresi, N. Nicoli Aldini, P. Torricelli, and B. Vicentini, "In vitro and in vivo behaviour of Ca- and P-enriched anodized titanium," *Biomaterials*, vol. 20, no. 17, pp. 1587–1594, Sep.

1999.

[119] V. . Frauchiger, F. Schlottig, B. Gasser, and M. Textor, “Anodic plasma-chemical treatment of CP titanium surfaces for biomedical applications,” *Biomaterials*, vol. 25, no. 4, pp. 593–606, Feb. 2004.

[120] M. Ask, J. Lausmaa, and B. Kasemo, “Preparation and surface spectroscopic characterization of oxide films on Ti6Al4V,” *Appl. Surf. Sci.*, vol. 35, no. 3, pp. 283–301, Jan. 1989.

[121] W. F. Cui, L. Jin, and L. Zhou, “Surface characteristics and electrochemical corrosion behavior of a pre-anodized microarc oxidation coating on titanium alloy,” *Mater. Sci. Eng. C*, vol. 33, no. 7, pp. 3775–3779, Oct. 2013.

[122] S. Tsunekawa, Y. Aoki, and H. Habazaki, “Two-step plasma electrolytic oxidation of Ti–15V–3Al–3Cr–3Sn for wear-resistant and adhesive coating,” *Surf. Coatings Technol.*, vol. 205, pp. 4732–4740, 2011.

[123] Y. L. Cheng, M. K. Mao, J. H. Cao, and Z. M. Peng, “Plasma electrolytic oxidation of an Al-Cu-Li alloy in alkaline aluminate electrolytes: A competition between growth and dissolution for the initial ultra-thin films,” *Electrochim. Acta*, vol. 138, pp. 417–429, 2014.

[124] Y. Cheng, F. Wu, J. Dong, X. Wu, Z. Xue, E. Matykina, P. Skeldon, and G. E. Thompson, “Comparison of plasma electrolytic oxidation of zirconium alloy in silicate- and aluminate-based electrolytes and wear properties of the resulting coatings,” *Electrochim. Acta*, vol. 85, pp. 25–32, 2012.

[125] Y. Cheng, J. Cao, Z. Peng, Q. Wang, E. Matykina, P. Skeldon, and G. E. Thompson, “Wear-resistant coatings formed on Zircaloy-2 by plasma electrolytic oxidation in

sodium aluminate electrolytes," *Electrochim. Acta*, vol. 116, pp. 453–466, 2014.

[126] A. L. Yerokhin, A. Leyland, and A. Matthews, "Kinetic aspects of aluminium titanate layer formation on titanium alloys by plasma electrolytic oxidation," *Appl. Surf. Sci.*, vol. 200, no. 1–4, pp. 172–184, Nov. 2002.

[127] S.-G. Xin, L.-X. Song, R.-G. Zhao, and X.-F. Hu, "Composition and thermal properties of the coating containing mullite and alumina," *Mater. Chem. Phys.*, vol. 97, no. 1, pp. 132–136, May 2006.

[128] E. Matykina, R. Arrabal, P. Skeldon, and G. E. Thompson, "Investigation of the growth processes of coatings formed by AC plasma electrolytic oxidation of aluminium," *Electrochim. Acta*, vol. 54, no. 27, pp. 6767–6778, Nov. 2009.

[129] M. Treviño, N. F. Garza-Montes-de-Oca, A. Pérez, M. A. L. Hernández-Rodríguez, A. Juárez, and R. Colás, "Wear of an aluminium alloy coated by plasma electrolytic oxidation," *Surf. Coatings Technol.*, vol. 206, no. 8–9, pp. 2213–2219, Jan. 2012.

[130] I. A. Aksay, D. M. Dabbs, and M. Sarikaya, "Mullite for Structural, Electronic, and Optical Applications," *J. Am. Ceram. Soc.*, vol. 74, no. 10, pp. 2343–2358, Oct. 1991.

[131] R. Torrecillas, J. M. Calderón, J. S. Moya, M. J. Reece, C. K. L. Davies, C. Olagnon, and G. Fantozzi, "Suitability of mullite for high temperature applications," *J. Eur. Ceram. Soc.*, vol. 19, no. 13–14, pp. 2519–2527, Oct. 1999.

[132] S. Aliasghari, P. Skeleton, and G. E. Thompson, "Plasma electrolytic oxidation of titanium in a phosphate/silicate electrolyte and tribological performance of the coatings," *Appl. Surf. Sci.*, vol. 316, no. 1, pp. 463–476, 2014.

[133] K. R. Shin, Y. G. Ko, and D. H. Shin, "Influence of zirconia on biomimetic apatite formation in pure titanium coated via plasma electrolytic oxidation," *Mater. Lett.*, vol.

64, pp. 2714–2717, 2010.

[134] K. R. Shin, Y. G. Ko, and D. H. Shin, “Effect of electrolyte on surface properties of pure titanium coated by plasma electrolytic oxidation,” *J. Alloys Compd.*, vol. 509, Suppl, pp. S478–S481, 2011.

[135] W. A. Badawy, A. M. Fathi, R. M. El-Sherief, and S. A. Fadl-Allah, “Electrochemical and biological behaviors of porous titania (TiO2) in simulated body fluids for implantation in human bodies,” *J. Alloys Compd.*, vol. 475, pp. 911–916, 2009.

[136] A. L. Yerokhin, A. Leyland, and A. Matthews, “Kinetic aspects of aluminium titanate layer formation on titanium alloys by plasma electrolytic oxidation,” *Appl. Surf. Sci.*, vol. 200, pp. 172–184, 2002.

[137] M. Avdeev and A. Kholkin, “Low-temperature Na4Ti5O12 from X-ray and neutron powder diffraction data,” *Acta Crystallogr. Sect. C*, vol. 56, no. 12, pp. e539–e540, Dec. 2000.

[138] P. J. P. Naeyaert, M. Avdeev, N. Sharma, H. Ben Yahia, and C. D. Ling, “Synthetic, Structural, and Electrochemical Study of Monoclinic Na4Ti5O12 as a Sodium-Ion Battery Anode Material,” *Chem. Mater.*, vol. 26, no. 24, pp. 7067–7072, Dec. 2014.

[139] R. X. Frscnnn, “Crystal structure of Al-rich mullite,” *Am. Mineral.*, vol. 79, pp. 983–990, 1994.

[140] J.-H. Xing, Z.-B. Xia, J.-F. Hu, Y.-H. Zhang, and L. Zhong, “Growth and crystallization of titanium oxide films at different anodization modes,” *J. Electrochem. Soc.*, vol. 160, no. 6, pp. C239–C246, 2013.

[141] M. A. Henderson, “A surface science perspective on photocatalysis,” *Surf. Sci. Rep.*, vol. 66, no. 6–7, pp. 185–297, Jun. 2011.

[142] S. Stojadinović, R. Vasilić, M. Petković, B. Kasalica, I. Belča, A. Žekić, and L. Zeković, “Characterization of the plasma electrolytic oxidation of titanium in sodium metasilicate,” *Appl. Surf. Sci.*, vol. 265, pp. 226–233, 2013.

[143] A. L. Y. and L. O. S. and N. L. G. and A. L. and A. P. and A. Matthews, “Discharge characterization in plasma electrolytic oxidation of aluminium,” *J. Phys. D. Appl. Phys.*, vol. 36, no. 17, p. 2110, 2003.

[144] L. O. Snizhko, A. L. Yerokhin, A. Pilkington, N. L. Gurevina, D. O. Misnyankin, A. Leyland, and A. Matthews, “Anodic processes in plasma electrolytic oxidation of aluminium in alkaline solutions,” *Electrochim. Acta*, vol. 49, no. 13, pp. 2085–2095, May 2004.

[145] S. M. Kramer, I. G. Gorichev, Y. A. Lainer, I. V Artamonova, and M. V Terekhova, “Calculation of the solubility of TiO2 and titanates in sulfuric acid solutions,” *Russ. Metall.*, vol. 2014, no. 9, pp. 704–707, 2015.

[146] C. S. Dunleavy, J. A. Curran, and T. W. Clyne, “Self-similar scaling of discharge events through PEO coatings on aluminium,” *Surf. Coatings Technol.*, vol. 206, no. 6, pp. 1051–1061, 2011.

[147] C. S. Dunleavy, I. O. Golosnoy, J. a. Curran, and T. W. Clyne, “Characterisation of discharge events during plasma electrolytic oxidation,” *Surf. Coatings Technol.*, vol. 203, no. 22, pp. 3410–3419, Aug. 2009.

[148] S. Stojadinović, R. Vasilić, M. Petković, and L. Zeković, “Plasma electrolytic oxidation of titanium in heteropolytungstate acids,” *Surf. Coatings Technol.*, vol. 206, pp. 575–581, 2011.

[149] C. S. Dunleavy, I. O. Golosnoy, J. A. Curran, and T. W. Clyne, “Characterisation of

discharge events during plasma electrolytic oxidation," *Surf. Coatings Technol.*, vol. 203, pp. 3410–3419, 2009.

[150] S. Aliasghari, "Plasma electrolytic oxidation of Titanium," *J. Serbian Chem. Soc.*, vol. 78, no. 5, pp. 1–223, 2014.

[151] S. Stojadinović, J. Jovović, M. Petković, R. Vasilić, and N. Konjević, "Spectroscopic and real-time imaging investigation of tantalum plasma electrolytic oxidation (PEO)," *Surf. Coatings Technol.*, vol. 205, no. 23–24, pp. 5406–5413, Sep. 2011.

[152] R. O. Hussein, X. Nie, and D. O. Northwood, "A spectroscopic and microstructural study of oxide coatings produced on a Ti–6Al–4V alloy by plasma electrolytic oxidation," *Mater. Chem. Phys.*, vol. 134, no. 1, pp. 484–492, 2012.

[153] M. M. S. Al Bosta and K.-J. Ma, "Suggested mechanism for the MAO ceramic coating on aluminium substrates using bipolar current mode in the alkaline silicate electrolytes," *Appl. Surf. Sci.*, vol. 308, no. 0, pp. 121–138, Jul. 2014.

[154] H.-J. Oh, J.-H. Lee, Y.-J. Kim, S.-J. Suh, J.-H. Lee, and C.-S. Chi, "Surface characteristics of porous anodic TiO2 layer for biomedical applications," *Mater. Chem. Phys.*, vol. 109, pp. 10–14, 2008.

[155] J.-H. Lee, S.-E. Kim, Y.-J. Kim, C.-S. Chi, and H.-J. Oh, "Effects of microstructure of anodic titania on the formation of bioactive compounds," *Mater. Chem. Phys.*, vol. 98, pp. 39–43, 2006.

[156] H.-J. Oh, J.-H. Lee, Y. Jeong, Y.-J. Kim, and C.-S. Chi, "Microstructural characterization of biomedical titanium oxide film fabricated by electrochemical method," *Surf. Coatings Technol.*, vol. 198, pp. 247–252, 2005.

[157] E. Matykina, A. Berkani, P. Skeldon, and G. E. Thompson, "Real-time imaging of

coating growth during plasma electrolytic oxidation of titanium," *Electrochim. Acta*, vol. 53, no. 4, pp. 1987–1994, 2007.

[158] J. J. Candel, V. Amigó, J. A. Ramos, and D. Busquets, "Sliding wear resistance of TiCp reinforced titanium composite coating produced by laser cladding," *Surf. Coatings Technol.*, vol. 204, pp. 3161–3166, 2010.

[159] A. Kazek-Kęsik, G. Dercz, I. Kalemba, K. Suchanek, A. I. Kukharenko, D. M. Korotin, J. Michalska, A. Krząkała, J. Piotrowski, E. Z. Kurmaev, S. O. Cholakh, and W. Simka, "Surface characterisation of Ti–15Mo alloy modified by a PEO process in various suspensions," *Mater. Sci. Eng. C*, vol. 39, no. 0, pp. 259–272, Jun. 2014.

[160] M. Fazel, H. R. Salimijazi, M. A. Golozar, and M. R. Garsivaz Jazi, "A comparison of corrosion, tribocorrosion and electrochemical impedance properties of pure Ti and Ti6Al4V alloy treated by micro-arc oxidation process," *Appl. Surf. Sci.*, vol. 324, pp. 751–756, Jan. 2015.

[161] L. Zhu, Z. Guo, Y. Zhang, Z. Li, and M. Sui, "A mechanism for the growth of a plasma electrolytic oxide coating on Al," *Electrochim. Acta*, vol. 208, pp. 296–303, Aug. 2016.

[162] L. O. Snizhko, A. L. Yerokhin, N. L. Gurevina, D. O. Misnyankin, A. Pilkington, A. Leyland, and A. Matthews, "A model for galvanostatic anodising of Al in alkaline solutions," *Electrochim. Acta*, vol. 50, no. 27, pp. 5458–5464, Sep. 2005.

[163] D. O. N. R.O. Hussein, X. Nie, "An investigation of ceramic coating growth mechanisms in plasma electrolytic oxidation (PEO) processing.pdf," *Electrochim. Acta*, vol. 112, p. 111, 2013.

[164] A. L. Yerokhin, X. Nie, A. Leyland, A. Matthews, and S. J. Dowey, "Plasma

electrolysis for surface engineering," *Surf. Coatings Technol.*, vol. 122, no. 2–3, pp. 73–93, Dec. 1999.

[165] B. Kasalica, J. Radić-Perić, M. Perić, M. Petković-Benazzouz, I. Belča, and M. Sarvan, "The mechanism of evolution of microdischarges at the beginning of the PEO process on aluminum," *Surf. Coatings Technol.*, vol. 298, pp. 24–32, Jul. 2016.

[166] L. Zhu, Z. Guo, Y. Zhang, Z. Li, and M. Sui, "A mechanism for the growth of a plasma electrolytic oxide coating on Al," *Electrochim. Acta*, vol. 208, pp. 296–303, Aug. 2016.

[167] A. K. Vijh, "Sparking voltages and side reactions during anodization of valve metals in terms of electron tunnelling," *Corros. Sci.*, vol. 11, no. 6, pp. 411–417, 1971.

[168] S. Ikonopisov, "Theory of electrical breakdown during formation of barrier anodic films," *Electrochim. Acta*, vol. 22, no. 10, pp. 1077–1082, 1977.

[169] W. L. W. J.R. Fuhr, "Optical emission spectroscopy studies of discharge mechanism and plasma characteristics during plasma electrolytic oxidation of magnesium in different electrolytes," *CRC Handb. Chem. Phys.*, vol. 205, no. 6, pp. 1651–1658, Dec. 1996.

[170] W. L. W. J.R. Fuhr, "Contact glow-discharge electrolysis," *CRC Handb. Chem. Phys.*, vol. 205, no. 6, pp. 1651–1658, Dec. 1996.

[171] W. L. W. J.R. Fuhr, "NIST Atomic Transition Probability Tables," *CRC Handb. Chem. Phys.*, 1996.

[172] X. Nie, E. I. Meletis, J. C. Jiang, A. Leyland, A. L. Yerokhin, and A. Matthews, "Abrasive wear/corrosion properties and TEM analysis of Al2O3 coatings fabricated using plasma electrolysis," *Surf. Coatings Technol.*, vol. 149, no. 2–3, pp. 245–251,

Jan. 2002.

[173] E. Matykina, R. Arrabal, P. Skeldon, and G. E. Thompson, “Transmission electron microscopy of coatings formed by plasma electrolytic oxidation of titanium,” *Acta Biomater.*, vol. 5, pp. 1356–1366, 2009.

[174] Y. Guan, Y. Xia, and G. Li, “Growth mechanism and corrosion behavior of ceramic coatings on aluminum produced by autocontrol AC pulse PEO,” *Surf. Coatings Technol.*, vol. 202, no. 19, pp. 4602–4612, Jun. 2008.

[175] H. Guo, M. An, S. Xu, and H. Huo, “Formation of oxygen bubbles and its influence on current efficiency in micro-arc oxidation process of AZ91D magnesium alloy,” *Thin Solid Films*, vol. 485, no. 1–2, pp. 53–58, Aug. 2005.

[176] T. Nakamura, T. Ichitsubo, E. Matsubara, A. Muramatsu, N. Sato, and H. Takahashi, “On the preferential formation of anatase in amorphous titanium oxide film,” *Scr. Mater.*, vol. 53, no. 9, pp. 1019–1023, Nov. 2005.